

#### Master's Degree in Automotive Engineering



Master's Degree Thesis

# Development of coatings on titanium alloys for protection against high-temperature oxidation in the automotive industry

**Supervisors** 

Candidate

Prof Stefano Paolo PASTORELLI

**Davlatjon BATIROV** 

**Co-supervisor:** 

**Prof. Dilshat TULYAGANOV** 



## Acknowledgements

I would like to convey my sincere appreciation to my supervisors, Prof. **Stefano Paolo Pastorelli** and Prof. **Dilshat Tulyaganov**, as well as the committee chair, for their consistent patience, invaluable advice, and ongoing support. Their willingness to share their knowledge and expertise has played a crucial role in the successful completion of this thesis.

I am also truly grateful to my classmates and fellow cohort members, especially those I share an office with, for their help with editing and steadfast moral support. Additionally, I extend my heartfelt thanks to the university librarians, research assistants, and study participants whose contributions and insights have greatly enhanced my research experience.

Lastly, I must recognize the unwavering support of my family, particularly my parents and wife. Their constant belief in me has been an enduring source of motivation throughout this journey.



## Summary

This thesis explores the characteristics, manufacturing methods, and applications of titanium, with a focus on its surface protection against high-temperature oxidation. In Uzbekistan, the growing interest in sports cars and racing has increased the demand for advanced automotive technologies. One significant challenge is the overheating of exhaust systems, particularly in vehicles using nitrous oxide ("nitro"), which can lead to reduced efficiency, safety risks, and potential damage. This research investigates material enhancements and protective coatings to improve oxidation resistance and thermal stability.

The first section reviews titanium metallurgy, including its crystal structure, phase transitions, and alloy classifications, as well as its physical, mechanical, and chemical properties. It discusses conventional and advanced machining methods and examines various surface protection techniques—such as silicon, aluminum, and glass-ceramic coatings—to combat oxidation.

The second section addresses adhesion theories and coating application mechanisms, including mechanical interlocking and chemical adsorption. It evaluates coating deposition methods, causes of failure, and factors influencing adhesion strength, focusing on titanium coatings for harsh environments.

An experimental part is carried out in Turin polytechnic university in Tashkent, under the co-supervision of Prof. Dilshat Tulyaganov who serves as a faculty member and coordinator of the laboratory where the research activities were carried out. Titanium substrates underwent cutting, polishing, and contamination removal to enhance adhesion, with comparative data collected from glass substrates. Coatings were applied under controlled conditions, followed by heat treatments to improve stability and microstructural integrity. A prototype titanium component was developed to demonstrate practical viability.

Characterization techniques and analysis including metallographic microscopy, thermal shock resistance assessments, thermal distribution in a coated exhaust system, SEM, FTIR, EDS, and XRD, were employed to evaluate adhesion quality, thickness uniformity. Results indicate that titanium coatings significantly enhance thermal management and durability, offering solutions to overheating issues in sports car exhaust systems.

These findings are vital for mitigating overheating in high-performance exhaust systems, as material enhancements can lower thermal stress and oxidation rates, thereby extending component lifespan. By utilizing advancements in titanium coating research, the automotive industry can develop innovative exhaust designs that improve safety and promote sustainable high-performance vehicles. Future research should prioritize customizing coatings for extreme combustion conditions to ensure reliability during nitro-boosted operations.



## **Table of Contents**

Sı	umm	ary		iii
Li	ist of	f Table	es	vi
List of Figures		vii		
A	Appendix A			xi
A	cron	yms		xii
1	Int	oduct	ion	1
	1.1	Meta	llurgy of titanium	3
		1.1.1	Crystal structure and plastic deformation	6
		1.1.2	$\beta/\alpha$ -transformation	
		1.1.3	The classification of titanium alloys	12
	1.2	Prope	erties of titanium	
		$1.2.\bar{1}$	Physical and mechanical properties	14
		1.2.2	Chemical properties	15
	1.3	Fabri	cation techniques	15
		1.3.1	Production of pure titanium	16
		1.3.2	Production of titanium alloys	17
		1.3.3	Conventional and advanced machine	
	1.4	Titan	ium in the automotive industry. Existing challenges	21
		1.4.1	•	
		1.4.2	<del>-</del>	
		1.4.3	Limited availability of raw materials	32
		1.4.4	Prospects and potential solutions	32
	1.5	Prote	ction of titanium against high temperature oxidation	34
		1.5.1	Surface protection using silicon	
		1.5.2	Surface protection using aluminum	35
		1.5.3	Surface protection using glass and glass-ceramics	
	1.6	Conc	lusion	
2	The	ories a	nd mechanism of adhesion	38
	2.1	Coati	ng deposition process and techniques	39





## Master's Degree Thesis AUTOMOTIVE ENGINEERING – A.Y. 2024/2025

	2.2	Theory of adhesion	47
		2.2.1 Mechanical interlocking theory	47
		2.2.2 Chemical/adsorption theory	48
		2.2.3 Acid-base theory	49
		2.2.4 Diffusion or interdiffusion theory	50
		2.2.5 The electrostatic attraction theory	51
	2.3	Thermodynamic theory of adhesion	51
	2.4	Macroscopic adhesion testing	52
		2.4.1 Cause of failure	55
		2.4.2 Adhesion test	56
	2.5	Influence of different factors on coating adhesion	64
	2.6	Other considerations	
	2.7	Application of coated titanium in the automotive in	dustry 76
		2.7.1 Cost and feasibility analysis	78
	2.8	Conclusion	
3	_	perimental parts	90
	3.1	b' $b'$ $1$	
	3.2	Cleaning and preparation procedure of Ti substrate	
	3.3	Glass powder preparation	
	3.4	Characterization of glass	
	3.5	Coating deposition and functionalization	
	3.6	Heat treatment process optimization	
		3.6.1. Preparation of sample cross section for microstr	ructural
		analysis	
	3.7	Scanning electron microscopic (SEM) analysis	
	3.8	EDS analysis	103
		3.8.1 EDS analysis of Ti substrate	
		3.8.2 EDS analysis of glass ceramic coating	105
	3.9	, ,	
	3.10	) XRD analysis of Ti substrate and glass coating	110
	3.11	Metallographic analysis of glass coating	112
	3.12	2 Thermal shock analysis of glass coating and Ti subs	strate 113
	3.13	Simulation of exhaust system at high temperatures.	117
4	Con	nclusions	120
5	App	pendix A	123
6	Bib	oliography	129



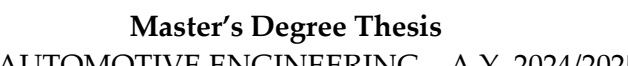
## List of Tables

1.1. Superplastic deformation of Ti-6Al-4V alloy in different strain rates	9
1.2. Main titanium microstructural phases	10
1.3. Comparison of Coating Methods	34
2.1. Cost analysis of CVD coatings (thickness 75 µm) for titanium	
exhaust systems	80
2.2. Cost analysis of CVD coatings (thickness 100 μm) for titanium	
exhaust systems	81
2.3. Property of Titanium sample	81
2.4. Titanium substrate cost estimation	84
2.5. Total cost of Titanium sample	85
2.6. Thermal spray with glass-ceramic on titanium	86
2.7. Comparison: CVD vs thermal spray for class-ceramic coating	
on titanium	87
3.1. Chemical compositions (batches) of the investigated glasses	
G-1d and G-1e (the composition of glassG-1b is presented	
or comparison purposes)	93
3.2. Characteristic temperatures (Tg and Ts) of the glasses G-1b, G-1d and	
G-1e and their thermal expansion coefficients (CTE) for the temperature	
ranges of 200–400°C and 200–500°C determined from the	
dilatometry curves forty	96
3.3. The mass and atomic ratio of Titanium sample	105
3.4. The mass and atomic ratio of the front and back sides	
of the coated sample	106
3.5. Thermal shock resistance test	113



# List of Figures

1.1. Breakdown of thermal challenges in nitro-fueled exhaust systems	1
1.2. Titanium 3D printing automotive exhaust manifold adopts	
DMLS 3D printing	2
1.3. Schematic flowchart of titanium production	4
1.4. Titanium alloy processing and product flow diagram	5
1.5. Pure titanium crystalline structure of (hcp) $\alpha$ -phase and (bcc) β-phase	7
1.6. The behavior of superplastic deformation in the Ti-6Al-4V alloy	8
1.7. Impact of (a) alpha and (b) beta stabilizers on the microstructura	ıl
characteristics of titanium alloys. The black dotted lines delineate the	e
metastable region of $\alpha$ - $\beta$ alloys, while the red dotted lines indicate the	e
anticipated microstructure at ambient temperature. Additionally, (c) illustrate	S
a standard commercially pure $\alpha$ -titanium microstructure, and (d) depicts a	a
typical annealed Ti-6Al-4V $\alpha$ - $\beta$ alloy microstructure	11
1.8. Comparative mechanical properties of Titanium, Steel, and Aluminum	15
1.9. Concept of Ti-1Cu alloys	21
1.10. Key Applications of Titanium in Automobiles	23
1.11. Titanium fuel tank	24
1.12. Ti-1Cu muffler	25
1.13. (a) Yamaha Motor Co., Ltd. YZF-R1, (b) Ti-5Al-1Fe connecting rod	26
1.14. Titanium engine valve	27
1.15. Schematic diagram of PEFC	30
1.16. Structure of Bioglass 45S5	37
2.1. Scheme of Physical Vapor Deposition (PVD) process	39
2.2. a) Aluminum nitride (AlN) coating applied to carbon fibers,	
(b) fiber without coating	40
2.3. Techniques for PVD processing	41
2.4. Deposition of TiO2 coating on a glass substrate utilizing the CVD method	41
2.5. Plasma-Enhanced Chemical Vapor Deposition (PECVD) System	42
2.6. Outline of the Thermal Spray Procedure	42
2.7. Scheme of Plasma spray process	
2.8. Scheme of High-Velocity Oxy-Fuel spray technique HVOF	43
2.9. Morphology of plasma spray Ni20Cr coating deposited by	
plasma spray method	44





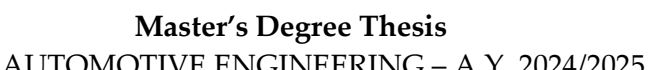
### AUTOMOTIVE ENGINEERING – A.Y. 2024/2025

2.10. Phosphate coating	45
2.11. Aluminum Electroplating Utilizing Bromide Salts	45
2.12. Rhodium dipping on yellow gold	46
2.13. Three types of superficial defects	47
2.14. Cross section of a steel/composite bonded interface	48
2.15. Chemical Interaction of Silane Adhesion Promoter with Steel Surface	49
2.16. Creation of $\pi$ -Ag, S-H and S-Ag bonds	50
2.17. Diffusion theory of adhesion	50
2.18. Electrical double layer formed at the interface between	
a polymer and a metal	51
2.19. Liquid drop on solid surface in equilibrium	52
2.20. Coalescence of molten powders	52
2.21. a) London forces, b) Keesom forces c) Debey forces	54
2.22. Theory of weak boundary layers	56
2.23. Cause of failure of coating/substrate system	56
2.24. Types of failure of coating/substrate system	57
2.25. Pull-o test	58
2.26. Cross-sectional view of (a) Mg0FHA and (b) Mg2FHA coatings on	
Ti6Al4V substrate	59
2.27. Cross-cut test	60
2.28. Scratch test	60
2.29. Three distinct scratch patterns were created through the application of	
constant load, progressive load, and incremental load	60
2.30. (a) acoustic emission and (b) penetration depth curves obtained by scratc	h
test on AlN coatings formed at different temperatures	62
2.31. Optical scratch images obtained on AlN coating at different loads	63
2.32. Indentation coating	64
2.33. Vickers interfacial fracture toughness on FeB/F e2B system: (a) 0.98 N,	
(b) 1.96 N, and (c) b2.94 N	66
2.34. Schematic representation of the thermographic	
detection of debonding area	66
2.35. Auger in-depth pro le chemical composition results of a W Ti coating	66
2.36. Auger in-depth pro le chemical composition results of a W Ti coating	67
2.37. HR-TEM micrographs of the interface substrate/interlayer zone	
of a W DLC:H coating	68
2.38. Representation of the device for laser treatment and thermal spray	69



#### AUTOMOTIVE ENGINEERING – A.Y. 2024/2025

2.39. SEM observations of Aluminum 2017(1) and Ti-6Al-4V (2) surfaces,	
(a) reference; (b) sand- blasted; (c) preheated by laser and (d)	
ablated by Laser	69
2.40. Cross section of Ni Al coatings on Aluminum 2107 surfaces sandblaste	
(a) and preheated (b)	
2.41. Schematic representation of laser textured surface	
2.42. Different interface characteristics before and after tensile test for	
grit-blasted surface, 100 µm distant holes and 200 -300 µm	
distant laser holes	72
2.43. Debonding strengths determined from LASAT of different surfaces	
2.44. FESEM cross-sectional micrographs of coated samples: (a) untreated	
surface, (b) treated surface at 300°C, (c) treated surface at 400°C, and (d)	
treated surface at 500°C	74
2.45. FESEM surface topography of Ti-6Al-4V: (a) untreated surface,	
(b) treated surface at 300°C, (c) treated surface at 400°C, and (d) treated	
surface at 500°C	75
2.46. Newly applied thick film at a corner	75
2.47. Typical Exhaust System model used in passenger cars and	
its components	77
2.48. Coating cost vs. maximum operating temperature of coating types	83
3.1. Preparation stage for Ti substrates prior to coating glass	89
3.2. Q11-1x1000 Cutting Machine with Foot Power	90
3.3. Grinding and Polishing Machine LS1 (Remet) in TTPU lab	90
3.4. Ultrasonic bath in TTPU lab.	91
3.5. Carbolite™ CWF Chamber Furnace in TTPU lab	92
3.6. Several cutting Ti substrates heated treated at 700 °C	92
3.7. Glass powder (G1-d) after grinding	
3.8. Dilatation curves of the glasses	96
3.9. Glass powder-glitserol slurry is deposited on surface of Ti substrate	97
3.10. Preparation of coating using glass powder-glycerol in proportion	
a) 70/30 b) 50/50 mass % ratio	
3.11. Drying was performed in a Memmert UN55plus drying cabinet	98
3.12. The graph showing the heating profile at 700 °C and 750 °C. Cooling p	rofile of
samples followed the cooling profile of furnace after switching off	100
3.13. Coated sample. The finished product from the furnace temperature	
at 700 °C (a) and 750 °C (b)	101
3.14. Individual images of coated samples heat treated at at 700 °C(a)	
and 750 °C(b).	101





#### AUTOMOTIVE ENGINEERING – A.Y. 2024/2025

3.1.5. Glass coating at round snape surfaces at heat treated at 750 °C	
concave(a) and convex(b).	101
3.16. Surface grinding and polishing, the type of carborundum	
surface (grit size)	102
3.17. Analytical SEM-EDS: JEOL JSM-IT200LA apparatus	103
3.18. Microstructure of polished cross section of glass coating – Ti substrate	
after heat treatment at 700 °C and 750°C	104
3.19. The microstructure of glass coating at 700C	104
3.20. The microstructure surface of Ti substrate	104
3.21. EDS of Ti substrate	105
3.22. EDS elemental mapping experiment of Ti substrate	106
3.23. EDS of the powders of the investigated coating glass	107
3.24. Spatial distribution of elements in glass coating	108
3.25. FTIR for coating at 700°C and 750°C	110
3.26. XRD pattern of Ti substrate after heating at 700 °C	111
3.27. XRD patterns of glass coatings heat treated at 700°C, 750 °C and 800 °C	111
3.28. Morphology of coating at 750 °C (magnification 12.5×)	112
3.29. Morphology of pure Ti substrate (magnification 12.5×)	112
3.30. Morphology of coating before the thermal shock test (sample 5)	114
3.31. Fracture occurs after 10th cycles (sample 5)	114
3.32. Fracture occurs after 7th cycles (sample 3 (a) and 4 (b)	114
3.33. Dual-exit performance exhaust system for Inline-4 engine	117
3.34. Thermal contour analysis (CFD by Ansys 2025 R1) of an exhaust	
system temperature value in Kelvin (K)	118
3.35. Thermal distribution in a coated exhaust system simulated under	
steady-state operating conditions	119
3.36. Temperature change along the Y-axis from the center	
of the pipe circumference radially outwards	119



# Appendix A

5.1. A Fourier Transform Infrared Spectroscopy coating at 700°C	120
5.2. A Fourier Transform Infrared Spectroscopy coating at 750°C	120
5.3. A Fourier Transform Infrared Spectroscopy coating at 800°C	121
5.4. A Fourier Transform Infrared Spectroscopy of Ti substrate	
tempered at 700°C	121
5.5. A Fourier Transform Infrared Spectroscopy of Ti substrate	
heated at 700°C	122
5.6. A X-ray of diffractograms of the Ti substrate after heating at 700 °C	122
5.7. A X-ray diffractograms of the glass-powder compacts heat	
treated at700°C	122
5.8. A X-ray diffractograms of the glass-powder compacts heat	
treated at800°C	123
5.9. A X-ray diffractograms of the glass-powder compacts heat	
treated at750 °C	123
5.10. A X-ray diffractograms of the glass-powder compacts heat	
treated at700°C	123
5.11. X-ray diffractograms of the Ti substrate sample 1 Grade 2	
5.12. (ASTM B348)	124
5.13. X-ray diffractograms of the Ti substrate	124
5.14. X-ray diffractograms of the Ti substrate sample 2 Grade 2	
5.15. (ASTM B348)	125
5.16 X-ray diffractograms of the Ti substrate	125



## **Acronyms**

#### **EBM**

Electron beam melting

#### $\mathbf{AM}$

Additive manufacturing

#### **SLM**

Selective laser melting

#### **HCP**

Hexagonal closed-packed

#### **BCC**

Body-centered cubic

#### **AWJM**

Abrasive water jet machining

#### LM

Laser machine

#### UM

Ultrasonic machining

#### **EDM**

**Electrical Discharge Machining** 

#### **EVOH**

Ethylene-vinyl alcohol copolymer

#### **PEFC**

Proton Exchange Membrane Fuel Cells

#### **MEA**

Membrane electrode assemblies

#### **FCV**

Fuel Cell Vehicle



#### FS

Fracture Splitting

#### **HSPT**

Hydrogen Sintering and Phase Transformation

#### **FFC**

Fray-Farthing-Chen

#### FIA

Formula One World Championship

#### **PVD**

Physical Vapor Deposition

#### CVD

Chemical vapor deposition

#### VAR

Vacuum arc remelting

#### **EBPVD**

Electron-beam physical vapor deposition

#### **PECVD**

Plasma-enhanced chemical vapor deposition

#### IAD

An ion-assisted deposition

#### **HVOF**

High Velocity Oxy-Fuel

#### **TEM**

Transmission Electron Microscopy

#### **TWEA**

Twin-wire electric arc

#### **LASAT**

Laser Shock Adhesion Test

#### **ROI**

Return on Investment

#### TTPU

Turin polytechnic university in Tashkent



## Chapter 1

## Introduction

The increasing interest in sports cars and racing in areas like Uzbekistan has led to a heightened demand for automotive technologies that can withstand extreme operating conditions. A significant challenge faced by high-performance vehicles is the overheating of exhaust systems, which can result in material deterioration, safety risks, and considerable drops in performance. This problem is especially pronounced in cars equipped with nitrous oxide (N<sub>2</sub>O or "nitro") systems, where combustion temperatures may surpass 1,600°C—significantly higher than the approximately 900°C observed in conventional engines. This extreme heat can cause exhaust components to visibly glow and accelerate oxidation processes. Traditional exhaust materials, such as stainless steel, start to lose their integrity at temperatures above 800°C, leading to issues like cracking or warping due to thermal cycling and oxidation rates that can be up to ten times greater in nitro-boosted combustion scenarios.

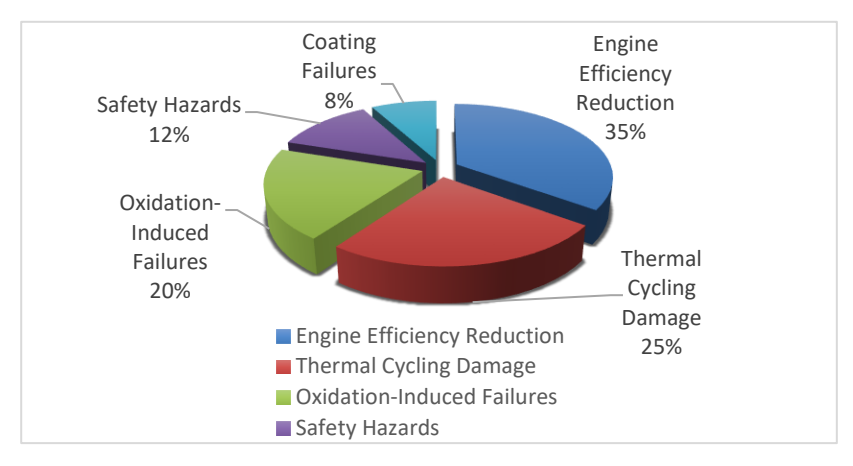


**Figure 1.1.** Breakdown of thermal challenges in nitro-fueled exhaust systems. Data compiled from sources: [F1–5].



The thermal stresses associated with these conditions account for around 12% of sports car fires result in measurable declines in performance, as each increase of 100°C in temperature can decrease engine efficiency by about 5% due to increased backpressure [1-6].

Existing thermal management strategies encompass coatings made from ceramics, such as zirconia, which have the capability to reduce surface temperatures by 200 to 300°C. However, these solutions frequently encounter challenges related to adhesion when subjected to thermal shock.

Titanium alloys, especially Grade 5 (Ti-6Al-4V), have become prominent alternatives due to their remarkable melting point of 1,668°C and a thermal expansion coefficient that is roughly 50% lower than that of stainless steel. Recent research has yielded significant advancements in this field, such as glass-ceramic coatings that can decrease oxidation by 75% at 1,200°C during lab tests, as well as hybrid coating systems that combine aluminum with silicon carbide nanoparticles, resulting in a 40% increase in adhesion strength [1-3].

Automotive companies like Porsche are investigating cutting-edge additive manufacturing techniques, creating 3D-printed titanium exhaust components with built-in cooling channels to improve thermal management (Figure 1.2.). The significance of these innovations is particularly pronounced in regions like Uzbekistan, where the importation of sports cars is rising at about 15% each year, leading to a pressing need for local thermal solutions. Concurrently, worldwide regulatory initiatives, such as the FIA's upcoming 2025 requirement for recyclable exhaust materials, are propelling research towards sustainable coating technologies. This study on titanium-based coatings tackles essential issues related to adhesion performance and thermal stability, providing viable solutions that improve the safety, longevity, and efficiency of high-performance exhaust systems. These advancements are in line with the specific requirements of Uzbekistan's developing motorsports sector and the overall global movement towards advanced automotive material science [6-8]





**Figure 1.2.** Titanium 3D printing automotive exhaust manifold adopts DMLS 3D printing [F6].

#### 1.1. Metallurgy of titanium

The metallurgy of titanium and its alloys has been the focus of extensive research over the past five decades. Titanium is distinguished by its exceptional properties, including a high strength-to-weight ratio and remarkable resistance to corrosive environments, making it suitable for a diverse array of applications. It is a robust metal characterized by limited ductility and a lustrous metallic white appearance. Its relatively high melting points also renders it valuable as a refractory material. Notably, titanium alloys possess several advantageous characteristics such as outstanding thermal resistance, significant load-bearing capacity, and resilience under various conditions, making them ideal for manufacturing cryogenic devices and components in aerospace engineering. Despite these benefits, titanium is less frequently utilized than aluminum or steel due to its elevated cost. The extraction process from its ores is complex and requires sophisticated processing techniques.

The strength of titanium surpasses that of aluminum alloys; thus, when substituted for aluminum, substantial weight savings can be realized despite its 60% higher density [9]. The metallurgy of titanium encompasses the stages of extraction, refining, alloying, and processing to attain specific mechanical and chemical properties suited for applications (Figure 1.3).

Titanium occurs in the earth's crust at an approximate concentration of 0.6%, positioning it as the fourth most abundant structural metal after aluminum, iron, and magnesium. The primary mineral sources include ilmenite (FeTiO<sub>3</sub>) and rutile (TiO<sub>2</sub>) [10]. However, due to its strong affinity for oxygen, titanium does not naturally exist in pure metallic form; therefore, complex extraction processes are necessary [11].



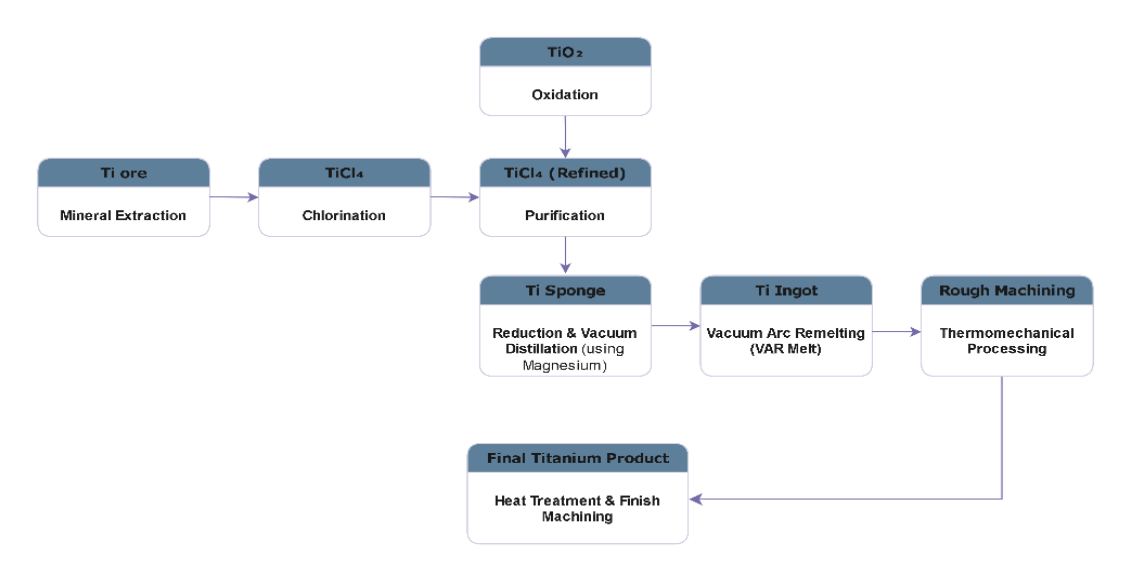


**Figure 1.3**: Schematic flowchart of titanium production [F7].

Titanium is primarily obtained from two ores. Chlorination at 900–1000 °C in the presence of carbon (as a reducing agent).

From rutile (TiO<sub>2</sub>) conversion:

From ilmenite (FeTiO<sub>3</sub>) chlorination:

Kroll process, reduction of Ti metal:

$$TiCl_4+2Mg \rightarrow Ti+2MgCl_2$$

The Kroll process remains the predominant method for extracting titanium. This involves converting titanium dioxide ore into titanium tetrachloride (TiCl<sub>4</sub>) via chlorination followed by reduction with magnesium in an inert atmosphere to yield sponge titanium. This sponge undergoes purification and processing into ingots through vacuum arc remelting (VAR) or electron beam melting (EBM) to eliminate impurities and enhance purity levels [12].

Titanium is frequently alloyed with elements like aluminum, vanadium, molybdenum, and iron to enhance mechanical properties. One notable alloy is Ti-6Al-4V which finds widespread application in aerospace and biomedical fields owing to its impressive strength-to-weight ratio along with excellent biocompatibility [13].

In the automotive sector, there is an increasing adoption of titanium because of its superior strength-to-weight ratio coupled with corrosion resistance and biocompatibility.



Various processing methods are employed for titanium and its alloys including casting, forging, powder metallurgy (PM), and additive manufacturing (AM), as detailed in Figure 1.4.

Due to titanium's heightened reactivity at elevated temperatures, specialized precautions are mandatory during processing to minimize contamination and oxidation which can adversely impact mechanical performance [14].

Casting represents one traditional approach utilized for forming titanium components but poses significant challenges attributed to the metal's high melting point combined with reactivity towards atmospheric gases like oxygen nitrogen or hydrogen. To mitigate these issues, vacuum or inert gas environments are typically utilized during casting operations preventing undesirable reactions that may compromise product integrity. Nevertheless, casting remains less prevalent for titanium compared to other metals owing to difficulties in achieving superior surface finishes alongside potential porosity within final structures [15].

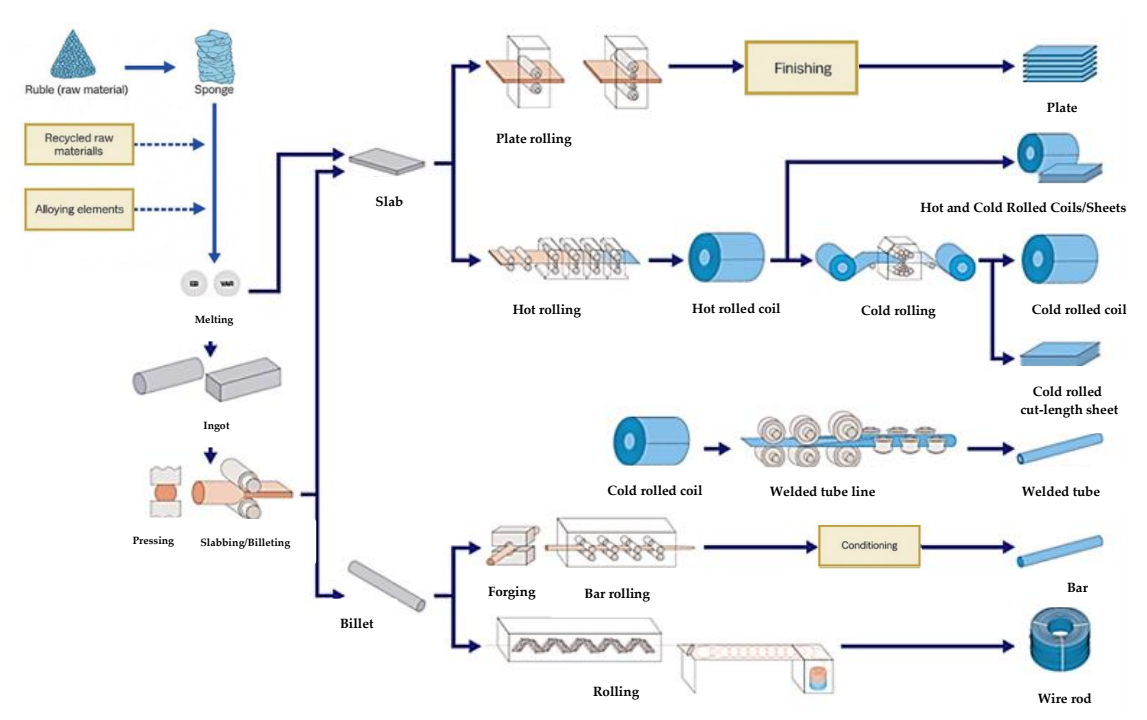


**Figure 1.4:** Titanium alloy processing and product flow diagram [F8]

Conversely forging has become a widely accepted method for producing robust titanium components where shaping occurs through compressive forces applied via hammering or pressing techniques enhancing mechanical attributes through microstructural refinement reduction of defects along with improved grain alignment.



However, the elevated temperatures required during forging increase oxidation risks necessitating protective coatings or controlled atmospheric conditions throughout this process [16].

Powder metallurgy presents another viable option facilitating fabrication while enabling production of intricate shapes featuring high material efficiency involving compaction followed by sintering processes at heightened temperatures . This method offers benefits including minimized material waste alongside tailoring capabilities regarding composition adjustment but shares challenges similar faced across other methodologies requiring stringent control measures against contaminants ensuring compliance with performance standards[15].

Additive manufacturing, commonly known as 3D printing, has seen notable advancements recently regarding utilizing titanium employing techniques such SLM/EBM allowing creation intricate geometries whilst minimizing material wastage. These approaches involve layer-by-layer deposition wherein powdered form gets melted fused utilizing laser/electron beams. Despite possessing numerous advantages AM faces hurdles concerning residual stresses microstructural inconsistencies necessitating post-processing treatments aimed at optimizing mechanical properties [17].

Beyond primary processing concerns machining inherently presents difficulties tied low thermal conductivity coupled high tensile strength resulting heat concentration cutting zones leading rapid tool wear potential damage workpieces .To address aforementioned issues specialized cutting tools composed carbide coated materials integrate effective cooling mechanisms notably involving high-pressure coolant systems cryogenic solutions aiding dissipating heat improving efficiency thereby guaranteeing precision component manufacturing meeting rigorous demands [18].

#### 1.1.1. Crystal structure and plastic deformation

Titanium undergoes polymorphic transformation, signifying its existence in various crystallographic structures that are temperature dependent. The element possesses two primary allotropes: the hexagonal close-packed (hcp)  $\alpha$ -phase, which is stable at room temperature, and the body-centered cubic (bcc)  $\beta$ -phase, which emerges at temperatures exceeding 882°C [19].

These phases have a profound impact on titanium's mechanical attributes and its capacity for plastic deformation (see Figure 1.5). The hcp  $\alpha$ -phase features a limited number of slip systems, resulting in restricted plasticity under ambient conditions [20].



Conversely, the bcc  $\beta$ -phase is characterized by an abundance of slip systems that facilitate greater ductility and ease of deformation. The incorporation of alloying elements such as molybdenum, vanadium, and niobium stabilizes this  $\beta$ -phase, thus enhancing the overall workability of titanium alloys. Plastic deformation in titanium primarily occurs through mechanisms of slip and twinning. Given the limited slip systems present in the hcp  $\alpha$ -phase, deformation in pure titanium frequently depends on twinning alongside slip.

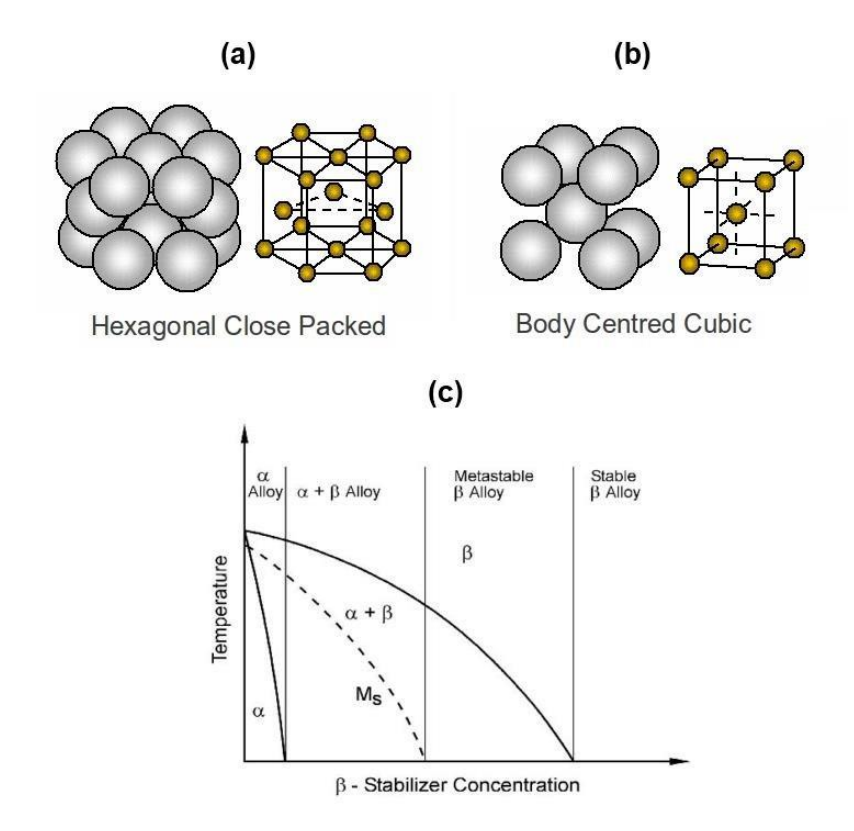


**Figure 1.5:** Pure titanium crystalline structure of (hcp)  $\alpha$ -phase and (bcc)  $\beta$ -phase [F9]

Twinning tends to be more prevalent at lower temperatures and higher strain rates since it enables materials to adapt to deformation when dislocation movement alone proves inadequate [21].



Temperature plays a critical role in influencing titanium's deformation characteristics. As temperatures rise, increased activity among additional slip systems enhance plasticity while diminishing the risk of brittle fractures. This factor is especially vital for titanium alloys where heat treatment and thermomechanical processing are implemented to refine mechanical properties tailored for specific uses [22].

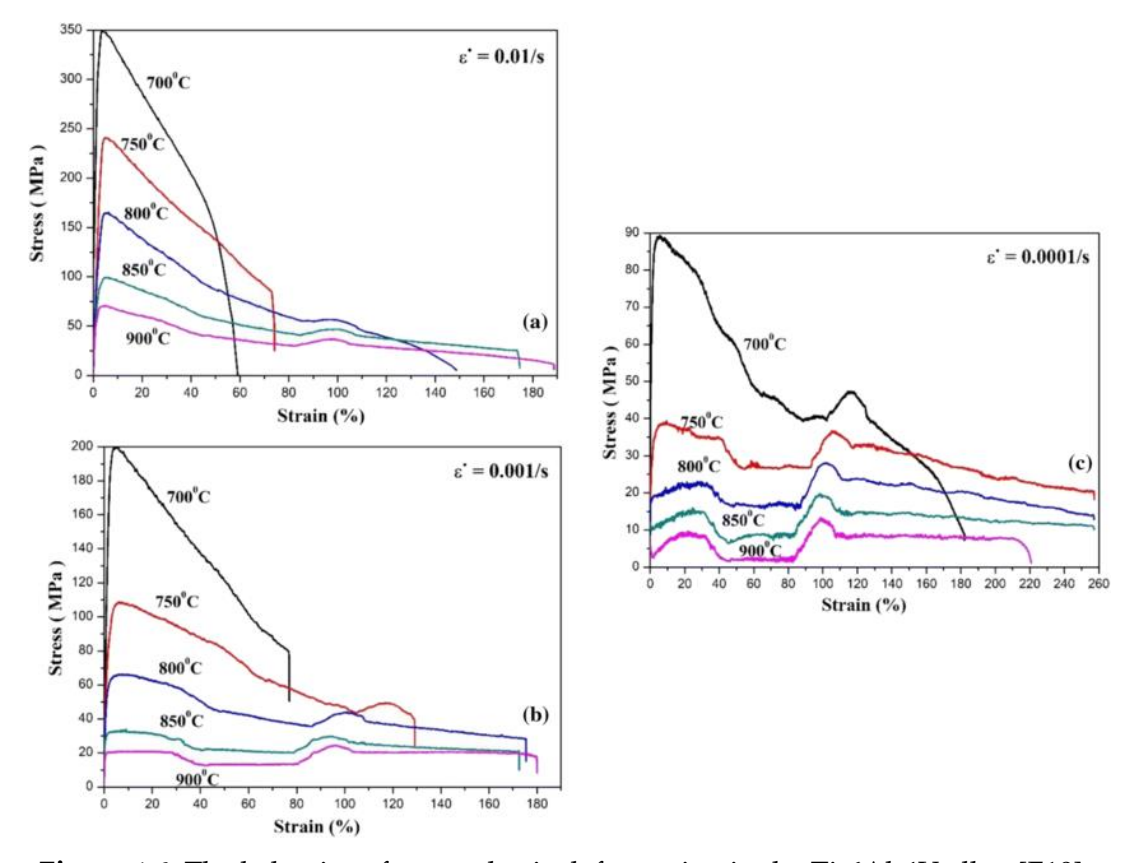


**Figure 1.6.** The behavior of superplastic deformation in the Ti-6Al-4V alloy [F10]

Work hardening also represents an essential aspect of plastic deformation in titanium. The interaction between dislocations and alloying constituents can result in strain hardening that bolsters the strength of titanium alloys while still preserving adequate ductility. However, excessive work hardening may impair machinability and formability; hence meticulous processing control is required [23].

Superplastic behavior significantly contributes to manufacturing lightweight components with complex geometries; notably, Ti-6Al-4V alloy exhibits superplastic properties applicable across various fields including hollow fan blades for gas



turbine engines and advanced heat exchangers. As shown in Figure 1.6, the research demonstrates that involving uniaxial tensile tests has been conducted within a temperature scope of 700 to 900 °C across different strain rates—0.01/s (High Strain Rate), 0.001/s (Medium Strain Rate), and 0.0001/s (Low Strain Rate). Results indicate an average elongation exceeding 50%, with elongations surpassing 200% observed from 750 to 900 °C at a strain rate of 0.0001/s—illustrating superplastic behavior in Ti-6Al-4V alloy (Table 1.1.) [24].

A comprehensive understanding of titanium's crystal structure and its plastic deformation behaviors is imperative for industrial applications. In aerospace engineering—where high strength-to-weight ratios are crucial—optimizing mechanisms related to slip and twinning ensure both durability and functionality for titanium components. Similarly, effective management of deformation behaviors in biomedical contexts are vital for ensuring implants' longevity and reliability [25].

In conclusion, titanium's polymorphic transformation between the hcp  $\alpha$ -phase and bcc  $\beta$ -phase significantly influences its mechanical properties and plastic deformation capabilities. The limited slip systems in the  $\alpha$ -phase restrict plasticity, while the  $\beta$ -phase enhances ductility through additional slip systems, particularly when alloyed with elements like molybdenum and vanadium. Understanding these characteristics is crucial for optimizing titanium's performance in industrial applications, especially in aerospace and biomedical fields. Work hardening and superplastic behavior further enhance titanium alloys' versatility, enabling the production of lightweight, complex components while ensuring durability and reliability. Effective management of these properties is essential for maximizing the benefits of titanium in various applications.

**Table 1.1.** Superplastic deformation of Ti-6Al-4V alloy in different strain rates [1]

Strain Rate (s-1)	Deformation Speed	Typical Behavior	Use Case
0.01	Fast	More brittle	Impact/dynamic tests
0.001	Moderate	Balanced	Standard tensile tests
0.0001	Slow	More ductile	Long-term or creep-like testing



#### 1.1.2. $\beta/\alpha$ -Transformation

Titanium experiences a phase transformation from a hexagonal close-packed (HCP) structure to a body-centered cubic (BCC) structure in response to temperature variations. At ambient conditions, commercially pure titanium predominantly exists in the  $\alpha$ -phase, characterized by its HCP configuration [26]. When temperatures exceed approximately 883 °C (1621 °F), it transitions into the  $\beta$ -phase, which is identified by the BCC arrangement [27]. This transformation notably influences the material's mechanical characteristics, including ductility and strength.

Titanium alloys primarily possess two principal crystalline structures: alpha ( $\alpha$ ) and beta ( $\beta$ ). The  $\alpha$ -phase features an HCP structure, while the  $\beta$ -phase is defined by a BCC arrangement. The delineation between these phases plays a crucial role in determining the mechanical properties of the material. Pure titanium has a specific transition temperature known as the beta transus temperature; above this threshold, it shifts from the  $\alpha$ -phase to the  $\beta$ -phase.

**Table 1.2.** Main titanium microstructural phases [2]

Phase	Symbol	Structure	Description
Alpha	α	НСР	Allotropic form of titanium at low temperature
Beta	β	ВСС	Allotropic form of titanium at high temperature
Alpha2	α2	НСР	A compound, Ti3Al, which appears in wide range of Al content
Gamma	γ		The intermetallic compound TiAl
Alpha prime	α'	НСР	Martensitic metastable structure
Alpha double prime	A''	OR	Orthorhombic metastable martensitic structure
Beta prime or omega	β' or w	ВСС	Metastable phase formed during quenching or aging

However, this transformation is reversible, meaning that commercial grades of pure titanium do not retain a stable residual  $\beta$ -phase when cooled from temperatures above this beta transus.



Prior to examining how alloying elements affect the stability of both phases, it's essential to recognize that titanium alloys—like many other metals—can form various stable and metastable phases. A detailed enumeration of these titanium alloy phases, along with their corresponding symbols and space groups can be found in Table 1.2.

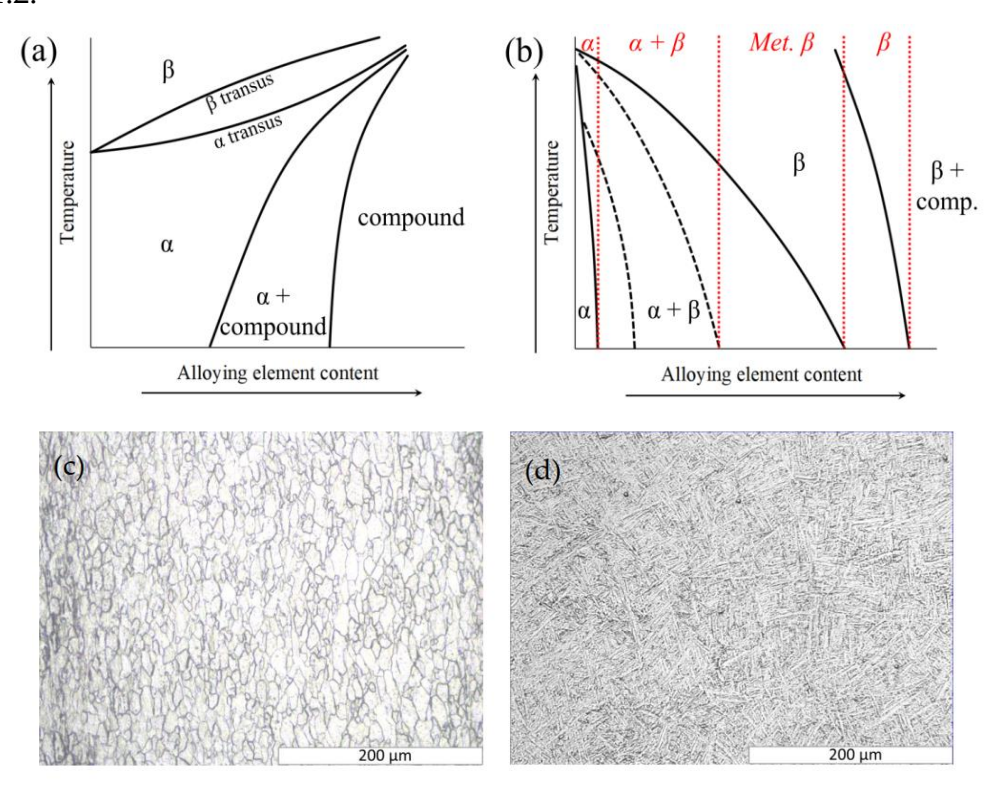


**Figure 1.7**. Impact of (a) alpha and (b) beta stabilizers on the microstructural characteristics of titanium alloys. The black dotted lines delineate the metastable region of  $\alpha$ - $\beta$  alloys, while the red dotted lines indicate the anticipated microstructure at ambient temperature. Additionally, (c) illustrates a standard commercially pure  $\alpha$ -titanium microstructure, and (d) depicts a typical annealed Ti-6Al-4V  $\alpha$ - $\beta$  alloy microstructure [F11].

These diagrams are rooted in thermodynamic principles, particularly Gibbs free energy minimization. The phase boundaries ( $\alpha$ ,  $\beta$ , and compound) are mathematically derived from equilibrium conditions and phase transformation.

$$G = H - TS$$

where: H: Enthalpy, T – temp. S – Entropy (Figure 1.7).

The addition of alloying elements is critical for modifying the properties of titanium



alloys. Traditionally, these elements are categorized into two groups based on their tendency to stabilize specific phases. Elements such as aluminum, tin, and zirconium promote stabilization of the  $\alpha$ -phase, thereby enhancing strength and hardness while raising the beta transition temperature [28].

Conversely, elements like molybdenum, Tungsten, chromium, iron, silicon, and copper favor stabilization of the  $\beta$ -phase; they enhance ductility and performance at elevated temperatures while lowering the beta transus temperature [29]. Vanadium and niobium can serve as either  $\alpha$ - or  $\beta$ -stabilizers contingent upon the alloy's composition [30].

Furthermore, lighter elements such as oxygen and nitrogen exert an  $\alpha$ -stabilizing influence with a neutral effect on beta transus temperature. The contribution of alpha and beta stabilizers in regulating microstructure within titanium alloys is succinctly illustrated in Figure 1.7.

In conclusion, titanium undergoes a phase transformation from a hexagonal close-packed (HCP)  $\alpha$ -phase to a body-centered cubic (BCC)  $\beta$ -phase at temperatures above approximately 883°C. This transformation significantly affects the mechanical properties of titanium, including ductility and strength. The addition of alloying elements is crucial for modifying these properties;  $\alpha$ -stabilizers like aluminum and zirconium enhance strength and raise the beta transition temperature, while  $\beta$ -stabilizers such as molybdenum and chromium improve ductility and performance at elevated temperatures. Elements like vanadium and niobium can act as either  $\alpha$ - or  $\beta$ -stabilizers depending on the alloy composition. Understanding these phase behaviors and the role of alloying elements is essential for optimizing the performance of titanium alloys in various applications.

#### 1.1.3. The classification of titanium alloys

The integration of these alloying elements facilitates the production of alloys exhibiting a diverse array of mechanical characteristics, biocompatibility, and resistance to corrosion. Traditionally, titanium alloys are categorized into five groups based on their chemical composition and the anticipated microstructure during service.



These categories include:

**Alpha Alloys** [31]: Mainly composed of  $\alpha$ -phase structures, this group includes both pure titanium and alloys enriched with  $\alpha$ -stabilizers, such as aluminum and tin, which are predominantly utilized in aerospace applications.

**Near Alpha Alloys** [32]: Characterized by a dominance of  $\alpha$ -phase with a minimal presence of  $\beta$ -stabilizers, these alloys strike a balance between strength and formability.

**Alpha-Beta Alloys** [33]: Featuring an equilibrium of  $\alpha$ - and  $\beta$ -phases, these alloys provide a blend of strength, ductility, and heat resistance, making them suitable for various applications.

Near Beta Alloys (or Beta Metastable) [34]: Largely consisting of β-phases with restricted amounts of  $\alpha$ -stabilizers; they trade off some mechanical strength to enhance ductility compared to  $\alpha$ - $\beta$  alloys.

**Beta Alloys** [35]: Composed primarily of  $\beta$ -phase matrices along with elements like vanadium and molybdenum.

Additionally, there exists another titanium-based structure that is classified as a nickel-titanium intermetallic compound. For the purpose of this review, Nitinol will be regarded as a titanium alloy despite its composition being approximately 55% nickel [36].

#### 1.2. Properties of titanium

Titanium is characterized by a distinctive set of physical, mechanical, and chemical attributes, making it exceptionally valuable across various sectors. It displays remarkable resistance to corrosion, an impressive strength-to-weight ratio, and superior biocompatibility.

Titanium dioxide (TiO<sub>2</sub>), a naturally occurring oxide of titanium, manifests in three crystallographic forms—rutile, anatase, and brookite—and is extensively utilized in multiple industries owing to its exceptional properties [37].

In the automotive sector, the unique characteristics of titanium provide substantial benefits, especially for high-performance and luxury vehicles. Its advantageous strength-to-weight ratio facilitates a reduction in vehicle weight without sacrificing structural integrity, resulting in enhanced fuel efficiency and overall performance.



Moreover, its outstanding resistance to corrosion contributes to the longevity and durability of essential automotive components such as engine parts and exhaust systems, suspension springs, and fasteners [38].

#### 1.2.1. Physical and mechanical properties

Titanium is a lightweight metal characterized by a density of 4.51 g/cm³, which is roughly 60% that of steel. This notable reduction in weight renders titanium particularly advantageous in sectors where minimizing mass is essential, such as aerospace and automotive engineering. The incorporation of titanium allows manufacturers to enhance fuel efficiency, boost performance, and decrease overall structural weight without sacrificing strength. Moreover, titanium possesses a high melting point of 1668°C, enabling it to retain its mechanical integrity even under extreme thermal conditions. Consequently, it serves as an optimal material for applications subjected to high heat, including jet engines, exhaust systems, and components used in space exploration [39].

From a mechanical perspective, titanium is distinguished by an exceptionally high strength-to-weight ratio that exceeds that of many traditional metals like aluminum and steel. This distinctive attribute empowers engineers to devise lightweight yet robust structures that improve efficiency in scenarios where both strength and weight reduction are paramount. Additionally, titanium exhibits remarkable fatigue resistance and superior toughness, allowing it to endure repeated stress cycles without significant deterioration. These qualities make it especially valuable in industries that demand long-term durability, such as aircraft manufacturing and structural engineering. Through appropriate heat treatment and alloying processes, titanium alloys can achieve impressive tensile strengths surpassing 1000 MPa, thereby further enhancing their mechanical capabilities [40].

Figure 1.8 illustrates a comparison of the mechanical properties among titanium, steel, and aluminum—emphasizing variations in tensile strength, modulus of elasticity, fatigue resistance, and melting point.

Another important mechanical attribute of titanium is its comparatively low modulus of elasticity, around 110 GPa, which is notably less than that of steel.



This characteristic enhances titanium's flexibility and impact resistance, rendering it particularly advantageous in scenarios requiring precise deformation control and effective stress distribution. Furthermore, its resistance to corrosion, compatibility with biological systems, and capacity to withstand extreme environmental conditions significantly broaden its utility across diverse industries [41].

#### 1.2.2. Chemical properties

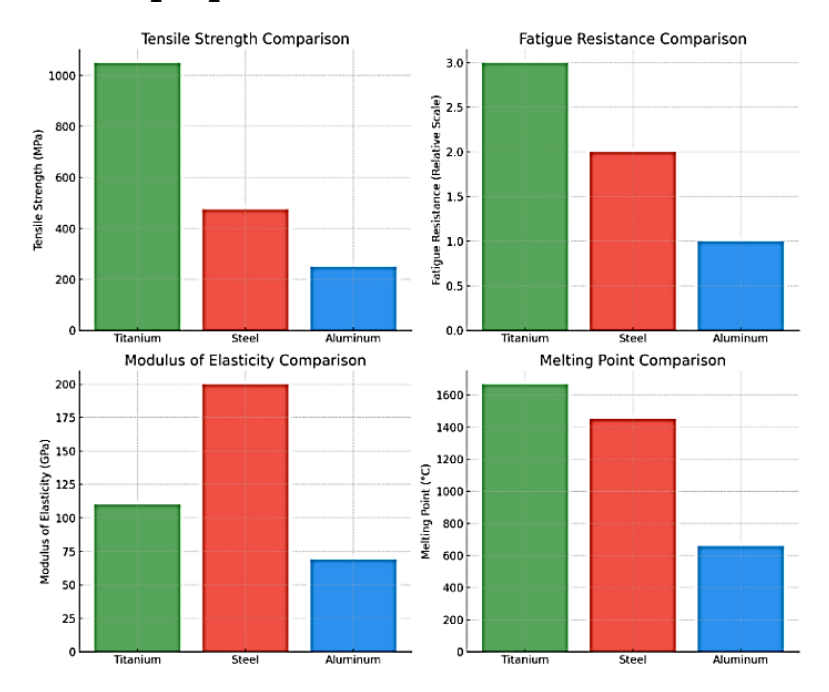


Figure 1.8. Comparative mechanical properties of Titanium, Steel, and Aluminum [F12].

One of Titanium's most notable characteristics is its outstanding resistance to corrosion. This property arises from the development of a stable and protective layer of titanium dioxide (TiO<sub>2</sub>) on its surface upon exposure to oxygen. This oxide coating serves as a shield, inhibiting further oxidation and degradation, which renders titanium remarkably resilient against corrosion in challenging environments, including seawater and acidic solutions [42].

In addition, titanium demonstrates strong chemical resistance against a variety of harsh substances, such as chlorides, sulfides, and potent acids, making it an ideal material for the chemical processing sector.



Unlike numerous other metals, titanium is immune to stress corrosion cracking, which significantly prolongs its durability in rigorous applications [43]. The combined physical, mechanical, and chemical attributes of titanium facilitate its extensive utilization across various industries [44].

Mechanically, titanium outperforms traditional metals like aluminum and steel in strength-to-weight ratio, fatigue resistance, and toughness, allowing for durable structures. Its low modulus of elasticity enhances flexibility and impact resistance, while a protective titanium dioxide layer ensures resilience in harsh environments. Additionally, titanium's strong chemical resistance and immunity to stress corrosion cracking further extend its lifespan in demanding applications. These combined attributes highlight titanium's significance in industries such as aerospace, automotive, and chemical processing.

#### 1.3. Fabrication techniques

Titanium and its alloys necessitate distinct fabrication methods owing to their exceptional characteristics, including significant reactivity at high temperatures and challenging machinability. The manufacturing techniques are tailored to optimize the material's performance while maintaining both cost efficiency and operational effectiveness.

#### 1.3.1. Production of Pure Titanium

The production of titanium is conducted through methods tailored to its distinct properties. The two historically significant techniques for yielding commercially pure titanium are the Kroll process and the Hunter process:

**Kroll Process** [45]: This method serves as the primary approach for extracting titanium metal from its ores. Initially, titanium tetrachloride (TiCl4) is produced by reacting titanium ores, predominantly ilmenite, with chlorine gas. Subsequently, TiCl4 is reduced to metallic titanium using magnesium in a high-temperature reactor, resulting in magnesium chloride as a byproduct. The process encompasses several stages: chlorination of the ore, condensation of TiCl4, reduction of TiCl4 via magnesium, and the separation of titanium sponge from magnesium chloride.



The titanium sponge generated contains impurities and necessitates additional processing steps for purification and refinement. Despite its intricate nature, the Kroll process remains essential for industrial titanium manufacturing, particularly within aerospace, medical, and various industrial sectors.

Hunter Process [46]: This alternative technique also produces titanium metal from ores through a similar initial step where titanium tetrachloride (TiCl4) is acquired via chlorination of ores such as ilmenite. However, instead of utilizing magnesium as a reducing agent like in the Kroll process, sodium or a sodium-potassium alloy is employed. The reduction occurs at lower temperatures than those required by the Kroll method. In this case, sodium or sodium-potassium alloy reduces TiCl4 to yield metallic titanium along with sodium or potassium chloride as byproducts. Although this method results in less energy consumption and operates at reduced temperatures compared to the Kroll process, it is not as widely adopted in industrial applications for titanium production.

#### 1.3.2. Production of Titanium Alloys

To manufacture titanium alloys from commercially pure titanium, it is essential to prioritize the prevention of oxidation. Consequently, only a limited number of technologies are widely adopted:

**Vacuum Arc Remelting** (VAR): This technique is frequently employed for melting and refining titanium alloys. It entails melting a consumable electrode under vacuum conditions using an electric arc, which aids in minimizing impurities and regulating the alloy's composition [47].

**Plasma Arc Melting** (PAM): Another vacuum-based method, PAM utilizes a high-energy plasma arc to melt the material. This technique provides enhanced control over composition and is particularly effective for producing specialty alloys [48].

**Induction Melting** (IM): Primarily used for small-scale production of titanium alloys, induction melting leverages electromagnetic induction to melt materials within a crucible under controlled atmospheric conditions [49].

**Powder Metallurgy**: While predominantly utilized as a near-net-shape manufacturing process for titanium components, powder metallurgy can also serve as an alloying method by mixing powders with diverse chemical compositions [50].



It is crucial to recognize that these production methods are highly specialized and necessitate rigorous process control due to the reactivity of titanium and its susceptibility to impurities. The selection of an appropriate production technique is influenced by various factors, including the desired alloy composition, required material quantity, and specific properties needed for the intended application.

#### 1.3.3. Conventional and Advanced Machining

Titanium's challenging machinability is primarily attributed to its low thermal conductivity and high chemical reactivity. Conventional machining methods entail:

- Turning, milling, and drilling: These processes necessitate specialized cutting tools and lubricants.
- Grinding and polishing: Employed to achieve precise surface finishes.

To enhance efficiency, advanced techniques have emerged, such as:

Electrical Discharge Machining (EDM) is an advanced metal removal method used for creating intricate geometries in titanium alloys and other conductive materials. It is particularly effective for titanium due to its hardness and difficult machinability. The process generates a controlled electrical discharge, or spark, between a tool electrode and the workpiece submerged in dielectric fluid, allowing for material removal without direct contact. The dielectric fluid acts as both a coolant and an insulator, flushing away eroded particles. Given the high melting points and poor thermal conductivity of titanium alloys, EDM enables precision cuts while minimizing thermal damage, a common issue with traditional machining. This technique is ideal for producing complex shapes and hardened surfaces typical in aerospace and medical applications. However, EDM has limitations, including slower material removal rates and surface finish quality, often requiring additional finishing steps. Despite these drawbacks, EDM is essential for machining hard materials like titanium alloys where conventional methods are inadequate.

In the automotive sector, titanium faces scalability challenges primarily due to machining difficulties. High costs limit broader adoption, and rapid tool wear increases maintenance needs and production downtime. Additionally, slow machining processes hinder efficiency, complicating mass production. Heat management is also a concern due to titanium's poor thermal conductivity, which can affect precision and machining quality.



Addressing these challenges requires advancements in cutting tool materials, optimized machining strategies, and hybrid manufacturing techniques to enhance efficiency and cost-effectiveness.

Abrasive Water Jet Machining (AWJM) is an effective material removal process for shaping titanium alloys and other hard-to-machine materials. Titanium alloys, known for their high strength and heat resistance, significantly benefit from AWJM. This method utilizes a high-velocity stream of water mixed with abrasive particles, such as garnet or aluminum oxide, to erode the material through kinetic energy. The controlled mixture allows for precise material removal, accommodating various thicknesses and complexities of the workpiece.

AWJM offers advantages for titanium alloys, particularly its non-thermal nature, which reduces the risk of heat-induced distortion or damage often encountered with traditional methods. Additionally, the lower mechanical stresses associated with AWJM minimize work hardening risks in titanium components. This technique is well-suited for intricate designs and composite structures found in aerospace, automotive, and medical applications involving titanium parts. However, secondary finishing processes may be necessary, as AWJM can leave surfaces slightly rough due to its abrasive action [53, 54].

**Laser Machining (LM)** is a promising method for shaping challenging materials like titanium alloys, known for their high strength and heat resistance. In LM processes, a focused high-energy laser beam melts or vaporizes material from the workpiece, allowing for intricate cuts and complex shapes required in various applications.

LM offers several advantages, including a non-contact approach that eliminates tool wear, reduces mechanical strain, and minimizes contamination risks from impurities. The localized heat input also reduces the affected zone, thereby lowering distortion and residual stress levels.

This technique is particularly suitable for sectors requiring precision, such as aerospace, military, and healthcare, where minimizing raw material loss is crucial. However, achieving optimal results may require adjustments based on alloy composition and thickness.

Additionally, post-processing measures may be necessary to address undesirable surface roughness generated during laser interactions.

**Ultrasonic Machining (UM)** offers unique advantages for working with hard substrates, such as titanium alloys. This method utilizes ultrasonic vibrations typically ranging from 20 to 40 kHz to facilitate efficient material removal without excessive temperature increases caused by friction.



The process involves pressing tools made from softer materials into contact with an abrasive slurry composed of particulate matter suspended in a liquid medium. This non-thermal characteristic prevents heat-related alterations, maintaining dimensional integrity throughout the machining process. As a result, UM is particularly beneficial in industries focused on aerospace components and medical implant fabrication. However, longer cycle times compared to standard methods may necessitate additional processing steps to achieve the desired finish.

Machining titanium alloys requires careful consideration of factors influencing optimal cutting conditions, including tooling choices, geometric configurations, and cooling/lubrication methods to mitigate temperature-related issues during machining. Additionally, the interactions between titanium and the tooling materials must be considered, leading to the development of alternative coatings that minimize degradation over time, ensuring consistent accuracy and adherence to quality standards. [58-59].

# 1.4. Titanium in the Automotive Industry: Existing Challenges.

Titanium is recognized for its lightweight nature, exceptional strength, and remarkable resistance to corrosion, making it a valuable material in various applications including aviation, heat exchangers that utilize seawater as a refrigerant, and desalination facilities. Its versatility has further extended into consumer goods, sporting equipment, and construction materials due to its thermal resilience, biocompatibility, aesthetic appeal, and overall functionality.

Moreover, the utilization of titanium in automotive components is on the rise owing to these advantageous properties. Specifically, vehicles that demand superior dynamic performance—such as racing motorcycles and cars—require enhancements in circuit timing and responsiveness. Consequently, titanium is frequently employed to significantly reduce weight while boosting power output. This paper presents examples of existing applications of titanium within automotive parts and discusses potential future uses for this material in additional components (Figure 1.9.) [60].



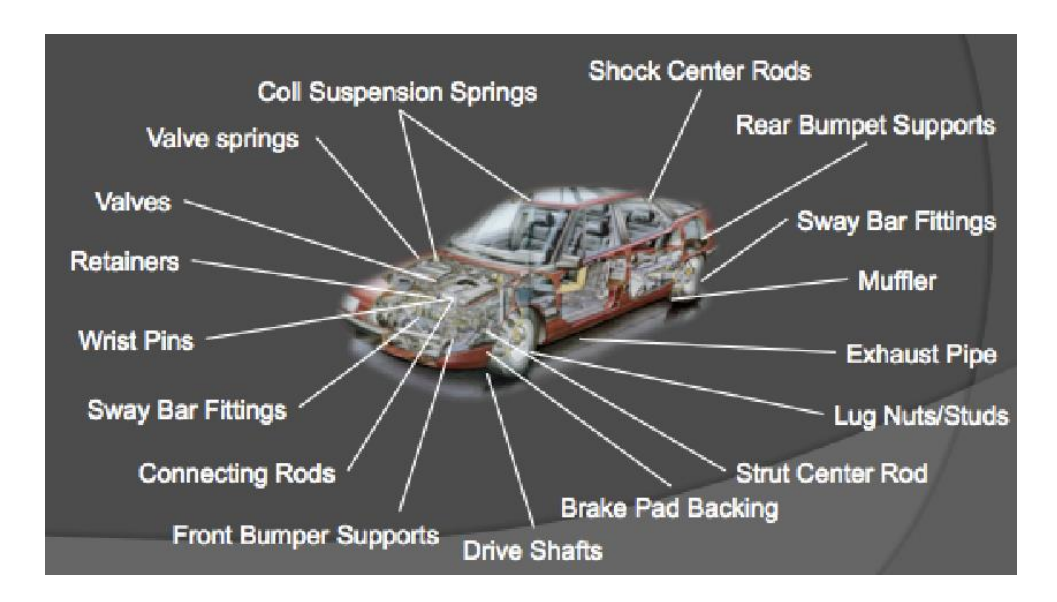


**Figure 1.9.** Key Applications of Titanium in Automobiles [F13]

**Fuel Tanks:** The reduction in weight of fuel tanks is a critical factor as it enhances fuel efficiency and dynamic performance by lowering the center of gravity, particularly for motorcycles.

In recent years, high-density polyethylene has emerged as a preferred lightweight material, however, to comply with stringent fuel gas permeation regulations set by EURO 5—implemented for motorcycles, since 2020—it must be combined in layers with ethylene-vinyl alcohol copolymer (EVOH) resin as a barrier layer. This necessity leads to an unavoidable increase in mass due to the added thickness (approximately 4–7 mm). Conversely, metallic materials exhibit lower fuel gas permeability, prompting consideration of lightweight metals such as aluminum and titanium. While aluminum alloys, particularly from the 5000 series, are potential candidates, they present challenges regarding weldability and press formability. Aluminum's low melting point and high thermal conductivity complicate the control of heat input during arc welding, increasing the risk of burn-through.

Additionally, spot welding aluminum requires elevated pressure, high current levels, and brief energizing durations, all of which elevate the initial costs associated with specialized equipment installation. Furthermore, aluminum's limited ductility and low Lankford value (r value) hinder its press formability for deep-drawn shapes like fuel tanks. These factors suggest that manufacturing thin-walled fuel tanks using standard equipment designed primarily for steel may pose significant challenges.





**Figure 1.10.** Titanium fuel tank [F14]

In contrast, titanium possesses a melting point comparable to that of iron and thermal conductivity akin to stainless steel, reducing the likelihood of burn-through during welding. Spot welding can be conducted simply by fine-tuning operational parameters without necessitating specialized machinery. Moreover, Titanium demonstrates outstanding deep draw formability due to its higher value. Commercially pure (CP) titanium classified under JIS Class 1 and ASTM Grade 1—with low oxygen content—exhibits overhang formability on par with that of low carbon steel for press forming applications, making it well-suited for fuel tank production.

However, unlike steel, titanium is susceptible to galling during processing; thus, adequate lubrication during press forming is essential. Ultimately, titanium presents fewer barriers to application in fuel tank manufacture compared to aluminum alloys. Indeed, following advancements in mass production techniques, including condition optimization, the world's first mass-produced motorcycle equipped with a titanium fuel tank was realized (Figure 1.10. Honda Motor Co., Ltd., 2017 model CRF450R). The incorporation of titanium has significantly reduced weight while markedly enhancing performance characteristics. Additionally, owing to its superior corrosion resistance properties, titanium does not require painting for corrosion protection and holds promise for use in automobile fuel tanks situated closer to ground level where higher corrosion resistance is paramount.



**Exhaust pipes:** The exhaust system components are constructed from a diverse range of materials, leading to significant weight reductions when titanium is utilized. This is particularly evident in motorcycles, where the aesthetic appeal of titanium has made it a popular choice for many years, especially for components like mufflers that are visibly exposed.

Initially, JIS Class 2 and ASTM Grade 2 CP titanium were predominantly employed; however, the implementation of stricter emission regulations necessitated the inclusion of catalytic converters, resulting in elevated exhaust gas temperatures. This shift required enhanced heat resistance—specifically high-temperature strength and oxidation resistance.

Additionally, there is a growing demand for high formability to achieve intricate shapes within these systems. To bolster strength at elevated temperatures, solid solution strengthening proves effective, often incorporating aluminum due to its superior performance in this regard. Furthermore, a minor addition of silicon is frequently implemented to enhance oxidation resistance at high temperatures.



Figure 1.11. Ti-1Cu muffler [F14]

Consequently, when designing titanium alloys for exhaust systems, aluminum and silicon are typically included. However, the incorporation of these elements can also lead to increased room temperature strength while reducing ductility. Notably, aluminum inhibits twinning deformation at room temperature, a factor that can impair formability.



Conversely, copper offers a strong solution strengthening effect at elevated temperatures without adversely impacting twinning deformation or formability at room temperature. This makes copper a valuable addition for achieving both high-temperature strength and desirable formability, two properties that often stand in contrast.

In light of this information, Super-TIX<sup>TM</sup> 10CU (Ti-1Cu) was developed with an approximate 1% copper content. Additionally, Super-TIX<sup>TM</sup> 10CUNB (Ti-1Cu-0.5Nb) was created with niobium added to further enhance oxidation resistance under high-temperature conditions. Niobium aids oxidation resistance by inhibiting oxygen diffusion across the titanium oxide layer while maintaining the solubility of copper; thus, it does not compromise high-temperature strength or room temperature formability.

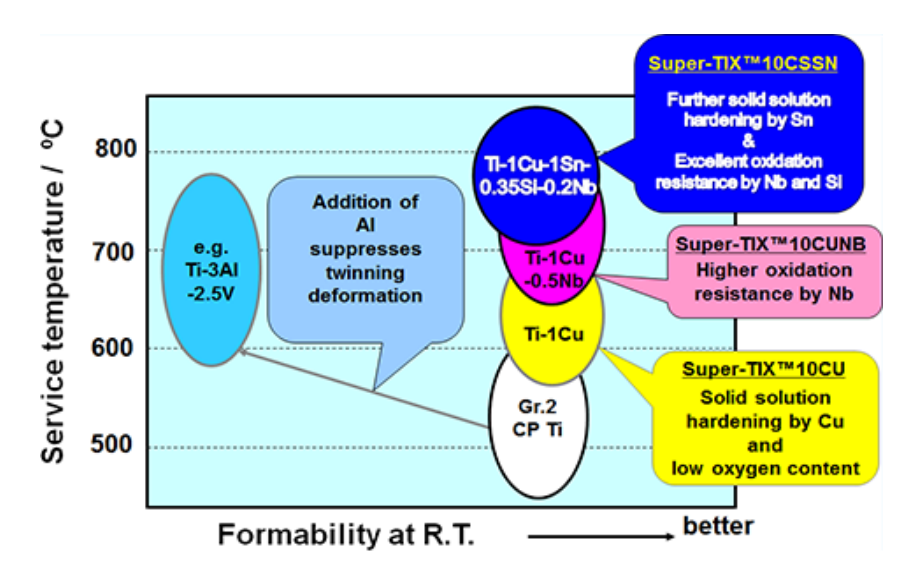


**Figure 1.12.** Concept of Ti-1Cu alloys [F14]

Moreover, Super-TIX<sup>TM</sup> 10CSSN (Ti-1Cu-1Sn-0.35Si-0.2Nb) has been formulated to improve high-temperature strength significantly (see Fig. 1.11). These advanced alloys have found applications in motorcycles and automobiles (refer to Figure 1.12. featuring Nissan Motor Co., Ltd.'s GT-R), operating effectively at temperatures reaching up to 700–800°C.

**Engine Components:** Engine components tend to be compact in size, and the impact of weight reduction is not dramatically pronounced.



Nevertheless, minimizing weight can diminish the inertia forces associated with rotational or reciprocating movements, thereby enhancing overall responsiveness. Furthermore, titanium outperforms other metals regarding specific strength within the operational conditions of engine components. It is particularly utilized in connecting rods and engine valves due to its favorable cost-performance ratio when employed in these applications.

Connecting Rods: The connecting rod serves as a crucial component within an engine, responsible for transforming the linear motion of the piston into rotational movement. Optimizing the weight of the connecting rod significantly enhances engine responsiveness, boosts power output by minimizing friction losses, and enables further weight reduction by allowing for smaller and simpler peripheral components. Thus far, Ti-6Al-4V has been utilized for connecting rods in motorcycles, while Ti-3Al-2.5V-REM has found application in automobiles. Given that vanadium (V) in these alloys is costly, Super-TIX<sup>TM</sup> 51AF (Ti-5Al-1Fe) was engineered to incorporate iron (Fe), a more economical alternative to vanadium.

This alloy exhibits nearly equivalent fatigue strength to the traditionally employed Ti-6Al-4V and demonstrates favorable hot workability. Additionally, it is particularly compatible with the Fracture Splitting (FS) method commonly used for steel connecting rods. With these advantages, Ti-5Al-1Fe facilitated the introduction of the world's first mass-produced titanium connecting rods via the FS method, featuring in Yamaha Motor Co., Ltd.'s 2015 model of the YZF-R1 and other models (see Fig. 1.13.). Moreover, this alloy is distinguished by its excellent machinability, contributing to reduced production costs for connecting rods.



**Figure 1.13.** Ti-5Al-1Fe connecting rod [F14]



Engine valves: Engine valves are components that operate with reciprocating motion, similar to connecting rods. Reducing their weight significantly enhances responsiveness at high RPMs. Additionally, it is feasible to minimize the size of associated peripheral components. When utilizing titanium for engine valves, it is imperative that the material possesses adequate fatigue strength to endure the stresses imposed by the camshaft and valve seat during each opening and closing cycle. Moreover, since exhaust valves are directly subjected to exhaust gases, they must exhibit both high-temperature fatigue strength and creep resistance.

Titanium alloys meeting these requirements are employed for both intake and exhaust engine valves (see Figure 1.14.). For intake engine valves, Ti-6Al-4V and Super-TIX<sup>TM</sup> 523AFM (Ti-5Al-2Fe-3Mo), which undergo various anti-wear treatments, are commonly used. The latter alloy is specifically engineered for enhanced beta-stabilizing capability and superior strength compared to Ti-6Al-4V, leading to its increasing adoption intake applications due to its exceptional strength and fatigue resistance. In contrast, near  $\alpha$ -type alloys developed for aircraft engines—such as Ti-6Al-2.7Sn-4Zr-0.4Mo-0.45Si and Ti-6242S (Ti-6Al-2Sn-4Zr-2Mo-0.1Si)—are predominantly utilized for exhaust engine valves.



**Figure 1.14.** Titanium engine valve [F14]



This preference arises from two key factors: (i) these alloys maintain a high proportion of the  $\alpha$ -phase, which is beneficial for high-temperature strength up to elevated thermal ranges, resulting in greater strength compared to Ti-6Al-4V and Ti-5Al-2Fe-3Mo in environments exceeding 500°C; (ii) at 800°C, their fatigue strength rivals that of heat-resistant steel SUH35 (Fe-0.55C-9Mn-21Cr-4Ni-0.45N), coupled with a notably high specific strength ratio (fatigue strength/density). For an in-depth exploration of the fatigue properties of engine valves, including the impact of microstructure and surface treatment, readers are encouraged to consult another article dedicated to this topic.

Reinforcement and stiffening components are occasionally employed to enhance the rigidity of a vehicle's structure, particularly when optimal responsiveness is required. Typical instances include strut bars that link the strut towers supporting the left and right suspension systems, as well as under braces that connect various elements beneath the vehicle chassis; these components are primarily fabricated from steel. Conversely, to mitigate the weight increase associated with adding new parts, weight reduction strategies are essential. Given that these components must fit within confined spaces, materials exhibiting high Young's modules and excellent formability are essential. In this context, titanium emerges as an ideal choice due to its relatively high Young's modulus combined with favorable formability characteristics among lightweight materials. Recently, there has been an uptick in the use of titanium for strut bars (refer to Figure 1.15. by Okuyama Co., Ltd.).

Additionally, as the urgency for reducing environmental impact grows, titanium offers benefits such as diminished painting requirements due to its superior corrosion resistance. Consequently, we anticipate a broader adoption of titanium in lower body components like subframes and braces.

**Body Panels:** As the automotive industry increasingly prioritizes weight reduction, optimizing the weight of body panels—such as roofs, hoods, and doors—emerges as a critical strategy due to their substantial mass. Notably, reducing the weight of the roof, positioned at the top of the vehicle's structure, can enhance dynamic performance by lowering the vehicle's center of gravity.

During vehicle assembly, the roof is attached to a frame primarily constructed from steel and subsequently undergoes a painting process. This process involves baking paint at approximately  $170^{\circ}$ C; however, if materials have a high coefficient of linear expansion, distortion may occur. Titanium possesses a coefficient of linear expansion of  $8.4 \times 10$ –6, which is relatively close to that of steel ( $12 \times 10$ –6).



Thus, incorporating titanium into roof designs could facilitate weight reduction while minimizing distortion risks. Looking ahead, advancements in technology are needed to address challenges associated with bonding dissimilar metals and achieving mass production; therefore, integrating titanium into body panels is highly desirable.

Fuel Cell and Electrification Components: Proton Exchange Membrane Fuel Cells (PEFC) are utilized not only in vehicles but also as distributed energy sources for residential applications due to their high-power density, lightweight nature, and compact design. As illustrated in Fig. 1.15, a PEFC consists of multiple layers within membrane electrode assemblies (MEA), which include a solid polymer membrane, electrodes, and gas diffusion layers, all encased in a structure featuring separators that secure both sides of the MEA. These separators are engineered with gas flow pathways that facilitate the supply of hydrogen and oxygen while effectively conducting current externally without permitting gas leakage.

The polymer membrane incorporates numerous sulfate groups to enhance conductivity; however, as degradation occurs over time, sulfate ions may leach into the generated water. Consequently, when selecting metal materials for separators, it is essential to ensure formability for the gas flow path, minimal contact resistance with electrodes, and resistance to corrosion in an acidic sulfuric acid environment.

Titanium emerges as a suitable candidate due to its excellent formability and inherent corrosion resistance along with electrical conductivity.

Nonetheless, the passivation layer on titanium surfaces exhibits high electrical resistance, necessitating improvements in contact resistance between the separator and electrodes. To address these challenges, research has focused on technologies that balance corrosion resistance with low contact resistance through methods such as precious metal plating (including Au and Pt) and carbon layer deposition. Notably, advancements in these areas have led to the incorporation of titanium separators in Toyota Motor Corporation's MIRAI Fuel Cell Vehicle (FCV).

Furthermore, there is growing interest in applying titanium to electric motors due to rising electrification demands. Similar to engines, motors feature rotating components where titanium alloys excel because of their lightweight yet robust characteristics.

Building on titanium's exceptional material properties, its use in automotive parts has progressively broadened from racing cars to mass-produced vehicles. Applications now encompass engine components such as connecting rods and valves as well as exhaust systems, fuel tanks, and even fuel cell elements.



As mobility evolves towards greater diversification in the future, we aim to further advocate for expanded utilization of titanium among automotive manufacturers as well as parts producers and material suppliers—all aimed at enhancing the benefits associated with automotive components. Despite these significant advantages offered by titanium, various challenges impede its widespread adoption for mass production purposes. The main hurdles include elevated costs associated with manufacturing complexities and limited availability of raw materials [60].

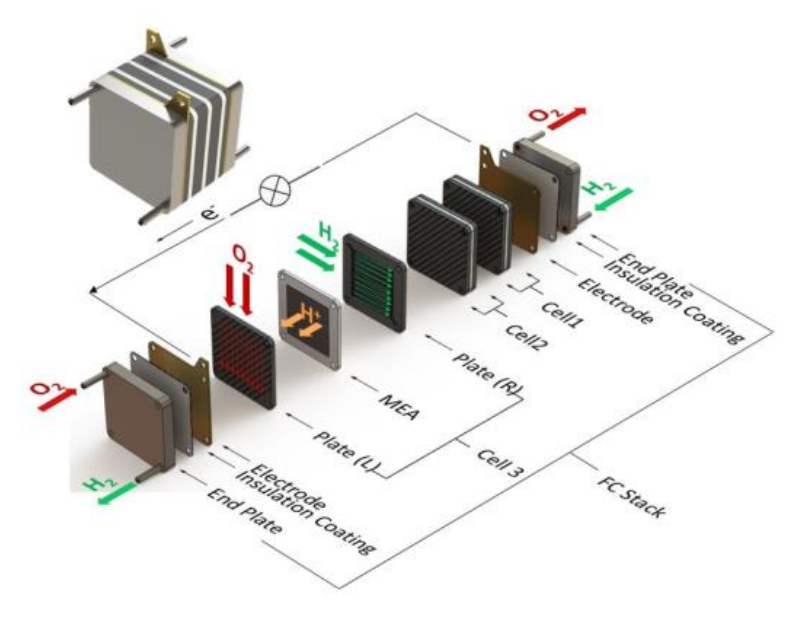


Figure 1.15. Schematic diagram of PEFC [F14]

In conclusion, titanium's unique combination of lightweight properties, exceptional strength, and corrosion resistance positions it as a highly advantageous material across various automotive applications. Its integration into components such as fuel tanks, exhaust systems, and engine parts not only enhances performance by reducing weight but also improves durability and efficiency. The ongoing development of advanced titanium alloys, such as Super-TIX<sup>TM</sup> variants, addresses the specific demands of high-temperature and high-stress environments, further broadening its applicability. Despite challenges related to manufacturing costs and raw material availability, the potential for titanium to contribute to the evolution of automotive design and engineering is significant, promising advancements in both performance and sustainability as the industry continues to prioritize weight reduction and efficiency.



# 1.4.1. High Cost and Economic Constraints

One of the major obstacles hindering the extensive adoption of titanium in the automotive sector is its elevated production expenses. The conventional Kroll process, commonly employed for extracting and refining titanium, is both energyintensive and costly. Specifically, the high-temperature reduction phase necessitates heating titanium tetrachloride (TiCl<sub>4</sub>) with magnesium at temperatures ranging from 800 to 1000°C, which consumes substantial amounts of energy. The chlorination stage, where titanium ore (TiO<sub>2</sub>) is transformed into TiCl<sub>4</sub> using chlorine gas at elevated temperatures, further exacerbates these energy requirements. Moreover, the batch processing characteristic of this method entails repeated cycles of heating, cooling, and handling, resulting in inefficiencies. The process also incorporates magnesium recycling; magnesium chloride (MgCl<sub>2</sub>) must undergo electrolysis, adding to the overall energy expenditure. Furthermore, intricate handling and purification procedures—such as vacuum distillation and the melting of titanium sponge—contribute to increased energy consumption. These combined factors render the Kroll process both costly and inefficient, thereby elevating the price of titanium production. In contrast to steel and aluminum—which can be produced through more economical methods—titanium manufacturing involves several complex stages that considerably inflate its cost. On average, titanium may be up to twenty times more expensive per kilogram compared to steel, making it less feasible for use in mass-market vehicles [61].

In addition to production costs, the price of raw materials further complicates titanium's economic viability. The extraction and processing of titanium ores like rutile and ilmenite entail expensive refining techniques. Fabrication methods such as forging, casting, and machining are also costly due to titanium's distinctive attributes, including high chemical reactivity and low thermal conductivity. While innovations in titanium processing have enhanced efficiency levels, overall production expenses continue to pose a significant barrier to its widespread implementation within the automotive industry [62].



# 1.4.2. Manufacturing and Processing Challenges

Titanium presents significant challenges in the manufacturing process due to its distinct physical and chemical characteristics. Its low thermal conductivity causes heat build-up during machining, which can lead to quick wear of tools and increased production costs. Conventional machining methods such as milling, drilling, and turning require specialized tools and cooling systems to manage the heat produced during processing. As a result, manufacturers face higher operational expenses when working with titanium compared to more traditional materials like steel or aluminum [63].

To address these challenges, new manufacturing techniques such as electrical discharge machining (EDM), laser cutting, and additive manufacturing (3D printing) have been explored. These advanced approaches improve the efficiency of titanium processing by reducing material waste and enhancing accuracy. However, they are still costly and not commonly employed for mass production due to their specific needs. Additionally, the forging and welding processes for titanium alloys necessitate high temperatures and sophisticated equipment, further limiting their use in large-scale automotive manufacturing [64].

# 1.4.3. Limited Availability of Raw Materials

Titanium extraction and processing are intricate processes. In contrast to aluminum and steel, which benefit from established supply chains, titanium production is contingent upon particular ores like rutile and ilmenite. These ores are sourced from specific locations such as Australia, Canada, and South Africa, resulting in constraints within the supply chain and fluctuations in pricing [65]. Furthermore, geopolitical considerations can affect both titanium mining operations and its global distribution, leading to market instability. The dependence on a limited number of mining areas coupled with the high costs associated with refining poses challenges for incorporating titanium into large-scale manufacturing.

Nonetheless, recent research indicates that titanium presents a low supply risk for electric vehicle (EV) production, positioning it as a viable option for future sustainable automotive uses [66].



# 1.4.4. Prospects and Potential Solutions

To address these challenges, researchers and manufacturers are actively investigating new techniques for cost reduction and innovative production methods. These include:

Alternative Extraction Methods: Emerging technologies such as the FFC Cambridge process and Hydrogen Sintering and Phase Transformation (HSPT) seek to decrease titanium production costs by minimizing energy usage and streamlining the extraction process. These advancements could enhance titanium's competitiveness against traditional materials like aluminum and steel [67].

Advancements in Additive Manufacturing: Techniques like 3D printing and powder metallurgy facilitate the effective creation of lightweight titanium components while generating minimal material waste. These methods improve manufacturing accuracy, lower costs, and provide greater design flexibility. However, the high initial investment associated with additive manufacturing poses a barrier to its widespread use in mass-market vehicles [68].

Development of New Titanium Alloys: Ongoing research is aimed at enhancing the machinability of titanium and creating cost-effective alloys with superior processing properties. By refining titanium compositions, manufacturers hope to lower fabrication costs and increase the material's applicability in automotive settings [69]. With persistent progress in material science and manufacturing technologies, it is anticipated that titanium will assume a more significant role within the automotive sector, especially in applications involving high-performance, electric, and luxury vehicles. Although cost-related challenges remain, continuous research and development initiatives are setting the stage for more affordable and efficient titanium solutions moving forward [70].

In summary, while titanium offers exceptional properties such as lightweight strength and corrosion resistance, its widespread adoption in the automotive sector is hindered by high production costs and complex manufacturing processes. The conventional Kroll process for titanium extraction is energy-intensive and costly, resulting in prices significantly higher than those of steel and aluminum. Additionally, titanium's unique characteristics necessitate specialized machining and fabrication techniques, further inflating operational expenses. Emerging technologies, including alternative extraction methods and advancements in additive manufacturing, show promise in reducing costs and enhancing efficiency.



# 1.5. Protection of titanium against high temperature oxidation

Titanium and its alloys, while known for their remarkable resistance to corrosion, experience accelerated oxidation when exposed to temperatures exceeding 600°C. This phenomenon leads to embrittlement and a deterioration of mechanical properties [71]. Such issues are particularly critical in industries like aerospace, automotive, and power generation, where materials frequently encounter high temperatures [72]. In contrast to stainless steel or nickel-based superalloys, titanium develops a non-protective and porous layer of titanium dioxide (TiO<sub>2</sub>) upon extended thermal exposure. This facilitates the diffusion of oxygen into the substrate [71], resulting in the creation of brittle  $\alpha$ -phase layers that are stabilized by oxygen, thus undermining the material's mechanical strength [73]. To mitigate the effects of hightemperature oxidation, a variety of surface protection methods have been introduced, including coatings based on silicon, aluminum, and glass-ceramics [70]. These sophisticated coatings act as barriers against diffusion, preventing oxygen from penetrating while preserving the essential characteristics of titanium alloys in harsh conditions. Table 1.3 shows, silicon, aluminum, and glass-ceramic-based coatings with an emphasis on enhancing adhesion and thermal stability specifically for automotive exhaust systems.

**Table 1.3:** Comparison of coating methods [3].

Coating Type	Deposition Method	Oxidation Resistance (°C)	Adhesion Strength (MPa)	Cost- Effectiveness
Aluminide (Al <sub>2</sub> O <sub>3</sub> )	CVD	800–1000	45–60	Moderate
Silicide (Ti₅Si₃)	Plasma Spraying	700–900	30–45	High
Glass-Ceramic	Slurry Coating	600-800	20–35	Low



# 1.5.1. Surface Protection Using Silicon

Silicon-based coatings significantly improve the oxidation resistance of titanium. By integrating silicon into titanium's surface, a protective silica (SiO<sub>2</sub>) layer is created, which acts as a barrier against oxygen penetration and degradation at elevated temperatures. Coatings like Ti<sub>5</sub>Si<sub>3</sub> and TiSi<sub>2</sub> are known for their excellent thermal stability and oxidation resistance, effective up to 1000°C. These coatings are usually applied using methods such as pack cementation, chemical vapor deposition (CVD), and slurry techniques. The primary benefit of silicon coatings is their ability to produce a dense, adherent oxide layer that inhibits further oxidation, making them particularly advantageous for aerospace components, turbine blades, and high-temperature industrial uses [70-75].

The SiO<sub>2</sub> layer exhibits remarkable stability in oxidative environments and avoids the spallation problems that can occur with pure TiO<sub>2</sub> layers. Moreover, silicide coatings have shown improved performance under cyclic oxidation conditions when compared to uncoated titanium alloys. Nevertheless, issues like brittleness during thermal cycling persist, prompting researchers to investigate composite silicide coatings that offer better ductility. Recent developments in nano-structured silicide coatings and multi-layered diffusion barriers made of silicon aim to enhance mechanical durability while preserving excellent oxidation resistance [70-74].

# 1.5.2. Surface Protection Using Aluminum

Aluminum-based coatings present an effective method for protecting against oxidation by creating a stable layer of aluminum oxide  $(Al_2O_3)$  on the surface of titanium. This oxide layer plays a crucial role in significantly limiting the diffusion of oxygen into the underlying metal, thereby preventing the development of embrittling oxygen-rich phases within the titanium structure.

Aluminide coatings are typically created using techniques such as pack aluminization, chemical vapor deposition (CVD), plasma spraying, and thermal diffusion processes. These coatings not only improve resistance to oxidation but also enhance wear and erosion resistance, making them suitable for components in aerospace engines, heat exchangers, and high-temperature industrial settings.



The generation of Al<sub>2</sub>O<sub>3</sub> is particularly advantageous due to its greater thermodynamic stability compared to TiO<sub>2</sub>; it forms a continuous and dense barrier that reduces oxidation at elevated temperatures. Furthermore, aluminum-modified titanium alloys (Ti-Al alloys) demonstrate improved thermal stability and mechanical strength, broadening their use in harsh environments. However, aluminide coatings have a potential drawback: they may lead to the formation of intermetallic compounds like TiAl and Ti<sub>3</sub>Al, which can affect the mechanical properties of the coated materials. To mitigate this issue, researchers are exploring graded aluminide coatings and hybrid aluminum-ceramic composites aimed at maximizing oxidation resistance while maintaining mechanical performance.

# 1.5.3. Surface Protection Using Glass and Glass-Ceramics

Glass and glass-ceramic coatings offer an alternative method for oxidation protection by creating a dense layer that obstructs oxygen infiltration. These coatings are generally made from borosilicate or phosphate-based glass, which bond effectively to titanium and demonstrate remarkable thermal stability. Acting as diffusion barriers, glass-ceramic coatings significantly restrict the movement of oxygen while preserving surface integrity in high-temperature environments. They are particularly advantageous for protective cladding in aerospace and energy sectors where extreme temperatures are frequently encountered.

A notable benefit of glass coatings is their capacity to autonomously repair minor cracks, providing sustained oxidation protection even amidst fluctuating thermal conditions. Furthermore, these coatings possess excellent chemical resistance, making them appropriate for demanding operational environments that involve exposure to corrosive gases and molten metals.

Nevertheless, issues such as mismatches in thermal expansion between the coating and titanium substrate need to be resolved to ensure long-lasting durability. Recent advancements in glass-ceramic formulations and multilayer hybrid coatings have shown potential in enhancing adhesion, resistance to thermal shock, and overall performance in high-temperature scenarios [72-75].



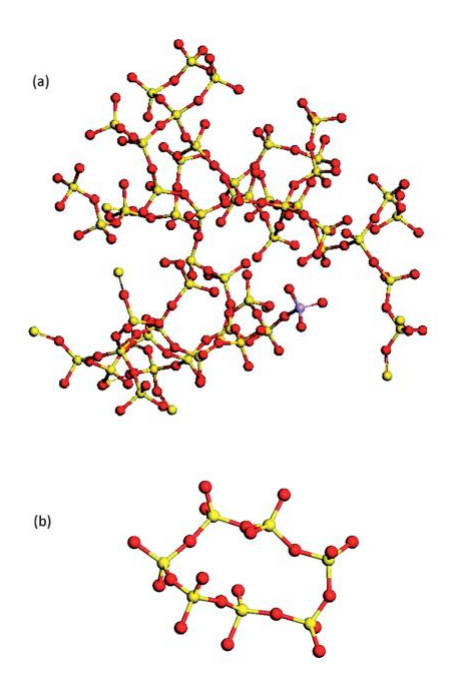


**Figure 1.16.** Structure of Bioglass 45S5 as determined by Molecular Dynamics (MD) simulation: a) the silicate backbone (SiO4), and b) a seven-membered silicate ring that illustrates short silicate units (with oxygen in red, silicon in yellow, and phosphorus in purple) [F15].

#### 1.6. Conclusion

The topics highlight the critical role of advanced coatings in enhancing the high-temperature oxidation resistance of titanium and its alloys, particularly for applications in automotive exhaust systems. Silicon-based coatings, such as silicides, effectively create a protective SiO<sub>2</sub> layer that inhibits oxygen penetration, demonstrating excellent thermal stability and oxidation resistance up to 1000°C. Glass-ceramic coatings provide an alternative by forming dense barriers against oxygen infiltration and exhibiting self-repair capabilities, although challenges related to thermal expansion mismatches remain.

Aluminum-based coatings, particularly aluminide layers, offer significant oxidation protection by generating a stable  $Al_2O_3$  layer, enhancing wear resistance, and improving thermal stability. However, they may also lead to the formation of intermetallic compounds that could affect mechanical properties.



Ongoing research into composite and graded coatings aims to optimize performance, addressing both oxidation resistance and mechanical integrity in high-temperature environments. These advancements are essential for expanding the application of titanium in demanding industries, ensuring its durability and functionality under extreme conditions.

# 2.Theories and mechanism of adhesion

The term "coating" refers to solid or liquid material applied to a substrate as either a continuous or discontinuous film. Coatings can serve functional, aesthetic, or combined purposes. They are employed to enhance or modify the surface characteristics of the substrate, such as its wettability, resistance to corrosion or wear, and may even impart entirely new properties like magnetic or electrical behavior. In contrast, aesthetic coatings focus solely on improving visual appeal. Coatings can be categorized into two types: all-over coatings that cover the entire surface of the substrate and non-all-over coatings that only cover specific areas [76].

# 2.1. Coating deposition process and techniques

Coating deposition methods can be categorized into various groups based on the mechanisms used for applying the coating:

**Vapor Deposition:** This technique involves the application of coating one atom or molecule at a time. The resulting thickness can range from a single atom to several millimeters, and it allows for the creation of multiple layers by using different materials.

There are two primary approaches within vapor deposition: **Physical Vapor Deposition** (PVD) and **Chemical Vapor Deposition** (CVD). In the PVD process, depicted in Figure 2.1, material is vaporized from either a solid or liquid source. The resulting atoms or molecules are then transported as vapor to the substrate, where they condense.



This procedure typically takes place under vacuum conditions or at low pressure.

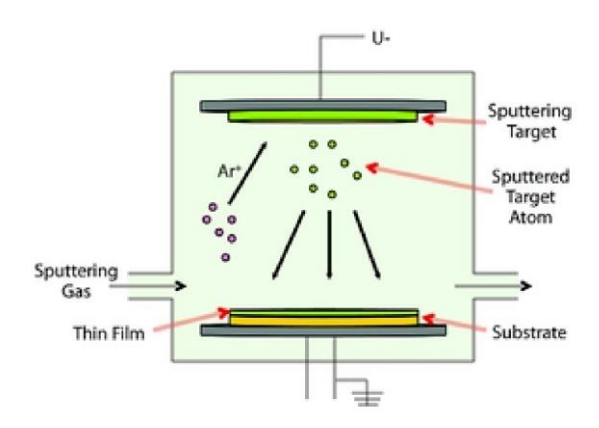


**Figure 2.1**. Scheme of Physical Vapor Deposition (PVD) process [F16]

This method enables the deposition of thin films ranging from a few nanometers to several nanometers in thickness. It is feasible to deposit either a single element or an alloy through a reactive deposition process, where a reaction occurs between the depositing materials and the surrounding gas or with a co-depositing material, resulting in compound formation. Various materials can serve as coatings or substrates; for instance, Figure 2.2 illustrates a PVD deposited coating on a carbon fiber substrate, which is coated with AlN.

The differences in surface characteristics between the uncoated fiber (b) and the fiber that has been coated with AlN (a) are clearly visible. There are several categories of PVD processes summarized in Figure 2.3: vacuum deposition, sputter deposition, arc vapor deposition, and ion plating. In vacuum depositions, also referred to as vacuum evaporation, the material intended for deposition is evaporated from a thermally heated source and travels to the substrate with minimal collisions against gas molecules. The vacuum environment helps reduce contamination within the deposition system. This process operates at a significantly higher rate compared to other methods.



Another method is **electron-beam physical vapor deposition** (EBPVD), which employs an electron beam to strike a target anode. This interaction causes atoms to be released from the target and enter a gaseous state, eventually condensing into solid form on the substrate to create a coating.

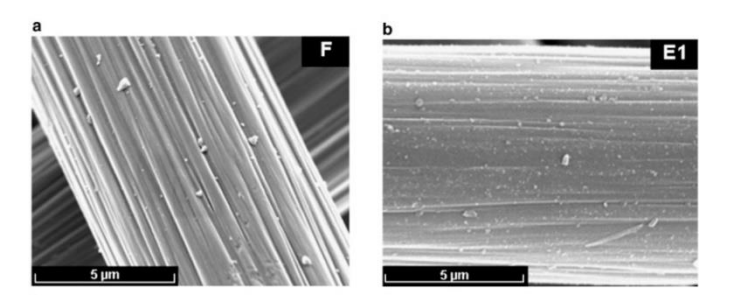


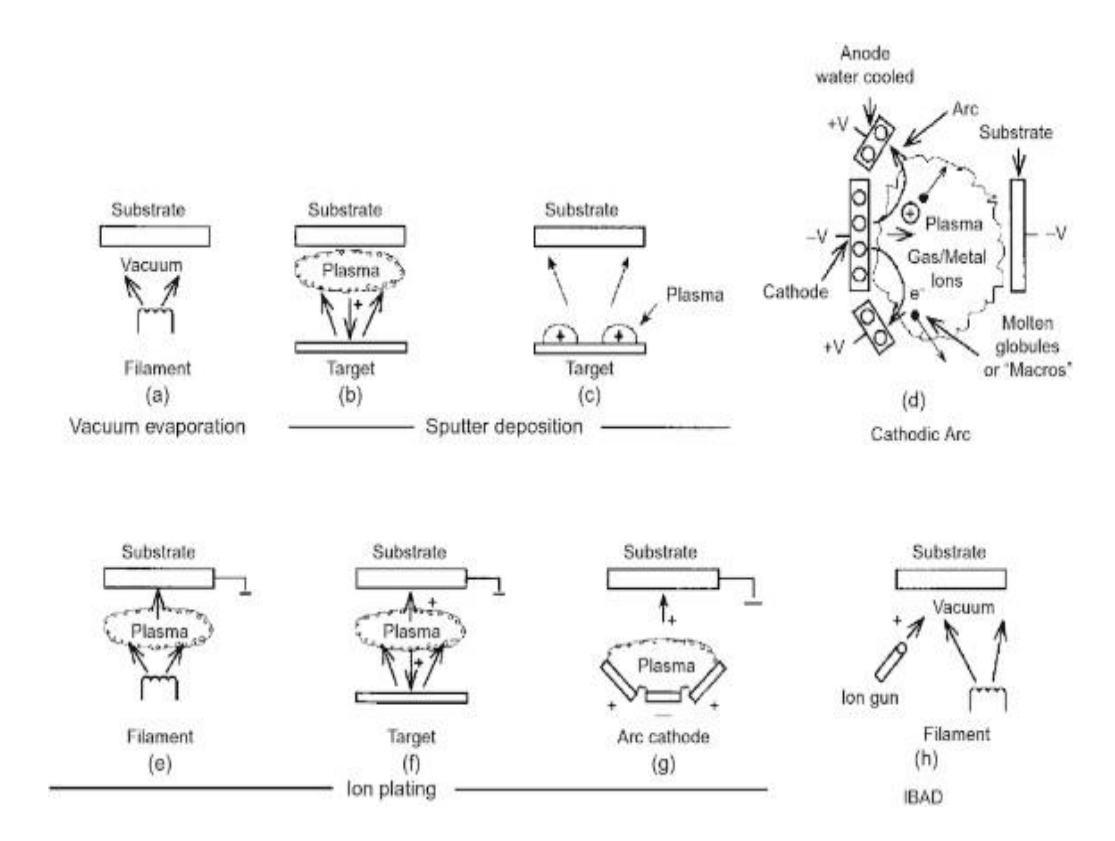
**Figure 2.2.** (a) Aluminum nitride (AlN) coating applied to carbon fibers, (b) fiber without coating [F17].

**Ion plating**, also referred to as ion-assisted deposition (IAD) or ion vapor deposition (IVD), involves either current or bombarding particles that facilitate the deposition of material vaporized through processes such as evaporation, sputtering, erosion, or decomposition of a chemical vapor precursor [77].

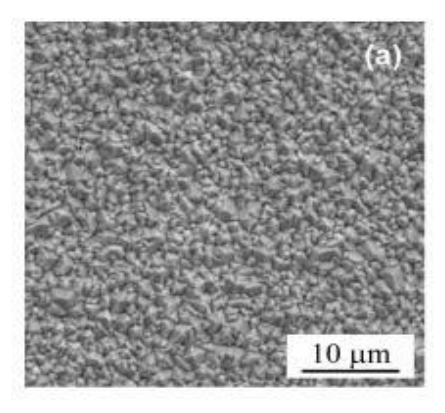
Chemical vapor deposition (CVD) is a technique that employs chemical vapor precursors, which are converted into atoms or molecules through reduction or decomposition processes. These transformed entities then react with one another on the surface to form a coating. Additionally, the atoms may interact with gases present in the system, leading to the formation of compounds that get deposited onto the substrate [76].

Figure 2.4 illustrates a TiO2 coating applied to a glass substrate using the CVD technique. This process can be categorized based on pressure levels into atmospheric pressure CVD, low pressure CVD, and high-pressure CVD. Furthermore, it can also be differentiated as hot wall and cold wall CVD depending on how heat is supplied: in hot wall configurations, the chamber is heated externally while in cold wall setups only the substrate is heated via induction or electric current, with the chamber remaining at ambient temperature [76-77].





**Figure 2.3**. Techniques for PVD processing: (a) Vacuum Evaporation, (b) Electron Beam Deposition, (c) Sputter Deposition in a Plasma Environment, (d) Sputter Deposition under Vacuum Conditions, (e), (f), (g) Ion Implantation in a Plasma Environment utilizing a Thermal Evaporation Source, a Sputtering Source, and an Arc Vaporization Source respectively, (h) Ion Beam-Assisted Deposition (IBAD)[F18].



**Figure 2.4**. Deposition of TiO2 coating on a glass substrate utilizing the CVD method [F19].



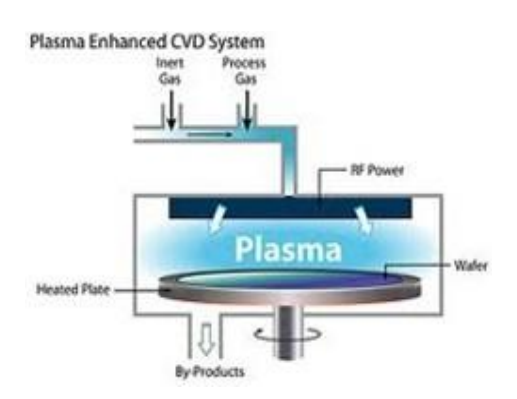


**Figure 2.5.** Plasma-Enhanced Chemical Vapor Deposition (PECVD) System [F20]

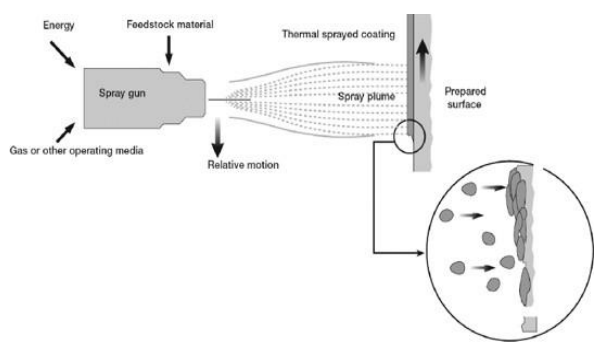


**Figure 2.6.** Outline of the Thermal Spray Procedure [F21]

An essential method is Plasma-enhanced chemical vapor deposition (PECVD) (refer to Figure 2.5). This process involves chemical reactions that take place following the generation of plasma formed from the reacting gases. Typically, this plasma is produced using radio frequency (RF) technology. The PECVD technique enables deposition at reduced temperatures, which is frequently vital for the production of semiconductors and organic coatings, including plasma polymers that have been utilized for functionalizing nanoparticle surfaces [78].

Spraying involves applying a coating to a surface using a device that utilizes compressed gas, typically air, to atomize and direct the particles. This method is primarily employed to achieve an even liquid coating over extensive areas. The materials used for coating can be in the form of powder, wire, or rod, which are supplied to a torch or gun where they are heated close to or slightly above their melting point.



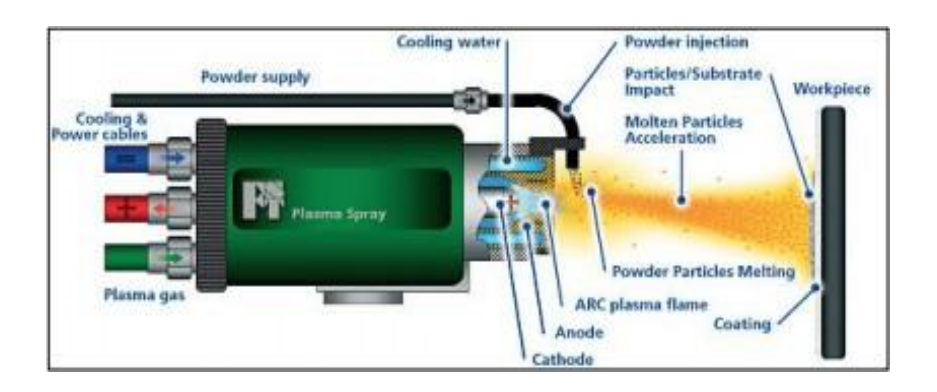


Figure 2.7. Scheme of Plasma spray process [F22]

There are various forms of this process. Generally, thermal spraying is a method whereby coating materials are melted through electrical or chemical means and then sprayed onto surfaces as micrometer-sized particles (see Figure 2.6).

The resulting coating can vary in thickness from a few microns to several millimeters. The plasma spray process (refer to Figure 2.7) employs a direct current electric arc to produce a stream of high-temperature ionized plasma gas, which serves as the heat source for the spraying operation. The powder intended for deposition is injected into the plasma outside the gun nozzle, where it melts and is propelled by the gas onto the substrate's surface. Upon reaching the substrate, these droplets flatten and solidify, forming the coating.

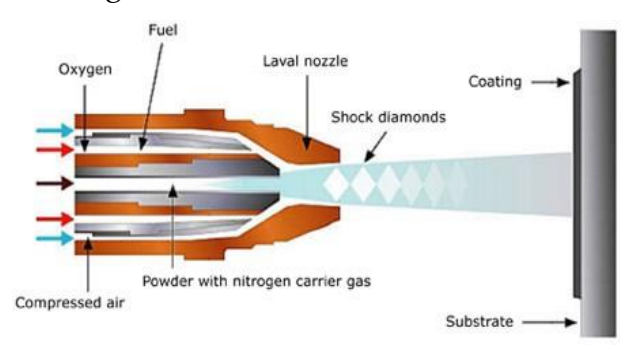


Figure 2.8. Scheme of High-Velocity Oxy-Fuel spray technique HVOF [F23]

By adjusting various parameters—such as the composition of the plasma gas, flow rate, type of feedstock, and the distance between the substrate and nozzle—it is possible to create coatings with specific desired properties.



A variant of the process is known as Vacuum Plasma Spraying, which occurs in a low-pressure chamber where the plasma is activated by an electrical field. Typically, any volatile plasma by-products are removed using a vacuum pump. This low-pressure plasma method offers several advantages, such as enhanced bonding and deposit density, better control over the thickness of the coating, and increased efficiency in material deposition.

The high velocity oxy-fuel (HVOF) spray process, illustrated in Figure 2.8, is a relatively modern technique. This method utilizes a combustion chamber where a mixture of gaseous and liquid fuel along with oxygen is ignited. The resulting combustion generates high temperatures and pressure within the chamber. As the hot gases flow through the nozzle, powdered feedstock is injected into this gas stream, causing it to accelerate toward the surface intended for coating. Due to the rapid speed of the particles, the coatings produced are typically very dense, well-adhered, and may contain various inclusions [79].

An illustration of the surface produced using spraying techniques is presented in Figure 2.9. In this instance, Ni<sub>20</sub>Cr is utilized as the coating material, which is applied via the plasma spray method.

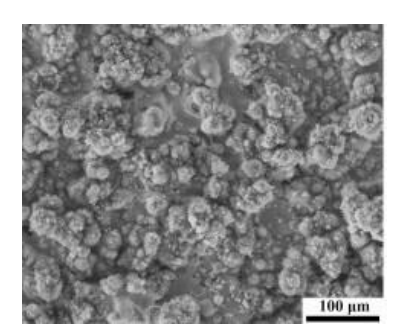


**Figure 2.9.** Morphology of plasma spray Ni20Cr coating deposited by plasma spray method [F24]

Additional techniques include conversion coatings, where the material's surface undergoes chemical and electrochemical reactions with the coating substance. Another notable method is plating, where a metal layer is deposited onto a conductive substrate. Various approaches exist for this process; one such technique involves placing a metal sheet on a solid base, followed by melting it through the application of heat and pressure.





**Figure 2.10.** Phosphate coating [F25]

Examples of these methods encompass chromate conversion coatings, phosphate conversion coatings, and blue or black oxide coatings applied to steel (refer to Figure 2.10).

Another approach involves electroplating, a process where metal in ionic form generates a non-ionic coating through the assistance of electrons. This system comprises a chemical solution containing the ionic metal, along with an anode and a cathode, where electrons are provided to facilitate the formation of the non-ionic layer. Additionally, one can achieve non-galvanic plating by leveraging concurrent reactions within an aqueous solution [76]. This method is employed to enhance aesthetic attributes or improve the properties of various substrates.

For instance, Figure 2.11 illustrates an aluminum substrate that has been electroplated using bromide salts to enhance its resistance to corrosion.

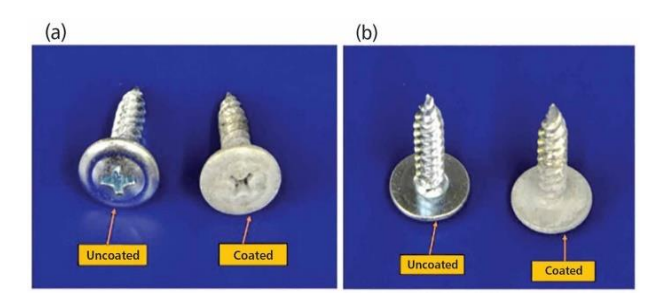


**Figure 2.11.** Aluminum Electroplating Utilizing Bromide Salts [F26]

In industrial applications, dip coating serves as a means to create thin films from solgel precursors. The procedure consists of several stages: the substrate is submerged in a coating material solution for a designated duration. As it is withdrawn from the solution, a thin layer adheres to the substrate.



Any excess liquid drains off the surface; subsequently, solvent evaporation leads to the formation of the thin layer. An example of this process is depicted in Figure 2.12, showcasing rhodium being dipped onto yellow gold.



Figure 2.12. Rhodium dipping on yellow gold [F27]

In conclusion, coating deposition methods are essential for enhancing material performance and durability across various applications. These techniques are categorized into vapor deposition, thermal spraying, and electrochemical methods, each with unique advantages. Vapor deposition methods, such as Physical Vapor Deposition (PVD) and Chemical Vapor Deposition (CVD), enable precise atomic-level coatings, producing thin films from nanometers to micrometers in thickness. Thermal spraying techniques, like plasma spraying and High Velocity Oxy-Fuel (HVOF) spraying, create robust coatings that withstand extreme conditions, enhancing wear resistance. Electrochemical methods, including electroplating and conversion coatings, improve surface properties and corrosion resistance through chemical reactions.

In the automotive industry, thermal spraying, particularly High Velocity Oxy-Fuel (HVOF) spraying, is particularly suitable due to its ability to produce dense, durable coatings that can endure high wear and thermal stress, making it ideal for components like engine parts and exhaust systems. Additionally, electroplating is commonly used to enhance corrosion resistance and aesthetic appeal on automotive surfaces. Choosing the appropriate coating method is crucial for optimizing performance in industries such as aerospace, automotive, and electronics. Ongoing advancements in these techniques, including hybrid and composite coatings, will enhance their effectiveness and broaden applications, meeting the growing demands for performance and sustainability.



# 2.2. Theory of adhesion

In a coating/substrate system, adhesion occurs between two distinct materials at their interface, necessitating the generation of intrinsic adhesive forces. The understanding of this adhesive phenomenon incorporates various fields, including surface chemistry, fracture mechanics, rheology, and materials mechanics.

When discussing adhesion theory, it is crucial to differentiate between intrinsic adhesion and measured adhesion. Intrinsic adhesion pertains to the direct molecular attractions between the coating and substrate, while measured adhesion refers to the bond strength that can be quantified through specific methods outlined later. Numerous models exist that elucidate the mechanisms of adhesion [80].

# 2.2.1. Mechanical interlocking theory

This model suggests that adhesion occurs due to the mechanical interlocking of the coating with the surface irregularities and pores of the substrate. Key factors influencing this theory include the substrate's roughness, porosity, and wettability. The tensile strength is influenced by the angle of crevices on the adhered surface, while an increase in roughness enhances shear strength.

Leeden and Frens identified three types of surface irregularities (see Figure 2.13), with only defect "b" being significant for interlocking adhesion.

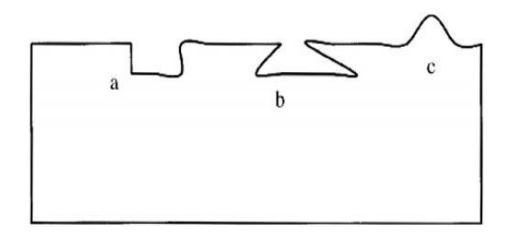


Figure 2.13. Three types of superficial defects [F28]

The impact of defects "a" and "c" varies based on the direction of the applied force. Furthermore, it is essential that the coating material possesses adequate viscosity to effectively fill the pores [43].

Mechanical interlock serves as the primary mechanism for explaining adhesion strength within a system comprising a metal substrate and a polymeric coating. Research conducted by Won-Seock et al. focused on a steel and carbon fiber reinforced polymer system (refer to Figure 2.14).



Their findings indicated that greater roughness enhances adhesion strength, while mechanical interlock leads to energy dissipation processes during the fracture phase [81].



Figure 2.14. Cross section of a steel/composite bonded interface [F28]

# 2.2.2. Chemical/adsorption theory

This framework, introduced by Sharpe and Schonhorn, relies on the interatomic and intermolecular interactions between the atoms and molecules present on the two surfaces. These interactions encompass secondary bonds, including Van der Waals and hydrogen bonds, as well as primary bonds such as covalent, ionic, and metallic bonds.

Paint formulations that include reactive functional groups like hydroxyl or carbonyl exhibit stronger adhesion to substrates that possess similar features. Consequently, bi-functional molecules are utilized as promoters of adhesion; one end is designed to react with the paint while the other end interacts with the substrate, resulting in robust and long-lasting connections. These molecules are typically silane-based and serve both as additives in paint compositions and as primers for glass and metal surfaces. An illustration of a covalent bond formed at the interface with a steel surface via chemisorption is depicted in Figure 2.15 [82].

Adsorption theory, often referred to as thermodynamic theory, encompasses knowledge related to wetting, rheology, and chemistry. To achieve effective wetting, the surface energy of the substrate needs to exceed that of the liquid coating, as will be elaborated upon later. Materials such as metal, glass, and certain polymers possess a higher surface energy than paint binders, making them suitable for use as substrates.

In some instances, specific plastic substrates with very low surface energy—like polypropylene, silicone rubber, and fluoroplastics—can serve as substrates if they undergo surface treatment processes (such as chemical treatment, flame treatment, or corona treatment) that enhance their surface energy. [82].



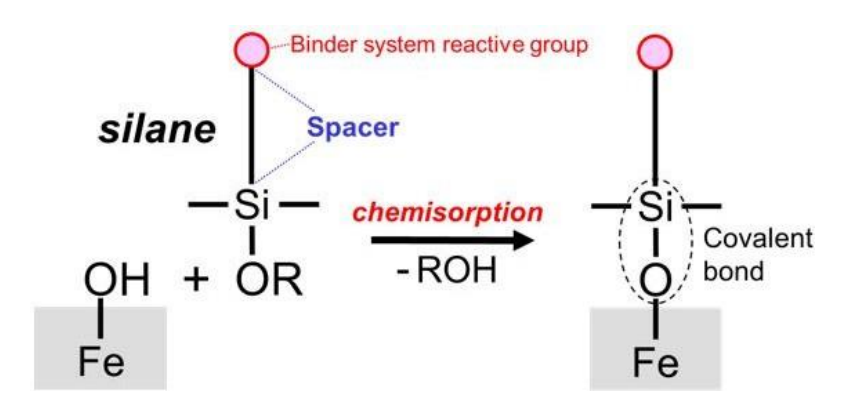


Figure 2.15. Chemical Interaction of Silane Adhesion Promoter with Steel Surface [F29]

# 2.2.3. Acid-base theory

Fowkes et al. identified acid-base interactions as a significant category of intrinsic adhesion forces. The two surfaces can function as an acid by either accepting electrons (a Lewis acid) or donating protons (a Brønsted acid), or they may act as a Lewis base by donating electrons or accepting protons, potentially exhibiting both acidic and basic characteristics [80][83].

Neubauer et al. investigated these mechanisms by examining the acid-base interactions of aromatic sulfur heterocycles adsorbed on Ag-Al2O3. As illustrated in Figure 2.16, three types of bonds are formed:  $\pi$ -Ag, S-H, and S-Ag. The first bond type,  $\pi$ -Ag, exhibits high adsorption energy and is generated through two mechanisms: silver cations form typical  $\sigma$ -bonds using their s orbitals, while the d orbitals of these cations can back-donate electron density to the antibonding  $\pi$ -orbital of the sulfur heterocycles. The S-Ag interaction is explained by hard and soft acid-base (HSAB) theory; specifically, the silver cation in Ag-Al2O3 acts as a soft acid, while the sulfur heterocycles serve as Lewis bases with two lone pairs of electrons—one  $\sigma$  lone-pair and one  $\pi$  lone-pair electron. Additionally, this S-Ag interaction aligns with HSAB theory: here, the silver cation behaves as a soft acid interacting with the sulfur heterocycle regarded as a soft base [84].



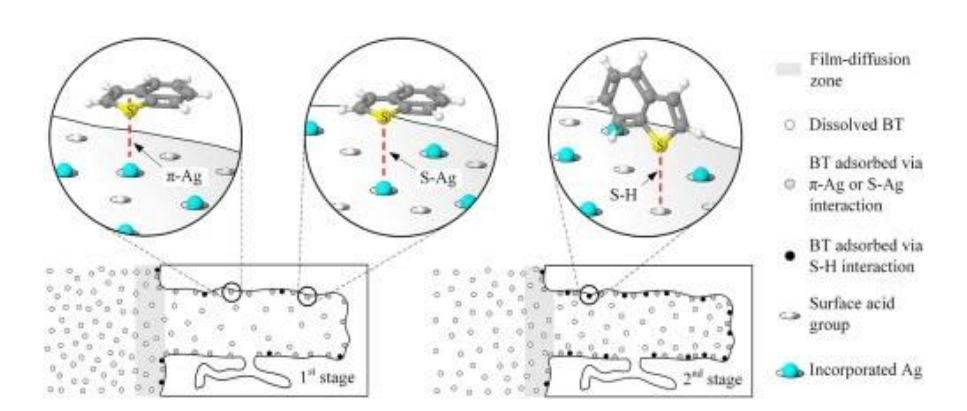


**Figure 2.16.** Creation of  $\pi$ -Ag, S-H and S-Ag bonds [F32]

# 2.2.4. Diffusion or interdiffusion theory

In this theory, adhesion arises from the interdiffusion of macromolecules between two materials (see Figure 2.17). Several conditions must be met: the molecules at the interface should possess sufficient mobility to intermingle, the materials need to have comparable solubility parameters, and they must be both miscible and compatible. Typically, this type of adhesion is observed between two polymers, where a transient zone develops due to the interaction of macromolecules in the outer layers. Macromolecules are crucial in determining bond strength, which is affected by factors such as chain length, polymer structure, contact duration, concentration, and temperature [80].

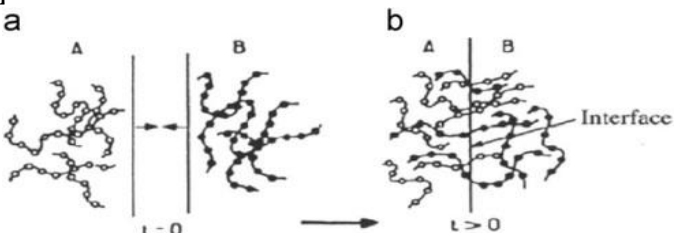


Figure 2.17. Diffusion theory of adhesion [F29]



# 2.2.5. The electrostatic attraction theory

The theory of electrostatic attraction is grounded in the shared interaction of electrons at the boundary between two different materials. Here, an electrostatically charged double layer of ions develops at the interface, allowing the system to be conceptualized as a capacitor. This framework is relevant for pairs of incompatible materials, like metal and polymer, illustrated in Figure 2.18. Attractive forces arise when one surface possesses a net positive charge while the other exhibits a net negative charge. The strength of these forces at the interface is influenced by charge density [80]. For instance, such adhesion bonds are formed between low-density polyethylene (LDPE) and an aluminum substrate. Furthermore, the presence of this electric double layer significantly impacts the mechanical properties observed at the interface. This model proves useful when dealing with incompatible materials, including polymers and metals.



**Figure 2.18.** Electrical double layer formed at the interface between a polymer and a metal [F29]

# 2.3. Thermodynamic theory of adhesion

From a thermodynamic point of view, the adhesion of a coating to a substrate depend on different parameters, such as free energy of the surface, wettability, forces of attraction. When a liquid drop is deposited on a surface, the liquid can spontaneously spread on the surface forming a thin film or can form a sessile droplet on the surface. In the first case, an intimate molecular contact is established and results in the elimination of air pockets and in the penetration of the liquid in the asperities of the surface. In the second case, the adhesion of the lm to the substrate is worse. The behavior depends on the surface tension of the two components, and it is possible to de ne a contact angle by the Young's equation:

$$\gamma s = \gamma s l + \gamma l \cos \theta$$



where In this equation,  $\gamma s$  represents the surface tension of the solid substrate in equilibrium with the saturated vapor of the liquid;  $\gamma sl$  denotes the interfacial tension between solid and liquid;  $\gamma l$  indicates the surface tension of the liquid in equilibrium with its own saturated vapor; and  $\theta$  signifies the contact angle at the solid-liquid interface (see Figure 2.19).

The value of superficial tension—and consequently that of the contact angle—determines whether a liquid will wet a given surface. This characteristic is crucial for establishing adhesive bonds: coatings with lower surface energy than that of their substrates will effectively wet those surfaces. If sufficient intimate contact is made between coating and substrate, strong physical interactions develop that lead to robust bonding. It is important to note that while spreading enhances adhesion by maximizing contact area and reducing interfacial flaws or defects, it is not the sole requirement for good adhesion.

When molten powders are applied to a surface, coalescence must take place (refer to Figure 2.20). This process depends on factors such as surface tension, particle curvature radius, and viscosity of the molten material.

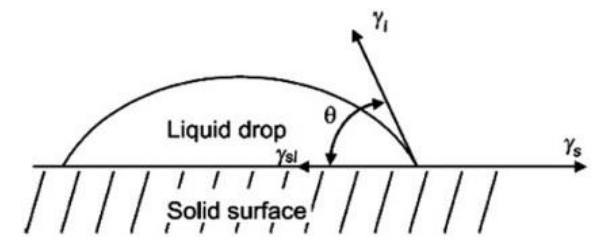


**Figure 2.19.** Liquid drop on solid surface in equilibrium [F29]

To reduce coalescence time effectively, conditions such as low viscosity, small particle size, and low surface tension are essential.

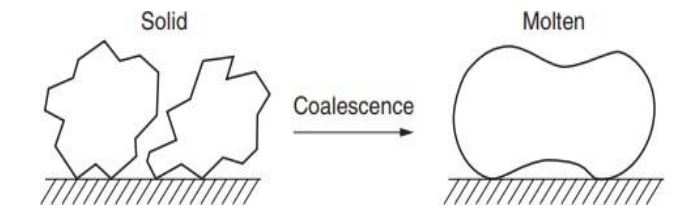


**Figure 2.20.** Coalescence of molten powders [F30]

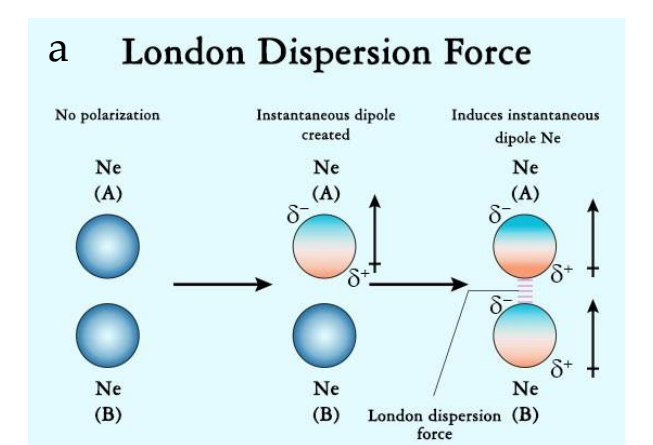


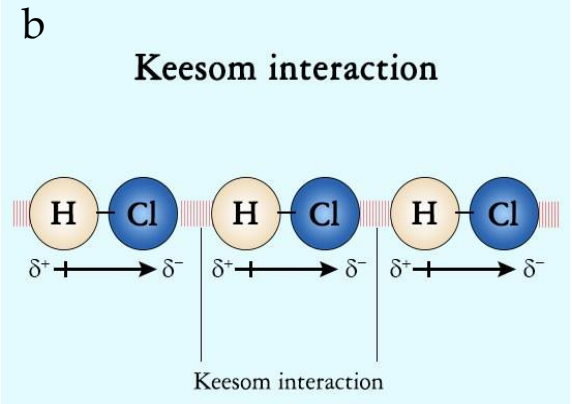
Another significant factor to consider is the role of attraction forces, known as Van der Waals forces. When atoms or molecules come sufficiently close together, they exhibit an attractive interaction. However, under certain conditions, repulsion may occur, particularly when there are fixed distributions of electrical charges or magnetic polarization, or when matter is compressed to the point that outer electron shells start to overlap. Van der Waals forces consist of three main components. The first component is referred to as London forces or dispersion forces, which arise from fluctuations in electron density leading to temporary electric dipoles that create attraction (see Figure 2.21 a).

These interactions are ubiquitous across all types of matter; despite their relatively weak nature, their cumulative impact can be substantial. The second component involves Keesom forces, which describe the attraction between permanent dipoles and rely on the dipole moments of the interacting molecules (see Figure 2.21 b).

The third contribution comes from Debye forces, which are the dipole-induced dipole interactions. These forces occur when a permanent dipole induces a dipole in an adjacent molecule, resulting in a potential energy of interaction that is proportional to the molecular polarizability (refer to Figure 2.21 c).

Additionally, acid-base interactions result in robust bonding. Examples include hydrogen bonding, Lewis acid-base interactions, and Bronsted-type acid-base interactions [80][83][85].







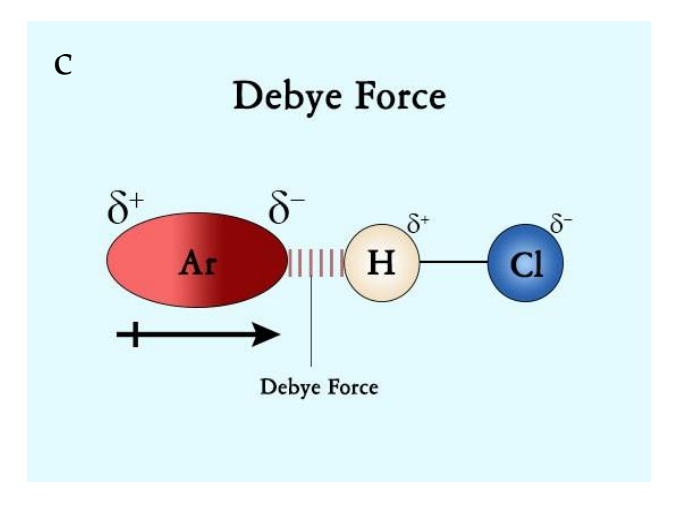


Figure 2.21. a) London forces, b) Keesom forces c) Debey forces [F31]

# 2.4. Macroscopic adhesion testing

As previously mentioned, coatings are applied to enhance or impart specific properties and characteristics to the substrate. To achieve this objective, it is crucial that the coating adheres well to the substrate without compromising the overall performance of the system. To assess adhesion, tests are conducted on both the coating and the substrate to analyze the level of adhesion. By evaluating how well coating adheres, one can investigate the pre-treatment processes of the component and examine how various parameters influence coating performance.

The American Society for Testing and Materials (ASTM) defines adhesion as "the state in which two surfaces are held together by interfacial forces which may consist of valence forces or interlocking forces or both." [86]. Experimental adhesion can be characterized as the maximum force per unit area applied when separating two materials, or as the work required to disconnect them. In practice, plastic deformation often occurs, complicating the assessment of true adhesion work [87].

The weak boundary layer theory elucidates that bond failure at an interface may arise from either cohesive failure or a compromised boundary layer. Such failures can take place in either the adhesive or adherend if impurities accumulate near the bonding surface, leading to weak connections with the substrate.

Bikerman identified seven distinct categories of weak boundary layers (see Figure 2.22), including air pockets, interface impurities, and chemical reactions between tw components [80][88].



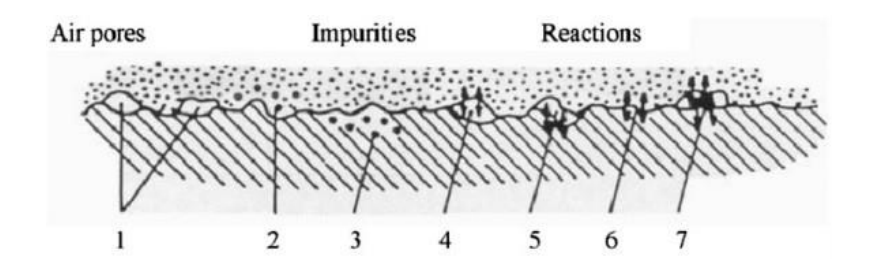


**Figure 2.22.** Theory of weak boundary layers. (1) air pores, (2) and (3) impurities at the interface, (4), (5), (6), and (7) reactions between the two materials [F29]

#### 2.4.1. Cause of failure

Different elements, whether acting individually or together, can stress the bond between a coating and its substrate, potentially leading to system failure (Figure 2.23). One of the primary causes of such failure is mechanical stress, which can affect both the bulk material and the interface zone. In this context, two prevalent types of stress are tensile stress, which acts perpendicular to the surface, and shear stress, which occurs along the plane of contact. Additionally, variations in temperature may also lead to system failure; when materials possess differing coefficients of thermal expansion, stress can develop at the interface. This situation is particularly problematic since the impact of temperature changes is often less noticeable compared to mechanical or chemical factors. Furthermore, a chemical cause for failure may arise if molecules like water, gases, or ions infiltrate the coating and reach the interface zone, resulting in diminished adhesion.

The nature of potential failures that can manifest during adhesion testing will vary based on the properties of both substrate and coating. Failure may initiate from the surface and propagate into the substrate (Figure 2.24) [85].



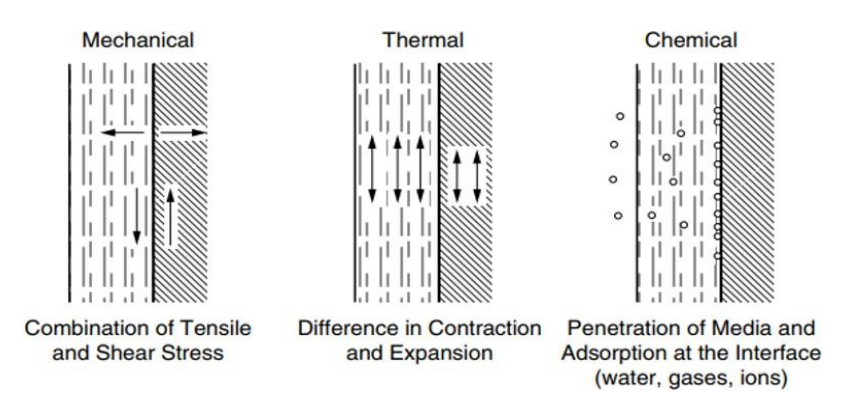


**Figure 2.23.** Cause of failure of coating/substrate system [F30]

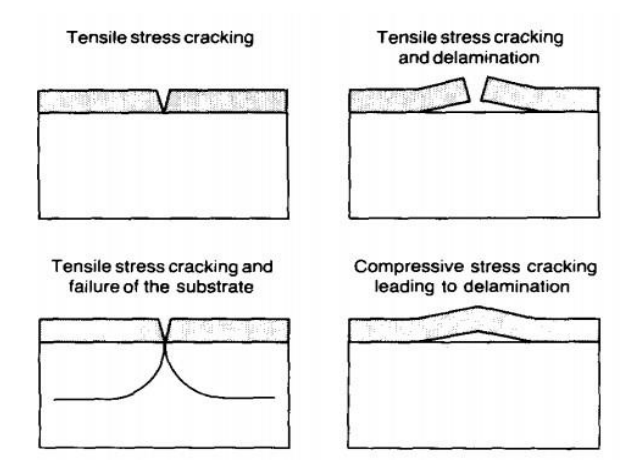


**Figure 2.24.** Types of failure of coating/substrate system [F33]

#### 2.4.2. Adhesion test

Adhesion testing techniques can be categorized into three main groups: nucleation methods, mechanical methods, and miscellaneous methods. Nucleation methods assess the failure of individual atomic bonds between the coating and substrate; the collective strength of these atomic forces results in overall macroscopic adhesion. These approaches rely on measuring factors such as nucleation rate, critical condensation, and the residence time of atoms during deposition. In contrast, mechanical methods involve various techniques to detach the coating from the substrate.



These can be further classified into two subcategories based on whether there is a normal detachment from the film's lateral surface relative to the substrate. Lastly, miscellaneous methods refer to techniques that do not qualify as practical tests but may hold academic significance [87][89].

The most widely utilized methods include:

Pull-off Test: This is the most straightforward and commonly employed assessment for determining the adhesion between a coating and its substrate. The ASTM D4541 standard outlines the necessary equipment and procedures: a dolly is affixed to the coated surface, which is then subjected to a perpendicular pulling force to detach the coating (see Figure 2.25) [89].

Typically, a two-component epoxy adhesive is used for bonding the dolly to the coating. This test allows for an evaluation of:

- 1. The maximum perpendicular force that can be applied to the surface area before material detachment occurs.
- 2. Whether the coating remains intact at a specified load.

However, this method has several drawbacks: it combines tensile and shear forces, making it challenging to differentiate and interpret them; perfect alignment at the interface is crucial for achieving uniform loading; and there is a risk that either the adhesive or solvent used during testing may infiltrate the coating, altering its properties and performance.

A pull-off test was carried out by Yanli Cai et al. on magnesium-containing hydroxyapatite (MgxFHA) coatings applied to a Ti-6Al-4V substrate. An aluminum rod was adhered to the coating surface with epoxy resin and allowed to cure at room temperature for 24 hours. Scanning Electron Microscopy (SEM) analysis was conducted to assess the mode of failure at the fracture interface. The outcomes of the pull-off tests on Mg0FHA (a) and Mg2FHA (b) coatings on Ti-6Al-4V are illustrated in Figure 2.26, revealing cohesive fractures in both instances [90].

A variation of this approach is the tangential shear or lap shear method, which involves applying a parallel force to the surface. The measured shear stress indicates the tangential force per unit area necessary to disrupt the bond between the coating and the substrate.

• **Ultra centrifugal method:** This technique eliminates the need for adhesives or solder by spinning the sample at extremely high velocities. Once a critical rotational speed is reached, the coating detaches from the substrate due to an inability to endure the centrifugal forces.



- Cross-cut test: To assess coating adhesion in this method, a lattice pattern is cut into the coating using various cutting tools. The evaluation relies on measuring how many flakes of coating detach from the substrate [85]. An illustrative example can be found in Figure 2.27.
- Scratch test: According to standard ASTM C1624-05 for scratch adhesion testing, different modes are defined for assessing both strength and failure of coatings applied on metallic or ceramic substrates. This test employs a diamond stylus to create a scratch on the coating's surface while applying a gradually increasing normal force at a consistent speed. Typically, a Rockwell C geometry stylus is utilized with varying radii to adjust contact pressure (Figure 2.28).

Upon completion of the scratch, microscopic examination of the surface reveals damages such as delamination, buckling, and deformation [91]. A critical load is established; this load signifies when separation between coating and substrate occurs consistently and correlates with both adhesion strength and damage resistance of the system. This value depends on characteristics of both the stylus and properties of the coating [87].

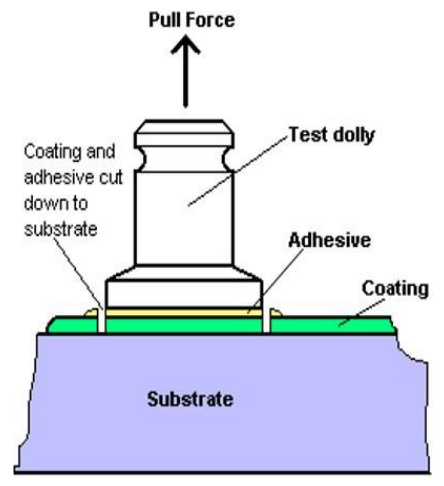


Figure 2.25. Pull-o test [F34]

As previously mentioned, the starch test can be conducted using three distinct methods:

- 1. **Constant Load**: In this approach, scratches are created by applying a uniform load. Additional scratches are produced by progressively increasing the load each time to identify the specific load that results in damage.
- 2. **Progressive Load**: This method involves applying a normal force with a linearly increasing load to create scratches. The critical load is defined as the threshold at which initial damage occurs.



3. **Incremental Load**: Here, scratches are formed by gradually increasing the applied load over time [91].

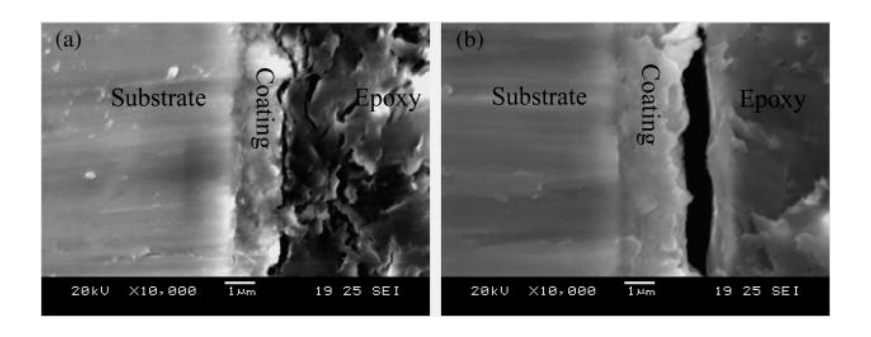


**Figure 2.26.** Cross-sectional view of (a) Mg0FHA and (b) Mg2FHA coatings on Ti6Al4V substrate [F35]

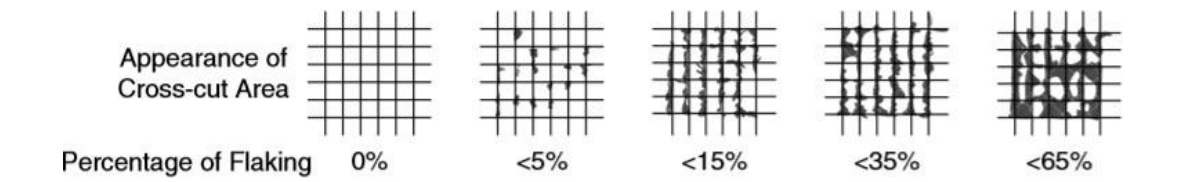


Figure 2.27. Cross-cut test [F36]

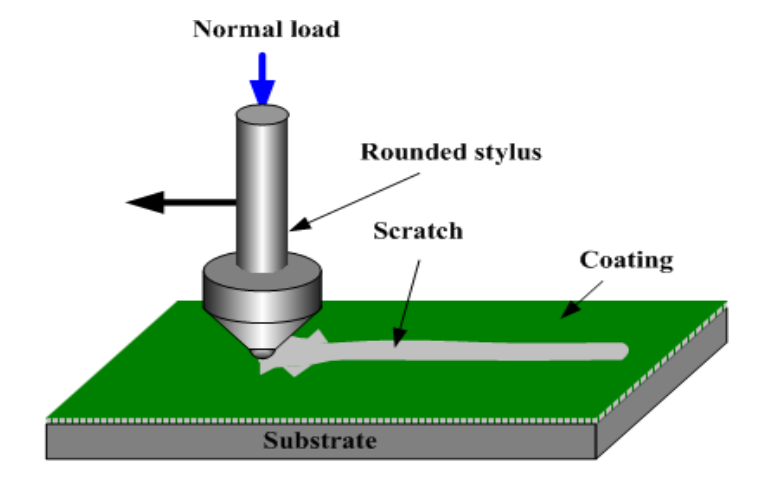
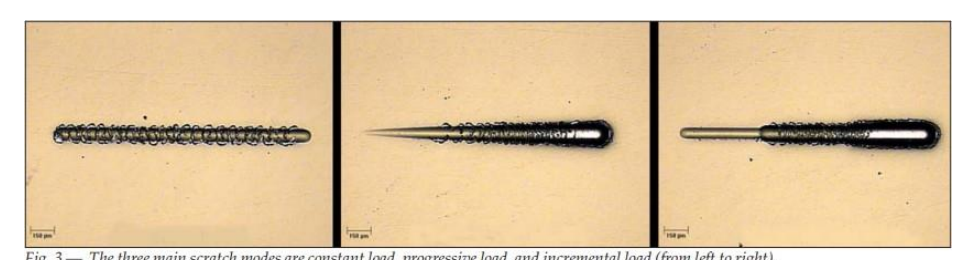


Figure 2.28. Scratch test [F37]



Figure 2.29 illustrates the scratches produced by various techniques. An acoustic emission sensor can be utilized to identify high-frequency elastic waves occurring within the coating/substrate system, signaling potential issues such as delamination, cracking, or chipping.



**Figure 2.29.** Three distinct scratch patterns were created through the application of constant load, progressive load, and incremental load. [F38]

Choudhary and Mishra investigated the adhesion properties of Aluminum Nitride coatings applied at various temperatures on a stainless-steel substrate, employing acoustic emission techniques during scratch testing. In Figure 2.30 (a), the acoustic emission curves obtained from scratch tests conducted at three distinct substrate temperatures are presented.

The recorded acoustic emissions remained relatively low, below 1.5%, indicating that the coating exhibits ductile characteristics and has a lower density of defects such as voids and cracks, along with minimal intrinsic stresses. The ductility of the AlN coating enhances with increased temperature; indeed, as depicted in Figure 2.30 (b), the penetration depth of the indenter rises when tested on coatings at elevated temperatures. Figure 2.31 displays optical images from a progressive scratch test performed on a coating developed at 400°C. Observations reveal that there is no adhesive delamination up to the maximum load of 20 N; furthermore, only minor pores appear along the scratch path after reaching this load [92].

Regarding indentation and shockwave-loading methods: a crack is induced at the interface between the coating and substrate through conventional indentation techniques. In this scenario, most deformation occurs within the film itself; however, there is some degree of debonding at the interface. The adhesion quality correlates with resistance to crack propagation. The bond between the coating and substrate is specifically linked to fracture resistance factors such as residual stress and defect strength control mechanisms.



This testing indicates that if cracks develop in the plastic zone created by indentation at the interface, this region will have reduced thickness compared to both coating and substrate layers involves residual stress and strength controlling defects. According to this test, should either the coating or substrate fail prior to interface separation occurring, then it can be concluded that the toughness of the interface is at least equal to that of its weaker component. Figure 2.32 illustrates a schematic representation of indentation adhesion for coatings and how crack size varies with increasing load levels. Certain methods aim to induce delamination through shockwave loading techniques using erosive particles or laser beams; outcomes depend significantly on how much energy is absorbed by the coating.

The laser technique utilizes a laser to examine the surface of a coating, where the energy absorbed creates a stress wave that can be detected. When the probing laser is pulsed, the movement of thermal waves aids in identifying areas with cracks or regions that have lost adhesion [87]. This investigation was carried out by Campos-Silva et al. to assess the adhesion between FeB and Fe2B on the boride surfaces of AISI 316 steel. Boriding is a thermochemical process aimed at enhancing hardness by diffusing boron into the clean surface of metal steel at elevated temperatures. Vickers interfacial indentation tests were conducted with loads ranging from 0.49 to 2.9 N, chosen according to the thickness of the FeB layer.

The results, illustrated in Figure 2.33, indicate that fracture resistance at the interface correlates with FeB layer thickness: an increase in this thickness enhances resistance against crack initiation and propagation at the interface. Similar trends were observed under various boriding conditions for the adherence of the FeB/Fe2B system. Furthermore, it was found that both compressive behavior and residual stress intensity diminished as the thickness of the FeB coating increased [93].

**Impact Test:** This test is crucial for assessing the resistance of coatings to stone chips. A steel ball strikes the surface, causing force transmission through the coating that results in debonding. Within the debonded region, two types of stress occur: compressive stress at the center of the circular detachment area and shear stress in the surrounding annular zone. By analyzing the dimensions of this debonding region, one can evaluate the adhesive forces of the coating (see Figure 2.34). Several factors must be considered in this assessment, including coating thickness, mass, diameter and velocity of the steel ball, as well as impact duration [85].



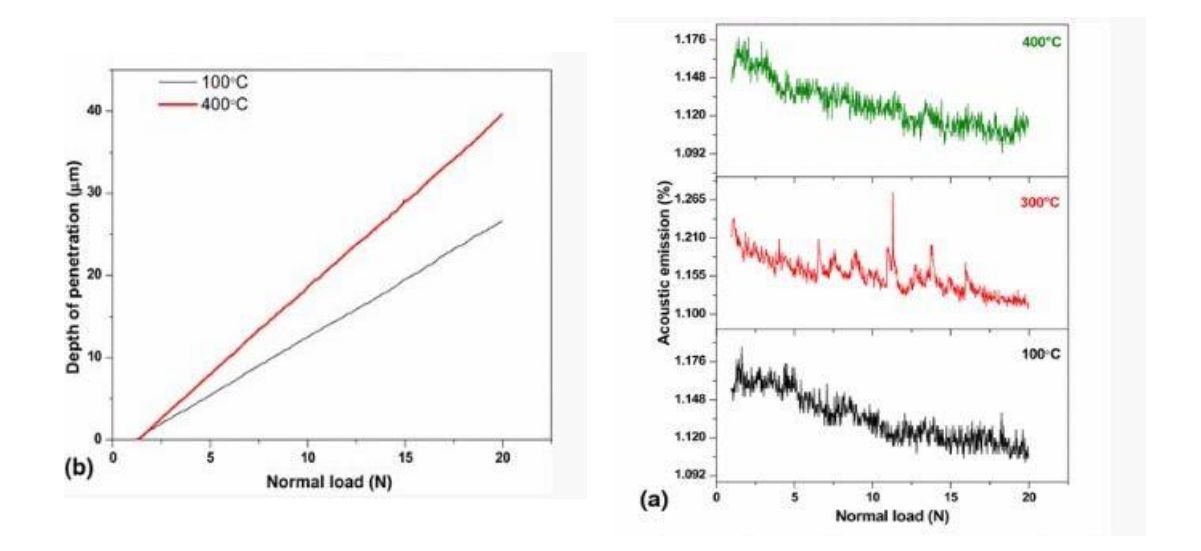


**Figure 2.30**. (a) acoustic emission and (b) penetration depth curves obtained by scratch test on AlN coatings formed at different temperatures [F38].

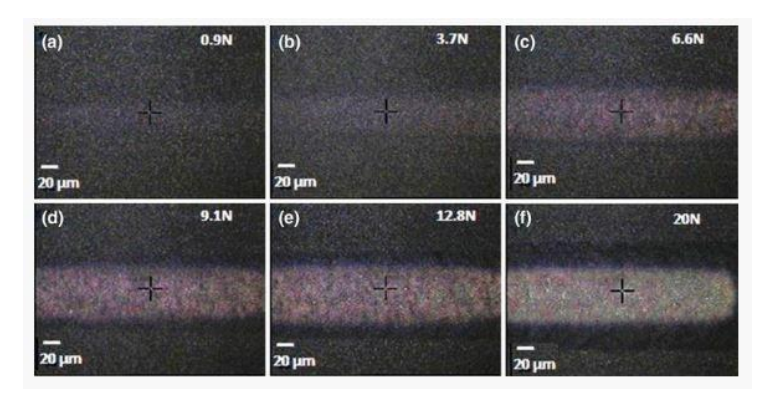


**Figure 2.31.** Optical scratch images obtained on AlN coating at different loads [F43]

Bouzakis et al. investigated the adhesion properties of TiAlN coatings produced via PVD using a nano-impact testing method. In this process, an indenter approaches and then re-accelerates from a short distance towards the film's surface. The automation used allows for repeated impacts at a designated location on the sample surface at a predetermined frequency. The progression of indentation depth during these successive impacts is monitored continuously.



The findings were compared with results derived from Finite Element Method (FEM) calculations. These comparisons indicate that the developed FEM simulation model can accurately describe loading conditions, fracture initiation, and subsequent evolution within the film [94].

**Thermographic Detection of Defects:** This technique enables the creation of a temperature distribution map on the surface. It allows for the identification of defects and areas of debonding, as the heat flux moves towards the surface uniformly unless interrupted by a defect or debonded section, which leads to variations in surface temperature, as illustrated in Figure 2.35 [85].

**Blister Method:** This approach involves injecting a fluid at the junction between the coating and substrate. The resulting increase in hydrostatic pressure causes the coating to detach from the underlying surface.

**X-ray Method:** This non-destructive technique utilizes X-ray spectroscopy to qualitatively assess the adhesion of epitaxial coatings applied to single-crystal substrates and evaluate bond strength. However, this method is applicable only under specific conditions and does not yield quantitative results.

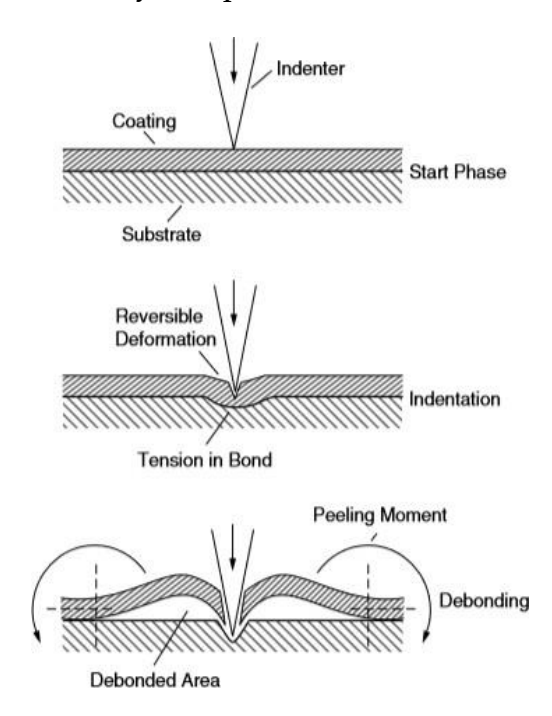


**Figure 2.32.** Indentation coating [F43]



**Pulsed Laser or Electron Beam Method:** In this process, only part of the substrate is coated while a laser or electron beam generates a compressive stress wave on the uncovered surface. This wave travels through the material, reflects off the coated surface, and transforms into a tensile wave [95].

# 2.5. Influence of different factors on coating adhesion

In any application, the effectiveness of the end product hinges on the bond established between the coating and the substrate. Consequently, numerous studies have been conducted to identify the factors influencing adhesion and enhancing system characteristics.

For instance, surface treatments can significantly improve interfacial adhesion between coatings and substrates. A well-prepared surface is crucial for achieving optimal adhesion and forming a robust bond at the interface. Primarily, it is essential that the surface is free from contaminants; any absorbed molecules must be removed as they can evaporate upon contact with the coating, leading to splattering and pore formation. This ultimately results in reduced mechanical performance of both the coating and substrate along with diminished adherence [96].

Moura e Silva et al. [97] investigated adhesion issues in two systems: coatings of W-Ti-N and W-DLC:H (W-Diamond Like Carbon), applied using reactive unbalanced magnetron sputtering on (111) mono-oriented silicon and AISI M2 high-speed steel substrates. The substrates underwent cleaning in ultrasonic baths containing acetone and ethanol before being placed into the deposition chamber. Prior to deposition, they were subjected to ion bombardment for additional cleaning. The findings were compared against earlier analyses conducted at a laboratory level on similar types of coatings. Results from scratch tests indicated that the critical load, which depends on the partial pressure of reactive gas, was lower for industrially deposited W-Ti-N coatings compared to those deposited in laboratory conditions.



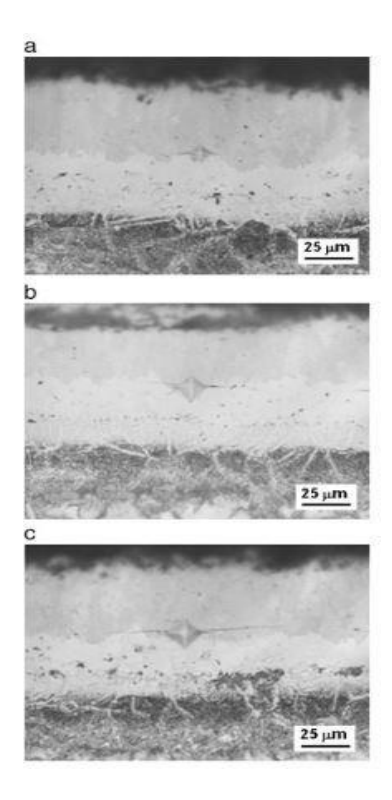


**Figure 2.33.** Vickers interfacial fracture toughness on FeB/F e2B system: (a) 0.98 N, (b) 1.96 N, and (c) b2.94 N [F44]

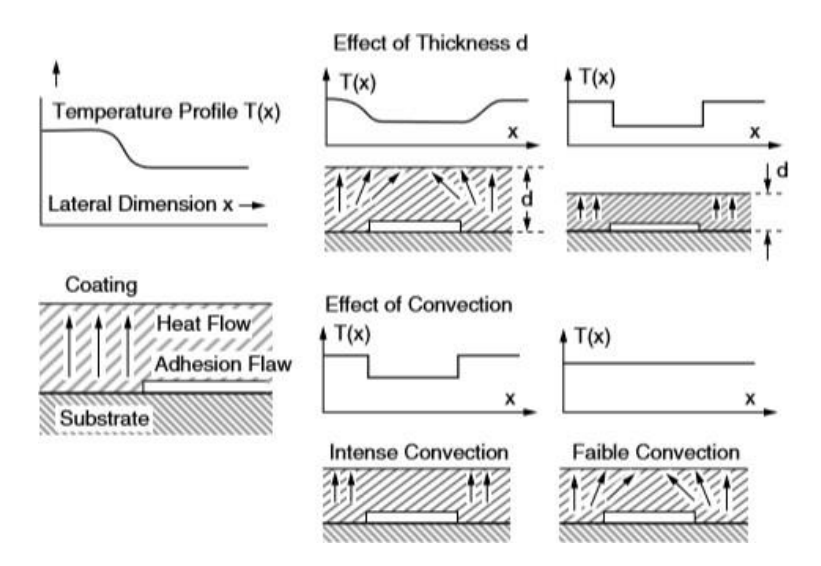


**Figure 2.34.** Schematic representation of thermographic detection of debonding area [F45]



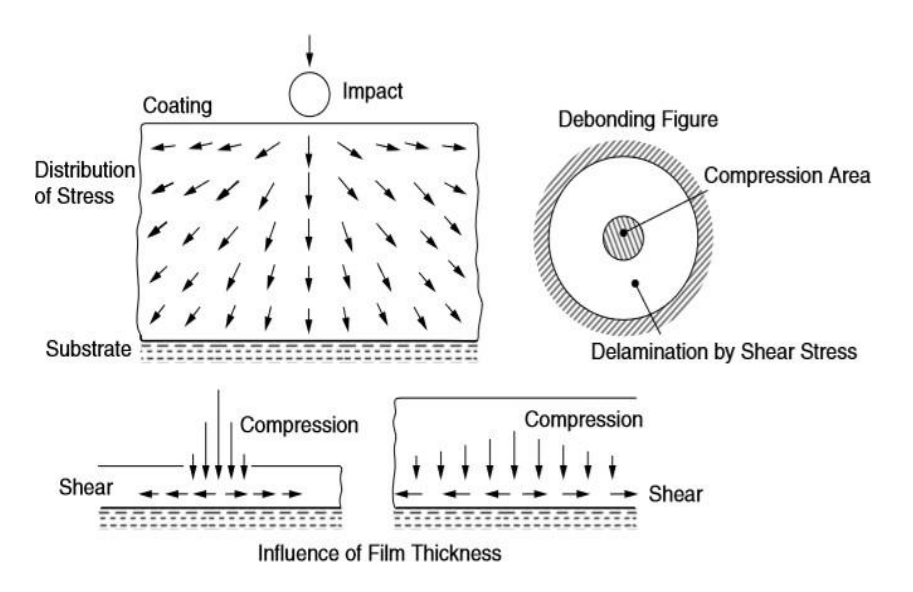


Figure 2.35. Impact test and stress involved [F45]

The findings for W-DLC:H coatings are consistent with previous results. To investigate the adhesion issue, an elemental spectrum obtained through RBS/ERDA (Rutherford Backscattering Spectrometry/Elastic Recoil Detection Analysis) was performed on W-DLC:H, which indicated a buildup of W at the substrate/interlayer boundary. For the W-Ti-N coating, Auger spectroscopy was conducted to determine whether contamination at the interface could be attributed to oxygen present in the residual atmosphere within the deposition chamber.

A very thin layer of W-Ti-N was applied to facilitate in-depth step analysis through Auger spectroscopy following the ion bombardment etching of the sample surface (Figure 2.36). The findings indicate that there is no marked increase in oxygen at the interface; however, an unexpected rise in W and Ti has resulted in the formation of a sub-layer between the coating and substrate. This is corroborated by the presence of a contamination layer, which is amorphous and exhibits uniform thickness, identified as the reason for adhesion failure, as illustrated in Figure 2.37 from TEM analysis. Another crucial factor influencing coating adhesion to a substrate is surface roughness: it enhances the contact area for particle-to-substrate interaction and improves coating anchorage. To achieve an appropriate surface profile while reducing grease and facilitating chemical and morphological alterations, degreasing and sandblasting techniques are employed.



The resulting surface features peaks and valleys created by high-velocity abrasive particles' impact. Following sandblasting, residual dust must be eliminated from the substrate using a solvent, after which it should be dried with clean compressed air. It is essential to apply the coating immediately after preparation to avoid oxidation and contamination [98].

Varacalle et al. [99] investigated the adhesion properties of Al and Al-Zn coatings on A36/1020 steel deposited via twin-wire electric arc (TWEA). The substrates were prepped using grit-blasting with both conventional grit (copper slag, coal slag, and chilled iron) and metallic grit.

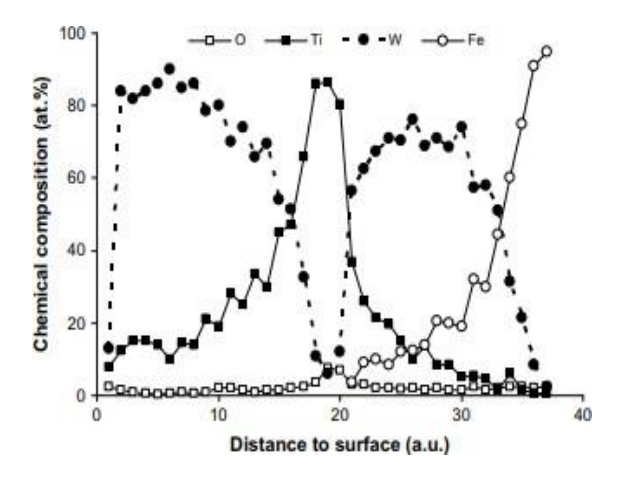


**Figure 2.36.** Auger in-depth pro le chemical composition results of a W Ti coating [F46]

They measured bond strength of the coatings and found that metallic grit generated greater surface roughness compared to conventional options. For Al coatings regarding their deposition method, they discovered correlations between bond strength and various factors: increased current significantly enhances bond strength, while spray distance and lower pressure have a lesser impact on adhesion force enhancement. In cases involving Al-Zn coated substrates, higher bond strength was also observed on surfaces treated with metallic grit, consistent with earlier findings. However, grit-blasting has its drawbacks: it can induce microcracks in the substrate leading to reduced mechanical properties, alongside concerns regarding chemical waste disposal [100]. As previously mentioned, sand inclusion on surfaces may yield counterproductive effects by diminishing coating adhesion. To mitigate these issues, physical and chemical modifications necessary for improved adhesion are achieved through innovative pretreatment solutions.



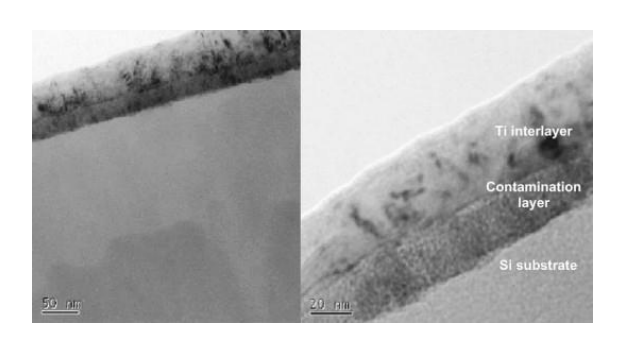


**Figure 2.37.** HR-TEM micrographs of the interface substrate/interlayer zone of a W DLC:H coating [F46]

Danlos et al. [100] explored an alternative approach for cleaning and preparing substrate surfaces utilizing a laser. This innovative technique merges the processes of cleaning and heating via lasers, which takes place prior to applying a coating using thermal spray methods. The process employs two lasers: a millisecond laser that heats the surface and a nanosecond ablation laser that cleans it (Figure 2.37). To enhance efficiency and achieve optimal surface temperatures, a delay is strategically implemented between the activation of the two lasers.

Preheating with laser technology is crucial to prevent substrate distortion or soot accumulation that often occurs with conventional methods. In their study, they examined two types of substrates: Aluminum alloy 2107 and titanium alloy Ti-6Al-4V, both of which were polished to a mirror finish before undergoing laser treatment. A scanning electron microscope (SEM) was used to analyze the morphologies of the surfaces, as depicted in Figure 2.39.

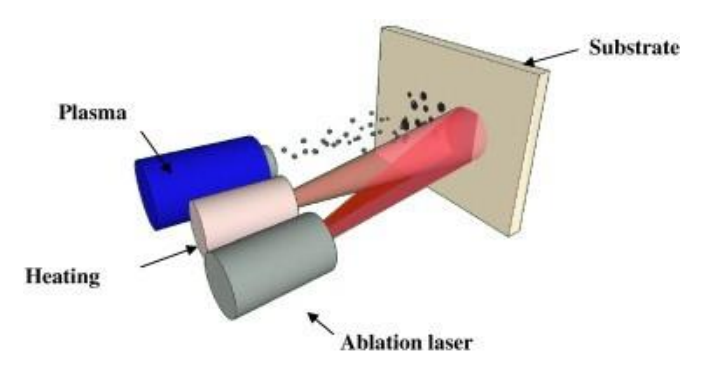


**Figure 2.38.** Representation of the device for laser treatment and thermal spray [F47]



This figure illustrates the differences between Aluminum 2107 (1) and Ti-6Al-4V (2) substrates at various stages: prior to treatment (a), after sandblasting (b), post-laser preheating (c), and following laser ablation (d). It is evident from the figure that the surfaces after sandblasting exhibit greater roughness compared to those before treatment due to high-velocity particle impacts on the substrates.

This figure illustrates the differences between Aluminum 2107 (1) and Ti-6Al-4V (2) substrates at various stages: prior to treatment (a), after sandblasting (b), post-laser preheating (c), and following laser ablation (d). It is evident from the figure that the surfaces after sandblasting exhibit greater roughness compared to those before treatment due to high-velocity particle impacts on the substrates.

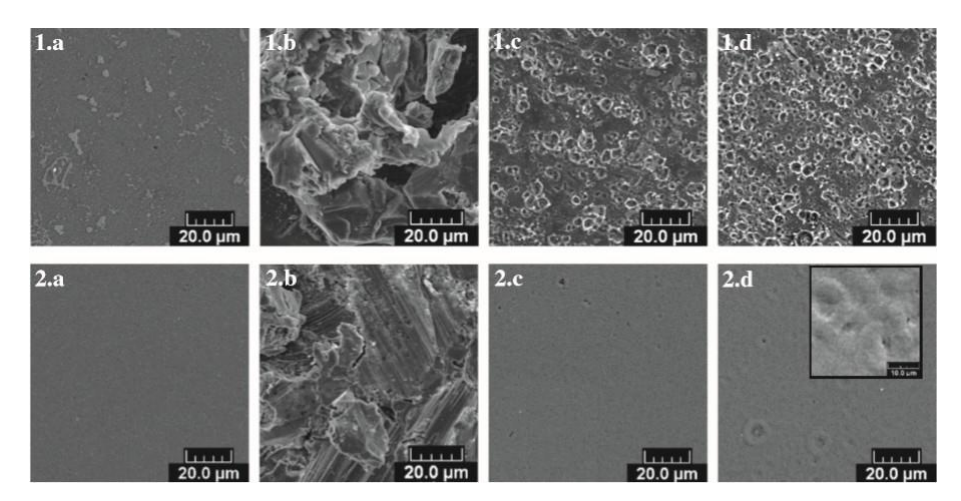


**Figure 2.39.** SEM observations of Aluminum 2017(1) and Ti-6Al-4V (2) surfaces, (a) reference; (b) sand- blasted; (c) preheated by laser and (d) ablated by laser [F47]

Significant differences are observed between Aluminum 2107 and Ti-6Al-4V following laser treatments: Aluminum 2107 displays an irregular surface with numerous craters, while Ti-6Al-4V achieves a smoother plane surface after preheating and ablation procedures. These variations relate to their differing thermal properties; Aluminum 2107 possesses higher mass heat capacity and thermal conductivity than its titanium counterpart, allowing it to dissipate thermal energy more effectively. Although Ti-6Al-4V has high absorptivity, it requires more energy to melt compared to Aluminum 2017, making the latter more responsive to temperature increases.



Furthermore, thermal diffusivity differs between the two materials: in Aluminum 2107, it is sufficiently high to promote thermal energy dissipation throughout its volume, leading energy concentration not just on surface defects but also deeper imperfections. Consequently, this results in increased crater formation; conversely, fewer craters appear on Ti-6Al-4V as energy remains focused on the surface, resulting in melting.

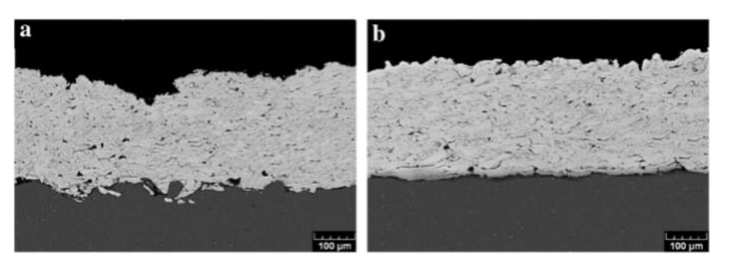


**Figure 2.40.** Cross section of Ni Al coatings on Aluminum 2107 surfaces sandblasted (a) and preheated (b) [F47]

To assess adhesion properties, a Ni-Al coating was applied on both sandblasted (a) and laser-treated (b) surfaces of Aluminum 2107 as illustrated in Figure 2.40, along with samples of Ti-6Al-4V. The results reveal that while the sandblasted surface's roughness allows molten particles to infiltrate its asperities—slowing crack propagation—the coating does not fully adhere at all points due to voids and grain inclusions present at the interface. In contrast, the irradiated surface demonstrates smoothness with effective contact between coating and substrate.

Adhesion assessments via interfacial indentation reveal a direct correlation between adhesion strength and roughness; specifically, interfacial adhesion is greater on sandblasted surfaces. Morphologically speaking, under identical laser treatments, Ti-6Al-4V exhibits smoother surfaces than those of Aluminum 2107. Regarding adhesion values, findings indicate that beyond mechanical anchorage factors play an important role through chemical affinity as well. An oxide layer has been identified on aluminum surfaces enhancing wettability and thereby increasing coating adhesion; however, no oxygen presence was detected on Aluminum 2107's surface. Therefore, a combination of mechanical anchorage along with chemical affinity appears most conducive for enhancing interfacial adhesion. Another laser technique aimed at enhancing the bond strength at the interface is the texturing laser. This method involves creating holes of specific diameters on the surface in accordance with a predetermined pattern (see Figure 2.41).



The effectiveness of this approach relies on parameters related to the laser and scanner, including hole geometry, as well as the frequency and power of the laser. These induced chemical and mechanical alterations expand the contact area between the coating and substrate.

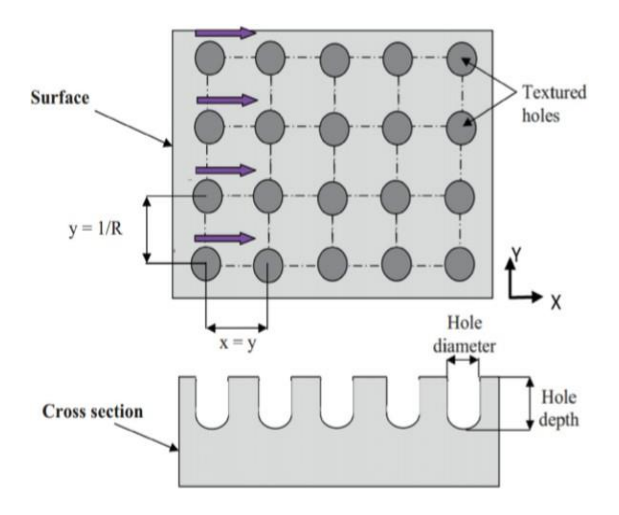
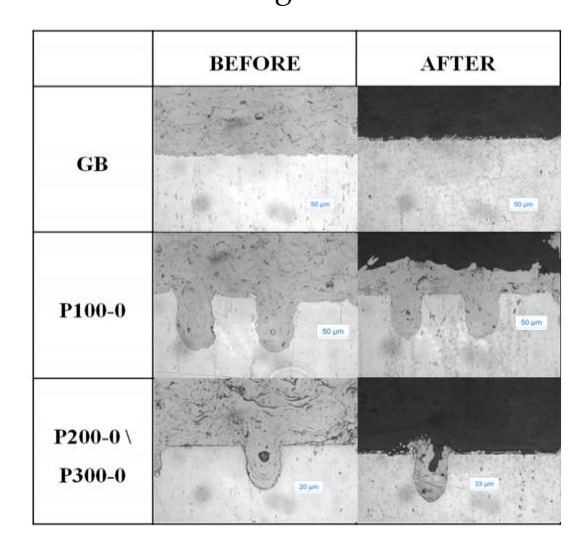


Figure 2.41. Schematic representation of laser textured surface [F48]

In their research, Kromer et al. examined how a Ni-Al coating, applied via atmospheric plasma spray, adhered to aluminum surfaces treated in two distinct manners: one through grit-blasting and another utilizing a laser surface texturing technique.



**Figure 2.42.** Different interface characteristics before and after tensile test for gritblasted surface, 100 µm distant holes and 200 300 µm distant laser holes [F48]



Both types of surfaces were analyzed both prior to and following the application of the coatings. For the laser-treated method, coating adhesion is influenced by factors such as pattern geometry and surface roughness; specifically, hole dimensions must correspond to both the average size of the sprayed powder and its viscosity. Additionally, optimizing hole depth and shape is crucial for minimizing stress concentration effects. Adhesion was assessed through two different tests: pull-off and LASER adhesion test (LASAT). Plasma-induced surface compression leads to relaxation that propagates throughout the sample, resulting in volumetric movement toward the rear surface. Damage detection can be achieved by measuring rear free surface velocity, which correlates with shock wave propagation as well as adhesion force. Results from pull-off testing indicate that surfaces treated with lasers yield stronger bonds compared to those treated conventionally via grit blasting; however, it was also observed that hole angle does not significantly affect adhesion values.

Figure 2.44 displays surfaces subjected to grit blasting versus those treated with lasers (with varying distances between holes) before and after testing.

The anchoring effect of these holes is clear; moreover, the morphology produced by laser treatment enhances crack energy release rates. Figure 2.45 illustrates results from LASAT testing. Both pull-off tests and LASAT results consistently show that bond strength on laser-treated surfaces surpasses that on grit-blasted ones. It has been noted that tighter patterning increases the energy required to separate the coating from its bond.

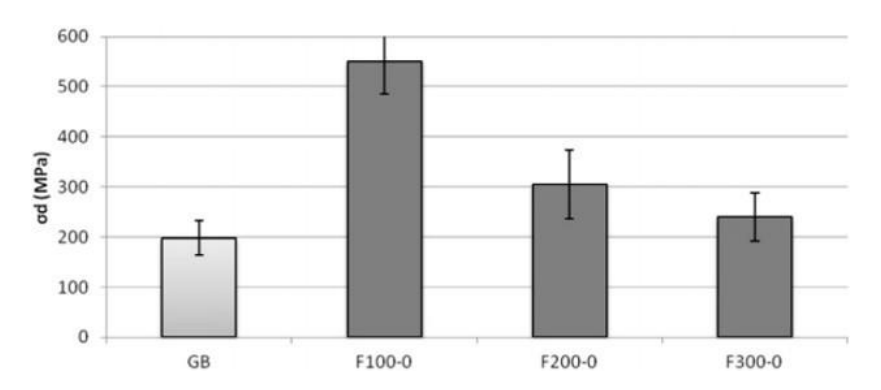
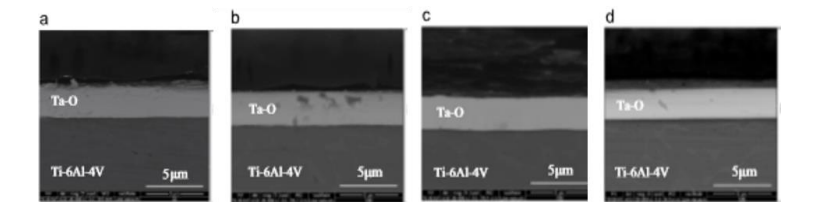


Figure 2.43. Debonding strengths determined from LASAT of different surfaces [F48]



Laser surface texturing allows you to obtain a better coating adhesion to the substrate. Is it possible to explain this considering that the crack propagating follows the surface. Holes represent obstacles, which increase the necessary energy for a crack to propagate. With tightened surfaces, the energy required to propagate at the interface is too high due to the irregularities, and crack propagates through coating [101]. Another crucial parameter in this process is the temperature during substrate treatment. Rahmati et al. investigated its influence by analyzing Ti-6Al-4V substrates coated with Ta-O that were subjected to heat treatments at 300°C, 400°C, and 500°C. The bond strength was assessed using scratch tests. Figures 2.44 and 2.45 illustrate FESEM images of Ti-6Al-4V samples: (a) untreated, (b) treated at 300°C, (c) treated at 400°C, and (d) treated at 500°C. These images reveal that varying treatment temperatures result in distinct morphological changes; specifically, higher temperatures lead to denser and smoother coatings temperatures result in distinct morphological changes; specifically, higher temperatures lead to denser and smoother coatings. Energy dispersive X-ray analysis indicates that surfaces treated at elevated temperatures exhibit a greater percentage of oxygen content, while untreated surfaces show the lowest levels of oxidation



**Figure 2.44.** FESEM cross-sectional micrographs of coated samples: (a) untreated surface, (b) treated surface at 300°C, (c) treated surface at 400°C, and (d) treated surface at 500°C [F49]

This suggests a gradual increase in oxidation during thermal treatment. Scratch test results demonstrate that adhesion values are highest for the system treated at 500°C, indicating an overall trend where adhesion improves with rising temperature.

This enhancement is attributed to the denser morphology achieved at higher temperatures, which strengthens adhesion to the substrate. Additionally, increased oxygen presence plays a significant role; free oxygen in the furnace reacts with tantalum to form Ta2O5 [102].



# 2.6. Other considerations

During the coating deposition process, various challenges can arise. To achieve a strong bond at the interface, it is crucial to be aware of potential issues and to identify solutions. One such issue involves sagging and slumping, which typically occurs in coatings applied to sloped surfaces, especially vertical ones. The influence of gravity causes a downward flow that can result in either sagging or slumping, depending on the characteristics of the coating fluid. To address this problem, managing the viscosity of the coating is essential; specifically, utilizing either a purely Newtonian or sheer-thinning system is recommended.

Additionally, during deposition, the applied material often lacks uniformity, leading to defects like waves or furrows. In this context, surface tension and coating viscosity play significant roles. The solution lies in leveling the coating, which helps reduce the film's surface tension. When a film is deposited around a corner, changes in surface tension may affect the thickness of the coating (see Figure 2.46) [87].

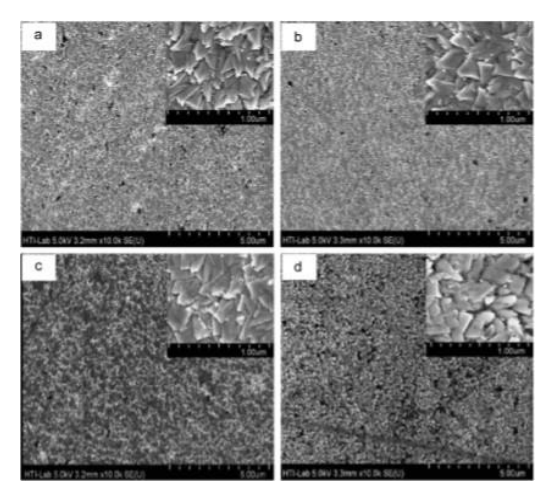


**Figure 2.45.** FESEM surface topography of Ti-6Al-4V: (a) untreated surface, (b) treated surface at 300°C, (c) treated surface at 400°C, and (d) treated surface at 500°C [F49]

If there is a gradient in surface tension across the surface, it can lead to local distortions. The movement of liquids from areas with lower surface tension to those with higher tension, driven by this gradient, results in the creation of depressions on the liquid's surface.



As polymer concentration increases and solvent evaporation leads to cooling, both the surface tension and density at the surface rise above those found in the bulk liquid. This situation establishes an unstable arrangement that seeks a more stable one where the surface material exhibits decreased surface tension and density.

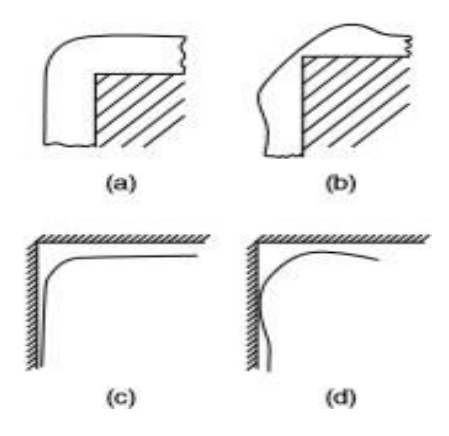


**Figure 2.46.** (a) Newly applied thick film at a corner; (b) decrease in the film thickness at the corner due to surface tension at a corner; (c) newly applied thin film at a corner; (d) increase in the film thickness at the corner due to surface tension [F50]

Additionally, craters—circular depressions on a liquid's surface—can form due to a low surface tension component present at the film's upper layer. The dispersion of this low-surface-tension component induces a bulk transfer of film materials, ultimately resulting in crater format.

# 2.7. Application of coated titanium in the automotive industry

To overview the actual combustion process generates exhaust gases. The exhaust system's main role is to bring the combustion gases or waste gases from the combustion process away from the engine to an exit point, generally at the rear of the vehicle, the tailpipe. The gases are toxic, hot, and corrosive, so they need to be removed from the occupants and also away from any sensitive mechanical components. It begins after the engine, where the heat shield protects areas near the air cleaner.



Underneath, we have the exhaust headers or manifold. The manifold's main function is to gather the gases. Exhaust gases come out of the cylinder head through exhaust ports into the manifold. In the exhaust header, the temperature is about 800°C.

The gases make their way along the pipe as they move and cool down. Once we reach the catalytic converter, the temperature is around 400-450°C. At the end of the tailpipe, the temperature is around 100-200°C. Thus, we have studied the cooling of the gases as they move through this system.

An automobile's exhaust system consists of multiple components. This system includes tubing designed to channel waste gases resulting from controlled combustion within the engine. The burnt gases are expelled through one or more exhaust pipes. Various devices, such as the cylinder head, exhaust manifold, turbocharger, catalytic converter, muffler, and silencer, facilitate the expulsion of these gases [111].

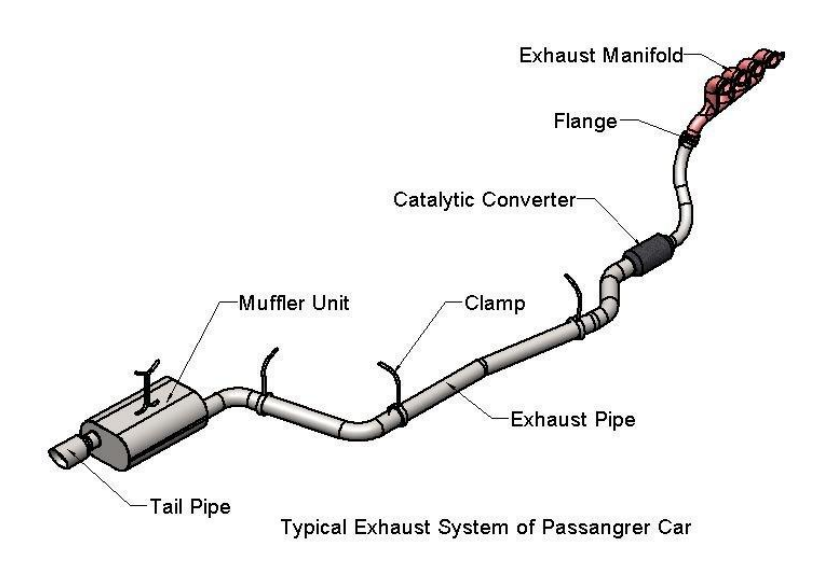


**Figure 2.47**. Typical Exhaust System model used in passenger cars and its components [F51]

#### **Foundational Concepts**

Coated titanium has become a vital component in the automotive industry due to its unique properties, which include:



High Strength-to-Weight Ratio: Titanium is known for being as strong as steel but much lighter, making it ideal for automotive applications where reducing weight is crucial for fuel efficiency [103].

Corrosion Resistance: Titanium exhibits excellent resistance to corrosion, particularly in harsh environments, which is beneficial for automotive components exposed to various chemicals and weather conditions [104].

Thermal Stability: With a high melting point and thermal conductivity, titanium can withstand extreme temperatures without losing its structural integrity [105].

### **Current Impact**

Today, glass ceramic coatings are integral to exhaust systems, offering several advantages:

Enhanced Durability: These coatings significantly increase the lifespan of exhaust components by providing a protective layer against oxidation and thermal fatigue [106]. Improved Performance: By insulating exhaust components, glass ceramic coatings help maintain optimal operating temperatures, improving overall engine efficiency [107].

Aesthetic Appeal: Glass ceramic coatings can provide a visually appealing finish, enhancing the vehicle's appearance [108].

#### **Potential Future Implications**

Looking ahead, the implications of using glass ceramic coatings in exhaust systems include:

Advancements in Engine Technologies: As automotive technologies evolve towards hybrid and electric vehicles, the demand for lightweight and efficient exhaust systems will increase, making coatings like glass ceramic even more essential [109]. Sustainability: Research into eco-friendly coating materials may lead to more sustainable production processes, aligning with the automotive industry's shift towards greener technologies [110].

In conclusion, the application of coated titanium and glass ceramic coatings in the automotive industry represents a convergence of material science and engineering innovation. Together, they enhance vehicle performance, durability, and efficiency, addressing the industry's evolving challenges and opportunities. As research continues to advance, the potential for new applications and improved technologies remains significant, paving the way for a more sustainable and efficient automotive future.



## 2.7.1. Cost and Feasibility Analysis

This report outlines the cost and feasibility of applying glass-ceramic coatings to titanium alloy exhaust systems in high-performance automotive applications. The analysis focuses on the application method, coating material, and thickness, alongside a comparative study of Chemical Vapor Deposition (CVD) and thermal spray techniques. The findings indicate that while CVD offers superior performance, cost and scalability challenges must be addressed for broader application [112].

The automotive industry continually seeks innovative solutions to enhance performance, durability, and weight efficiency. Titanium alloys, known for their excellent strength-to-weight ratio, are increasingly used in exhaust systems.

This report evaluates the economic and practical aspects of applying glass-ceramic coatings via CVD to titanium exhaust systems, focusing on cost implications, lifecycle benefits, and comparative analysis with alternative coating methods [113].

To determine the cost per square meter, three essential elements should be taken into account: the method of application, the type of coating material, and the thickness of the coating. In practical applications within high-temperature automotive settings, an assessment of costs and feasibility was performed for a glass-ceramic coating applied through chemical vapor deposition (CVD) on a titanium alloy exhaust system [112].

The thickness of titanium alloy utilized in sports car exhaust systems may vary based on design, manufacturer specifications, and specific components. Generally, exhaust pipes have a thickness ranging from 0.5 mm to 1.5 mm to ensure mechanical strength and weight optimization. Conversely, flanges, brackets, and smaller parts can be thicker, typically between 2 mm to 4 mm depending on structural demands. Heat shields or liners made from titanium are generally thinner as well, falling within the range of approximately 0.3 mm to 1 mm. Sports cars frequently utilize thinner sections of titanium compared to heavier vehicles due to titanium's favorable strength-to-weight ratio that permits durability at reduced thicknesses while contributing to overall weight reduction [113-115].

For high-performance or racing uses where thermal resistance is paramount, thicker coatings (around 75–100  $\mu$ m) may be employed. Leading providers like Jet-Hot and Cerakote usually apply ceramic coatings for exhausts in a range between 50  $\mu$ m and 75  $\mu$ m depending on specific requirements [114-115].



In the experimental phase, two samples of titanium were analyzed: one sourced from Titanium substrate (China) with a base thickness of 171  $\mu m$  and a minimum coating thickness of 75  $\mu m$ ; another Ti substrate grade 2 sample had a base thickness of 491.3  $\mu m$  with a minimum coating thickness set at 100  $\mu m$ . When protective or oxidation-resistant coatings are added to titanium alloys—such as those used in exhaust systems—the substrate's thickness typically remains unchanged while the coating forms an additional layer atop the surface.

To approximate the surface area that requires coating, simplified geometric shapes can be utilized; in this case, it is estimated at approximately 1.5 m<sup>2</sup>. To calculate the area for cylindrical pipes (or mufflers), use the formula:

$$A = 2\pi rh + 2\pi r^2$$

- To analyze the costs associated with CVD-applied glass-ceramic coatings on titanium exhaust systems.
- To compare the economic feasibility of CVD with thermal spray methods.
- To assess the lifecycle benefits and return on investment (ROI) for coated exhaust systems.

#### The analysis is based on a cost model that considers:

To assess the economic and practical feasibility of using a CVD-applied glass-ceramic coating on a titanium exhaust system, a cost model was developed. The coating is applied over an area of approximately  $1.5~\text{m}^2$  with a substantial thickness  $75~\mu\text{m}$  glass-ceramic coating is estimated at  $180/\text{m}^2$ . This yields a base coating cost of  $\xi$ 270. Including processing overheads such as surface cleaning, masking, energy consumption, labor, and post-coating inspection, the total cost per exhaust system is approximately  $\xi$ 330 (Table 2.1.).



**Table 2.1.** Cost analysis of CVD coatings (thickness 75 μm) for titanium exhaust systems

Parameter	Value	Notes
	CVD (Chemical Vapor Deposition)	Suitable for glass-ceramic coatings
Coating material	Glass-ceramic	High-temperature protection
Coating thickness	75 μm	Thin layer – cost-effective
Estimated surface area	1.5 m <sup>2</sup>	Total surface of exhaust system
Coating cost per m <sup>2</sup>	€ 180	Typical for thick CVD coatings
Base coating cost	€ 270	1.5 m <sup>2</sup> × €180/m <sup>2</sup>
Labor + Overhead per unit	€ 60	Estimated based on pre-treatment, masking, energy consumption, and quality control measures
Total estimated cost	€ 330	Cost per coated exhaust system

**Table 2.2.** Cost analysis of CVD coatings (thickness 100 μm) for titanium exhaust systems

Parameter	Value Notes		
Coating method	CVD	Suitable for dense, adherent coatings	
Coating material	Glass-ceramic	High thermal stability	
Coating thickness	100 μm	Balanced protection and material usage	
Surface area	1.5 m <sup>2</sup>	Full exhaust system coverage	
Estimated cost per m <sup>2</sup>	€ 200	Adjusted for moderate thickness	
Base coating cost	€ 300	1.5 m <sup>2</sup> × €200/m <sup>2</sup>	
Labor + processing overhead	€ 65	Estimated based on pre-treatment, masking, energy consumption, and quality control measures	
Total cost per unit	€ 365	For one coated exhaust system	

The second sample coating thickness of  $100 \, \mu m$ . Due to the increased material volume, the estimated coating cost is approximately  $\epsilon 200/m^2$ , leading to a base coating cost of  $\epsilon 300$ .



**Table 2.3.** Property of Titanium sample

Titanium Grade 2 (per ASTM B348)			
Property	Value		
Standard	ASTM B348		
Grade	2 (Commercially Pure Titanium)		
Tensile Strength (min)	~345 MPa		
Yield Strength (min)	~275 MPa		
Elongation	~20%		
Companion Desistantes	Excellent (especially in saline/body		
Corrosion Resistance	fluids)		
Biocompatibility	Excellent		
Used in	Dental implants, bone plates, screws		

Additional process-related costs, including surface treatment, masking, and quality control, bring the total per-part cost to approximately €365 (Table 2.2.).

#### Lifecycle Cost and ROI

Return on Investment (ROI) is a financial metric used to evaluate the profitability or efficiency of an investment. It measures the return relative to the investment cost, expressed as a percentage. A higher ROI indicates a more profitable investment. The formula for calculating ROI is:

$$\mathrm{ROI} = \frac{\mathrm{Net\ Return\ (or\ Benefit) - Investment\ Cost}}{\mathrm{Investment\ Cost}} \times 100$$

#### Where:

Net Profit is the total savings or gains from the investment minus the initial investment cost.

Investment Cost is the cost incurred to make the investment.

Lifecycle Cost and ROI Considerations. Assuming an untreated titanium exhaust system requires replacement after 3 years due to oxidation-related degradation, while the CVD glass-ceramic coated system extends lifespan to 9 years, the coating yields a 3× durability improvement.



If exhaust system replacement costs  $\in$ 700 (materials + labor), this translates into savings of  $\in$ 1400 over two avoided replacements. Subtracting the  $\in$ 330 coating cost results in net savings of  $\in$ 1070, indicating a strong return on investment.

Number of replacements = 9 years/3 years=3 times

#### Replacement cost of exhaust system:

Thus, the total replacement cost for the untreated exhaust system over the 9-year lifespan of the CVD-coated system is €2100. This figure is essential for calculating the net profit and ROI when comparing the costs of untreated versus CVD-coated exhaust systems.

- Net Return (Benefit) = Total savings or cost avoided = €2100 (cost of 3 replacements avoided by using coated system)
- Investment Cost = €330 (coated exhaust system)

$$ext{ROI} = rac{2100 - 330}{330} imes 100 = rac{1770}{330} imes 100 pprox 536.36\%$$

Table 2.2. Also calculated and result is ROI = 475%.

It means, for every €1 you invest in the coated exhaust system, you are effectively saving or gaining about €5.36 in avoided maintenance or replacement expenses. So, instead of spending money repeatedly on replacements, this one-time investment in the coating yields substantial long-term savings—making it economically efficient, sustainable, and cost-effective.

CVD stand out for their excellent thermal and oxidative stability. Compared to traditional TiN or TiAlN coatings applied by PVD, glass-ceramic coatings can withstand temperatures above 1000 °C and form a stable, adherent barrier on titanium substrates. While ceramic coatings such as yttria-stabilized zirconia (YSZ) also offer high-temperature performance, they often rely on thermal spray methods, which can lead to thicker, less uniform coatings [112-113].

The use of CVD allows for uniform deposition even on complex geometries but comes at the cost of longer processing times and higher energy consumption.

Thus, glass-ceramic CVD coatings offer a technically superior solution for extreme



environments, albeit with cost and throughput constraints that must be considered for volume manufacturing.

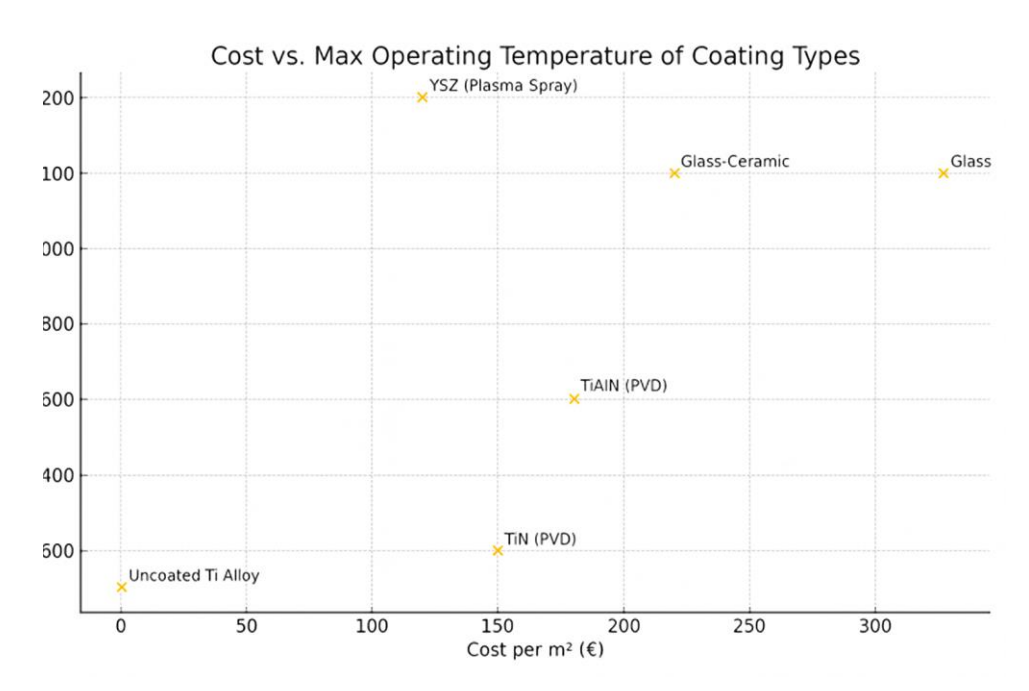


Figure 2.48. Coating cost vs. max operating temperature of coating types [F52]

The total cost of the coated exhaust system includes both the titanium substrate and the glass-ceramic coating. For a CP titanium sheet of 0.23–0.49 mm thickness, the estimated raw material cost is  $\in$ 81– $\in$ 98 per m². When combined with the CVD coating cost ( $\sim$ 6365 per part), the total cost of a coated 1.5 m² exhaust system ranges between  $\in$ 486.5 and  $\in$ 512. This value excludes machining, welding, and other component-level operations.



Table 2.4. Titanium substrate cost estimation

Parameter	Value		
Titanium type	Commercially Pure Titanium (Grade 2)		
Thickness range	0.23–0.49 mm		
Average thickness used	0.36 mm (mean of range)		
Density of Ti	4.51 g/cm <sup>3</sup>		
Area	1 m <sup>2</sup>		
Volume	$0.00036 \mathrm{m}^3 = 360 \mathrm{cm}^3$		
Mass	$360 \text{ cm}^3 \times 4.51 \text{ g/cm}^3 = 1.624 \text{ kg}$		
Titanium market price	~€50–€60/kg (Grade 2 sheet, 2024–2025)		
Material cost per m <sup>2</sup>	€81–€98		
Total titanium cost (1,5 m²)	€121.5–€147		

An alternative coating technique considered is thermal spray (specifically plasma spray) using a glass-ceramic material. With a target coating thickness of  $100 \, \mu m$  over a  $1.5 \, m^2$  surface area, the total estimated cost is between  $\mathfrak{E}245$  and  $\mathfrak{E}265$  per exhaust system.

**Table 2.5.** Total cost of Titanium sample

Component	<b>Estimated Cost (€)</b>
Titanium (1.5 m²)	€121.5–€147
Coating 1 (75 µm)	330
Total cost	€451,5–€477
Coating 2 (100 µm)	365
Total cost	€486.5–€512

Thermal spray offers faster processing than Chemical Vapor Deposition (CVD) and is more scalable for industrial use.



However, due to the brittle nature of glass-ceramics and thermal expansion mismatch with titanium alloys, delamination or cracking may occur. Proper surface preparation, including grit blasting and temperature control, is critical for adhesion and coating integrity.

While thermal spray reduces cost and improves throughput, further experimental validation is required to confirm adhesion, oxidation resistance, and thermal cycling behavior of the glass-ceramic layer on titanium substrates.

In conclusion, this report evaluates the cost and feasibility of applying glass-ceramic coatings to titanium alloy exhaust systems in high-performance automotive applications. The analysis highlights the advantages of Chemical Vapor Deposition (CVD) for achieving superior adhesion and thermal resistance, with coatings of 75 µm and 100 µm thicknesses costing approximately €330 and €365 per exhaust system, respectively. While CVD offers excellent performance, challenges such as higher costs and longer processing times compared to thermal spray methods must be addressed for broader application.

Thermal spray techniques present a more scalable option, with estimated costs ranging from €245 to €265 per unit. However, they may encounter issues related to coating integrity, such as delamination due to thermal expansion mismatches. The lifecycle benefits of CVD-coated systems are significant, as they extend the lifespan of exhaust components from three years to nine years, resulting in substantial cost savings and a return on investment (ROI) of 475%. Ultimately, while CVD glass-ceramic coatings provide a technically superior solution for high-performance applications, careful consideration of cost, scalability, and processing challenges is essential for their successful implementation in the automotive industry.

**Table 2.6.** Thermal spray with glass-ceramic on titanium

	Value		
Coating method	Thermal spray (plasma preferred)		
Coating material	Glass-ceramic		
Coating thickness	100 μm		
Area to be coated	1.5 m <sup>2</sup>		
Material + processing cost	~€130/m² (typical for ceramic TS)		
Base coating cost	€ 195		
Labor, surface prep, QC	€50–€70		
Total cost per unit	€245–€265		



**Table 2.7.** Comparison: CVD vs thermal spray for class-ceramic coating on titanium

Parameter	CVD (Chemical Vapor	Thermal Spray (Plasma		
1 arameter	Deposition)	Spray)		
Coating material	Glass-ceramic	Glass-ceramic		
Eggibility on titanium	Excellent adhesion	Possible, but risk of		
Feasibility on titanium	Excellent aunesion	delamination		
Coating thickness	Uniform, controllable (100 µm)	Controllable, may require		
Coating thickness	Officiality Controllable (100 μm)	post-processing		
Surface preparation	Clean and smooth	Grit blasting usually		
Surface preparation	Clean and smooth	required		
Adhesion strength	Very high	Moderate, depends on		
Adhesion stiength	very flight	spray parameters		
Coating uniformity	Excellent, even on complex	Moderate – limited by		
Coating uniformity	shapes	line-of-sight geometry		
Thermal stress risk	Low (slow deposition,	High (thermal mismatch,		
Thermal stress risk	controlled heating)	rapid cooling)		
Processing time	Long (slow deposition rates)	Short (fast application		
Trocessing time	Long (slow deposition rates)	rates)		
Scalability for	Limited – better for	More scalable for		
production	prototypes, R&D	industrial production		
Typical cost per 1.5 m <sup>2</sup> unit	~€365	~€245–€265		
Equipment	High - vacuum eyetom gae	Moderate - caray gun		
* *	High – vacuum system, gas	Moderate – spray gun, plasma torch		
cost/complexity	handling  Everylant (dense swife me	. 1		
Oxidation resistance	Excellent (dense, uniform	Good, but depends on		
	layers)	porosity and cracks		
Best use case	High-performance, low-	Mass production with		
	volume (e.g., motorsport)	cost constraints		



# 2.8. Conclusion

The exploration of coating deposition methods, adhesion mechanisms, and the application of advanced coatings in the automotive industry underscores the critical role these technologies play in enhancing material performance and durability. Coating methods, including vapor deposition, thermal spraying, and electrochemical techniques, each offer unique advantages tailored to specific applications. Vapor deposition techniques, such as Physical Vapor Deposition (PVD) and Chemical Vapor Deposition (CVD), provide precise atomic-level coatings, while thermal spraying methods, like High Velocity Oxy-Fuel (HVOF) spraying, deliver robust coatings capable of withstanding extreme conditions.

Electrochemical methods enhance surface properties and corrosion resistance, making them valuable in various industrial contexts.

Adhesion in coating/substrate systems is a multifaceted phenomenon influenced by surface chemistry, mechanical interlocking, and thermodynamic principles. Effective adhesion is critical for the longevity and performance of coatings, necessitating careful surface preparation and the use of appropriate adhesion testing methods. Ongoing research into adhesion mechanisms and surface treatments aims to improve the durability and effectiveness of coatings, particularly in demanding sectors such as automotive and aerospace.

The application of glass-ceramic coatings on titanium alloy exhaust systems exemplifies the intersection of material science and engineering innovation within the automotive industry. While Chemical Vapor Deposition (CVD) offers superior adhesion and thermal resistance, its higher costs and longer processing times present challenges for broader adoption. Conversely, thermal spray techniques provide a more scalable solution, albeit with potential issues related to coating integrity. The lifecycle benefits of CVD-coated systems, which significantly extend component lifespan and yield substantial cost savings, highlight the importance of evaluating both performance and economic factors in coating selection.

To sum up, the continued advancement of coating technologies and a comprehensive understanding of adhesion principles are essential for optimizing performance across various applications. As the automotive industry evolves, the integration of innovative coating will be pivotal in addressing emerging challenges, promoting sustainability, and enhancing overall efficiency.



# 3. Experimental parts

## 3.1. Cutting, marking, and polishing titanium samples.

Commercially pure titanium of Grade 2 (ASTM B348) was used as the substrate material for this study – in this study and named as Ti substrate in further discussion. The initial raw titanium sheets were acquired in dimensions of  $140 \text{ mm} \times 30 \text{ mm}$ . The preparation process consisted of the following sequential steps (Figure 3.1):

#### 1. Polishing:

The surfaces of the titanium sheets underwent mechanical polishing with a wheel polisher fitted with abrasive papers of varying grit sizes, from P240 to P1000. This procedure effectively eliminated surface imperfections and resulted in a consistent finish suitable for further coating and treatment processes.

#### 2. Sectioning:

Following the polishing step, the sheets were cut into smaller rectangular substrates measuring 10 mm × 10 mm utilizing a manual cutting machine specifically designed for metal foils. This approach ensured uniformity in sample size for testing and characterization purposes (illustrated in Figure 3.2).

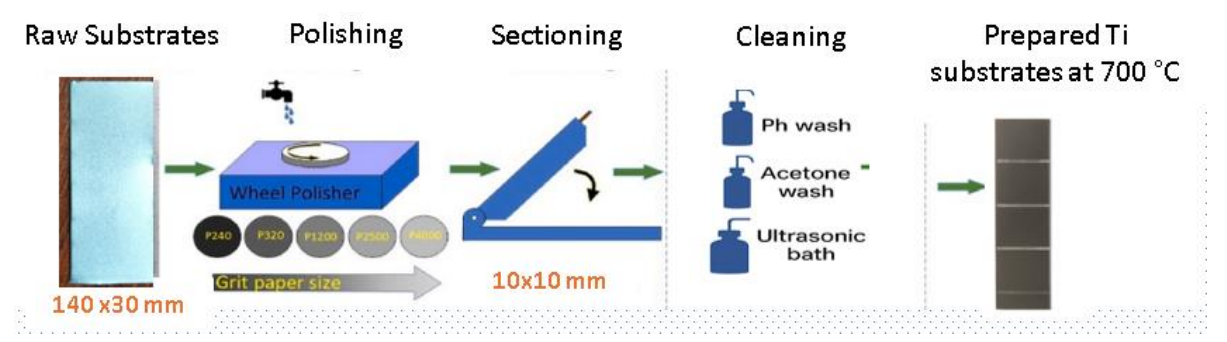


**Figure 3.1.** Preparation stage for Ti substrates prior to coating glass

The target of this study is to prepare uniform titanium substrates that are free from surface imperfections, ensuring a consistent substrate for further experimental processes, including coating and characterization.



For grinding and polishing Machine LS1 was used (Fig. 3.3).



**Figure 3.2.** Q11-1x1000 Cutting Machine with Foot Power in TTPU.



**Figure 3.3.** Grinding and polishing Machine LS1 (Remet) in TTPU lab.

# 3.2. Cleaning and preparation procedure of Ti substrates.

#### 1. Cleaning:

The sectioned samples underwent a comprehensive three-stage cleaning process designed to remove surface impurities:

- Rinsing with pH-balanced water
- Washing with acetone (referred to as acetone wash)
- Immersion in an ultrasonic bath containing Isopropyl Alcohol (IPA) to eliminate any residual particles or surface oils.

To address potential contamination from previous treatments, the titanium coupons were subjected to an exhaustive cleaning regime. Initially, the samples were placed in a beaker filled with acetone, ensuring that the marked surface was in direct contact with the bottom of the vessel. The beaker was placed in an ultrasonic bath for a duration of 5 minutes (Fig. 3.4).

In the next phase, the samples were transferred to a separate beaker containing a sufficient volume of ultrapure water, while the used acetone was set aside for disposal. The water-filled beaker underwent sonication for 10 minutes; this procedure was then repeated using fresh ultrapure water for another 10 minutes.



Ultrasonic cleaning is essential for dislodging surface contaminants and residues. This process utilizes high-frequency mechanical vibrations (~20 kHz) produced by electric currents, which are converted into acoustic energy, creating microscopic cavitation effects between the cleaning solution and the sample surfaces.

After completing the cleaning cycle, the samples were dried under a laminar flow cabinet and subsequently sealed in appropriate packaging for storage.



**Figure 3.4.** Ultrasonic bath in TTPU lab.

#### 3. Thermal treatment:

To enhance the structural stability and surface integrity of Ti substrate tempering at 700°C for 30 minutes was done in Carbolite<sup>TM</sup> CWF Chamber Furnace (Fig. 3.5). This thermal treatment occurred within a chamber furnace, where samples were carefully positioned on a ceramic tray to ensure homogeneous heat distribution (Fig.3.6).

The furnace was preheated to reach the target temperature of 700°C, and samples were maintained at this temperature for 30 minutes to stabilize their internal microstructure. This step is crucial for alleviating residual stress introduced during earlier mechanical processing and polishing operations while fostering a uniform surface condition favorable for subsequent modifications.

Upon completion of the tempering cycle, the furnace was turned off, allowing the Ti substrates to cool naturally in ambient air until they reached room temperature.



This gradual cooling process is vital in preventing thermal shocks or microcracks that could otherwise affect both mechanical strength and chemical performance during high-temperature applications.



**Figure** 3.5. Carbolite<sup>TM</sup> CWF Chamber Furnace in TTPU lab.



**Figure 3.6.** Several cutted Ti substrates heat treated at 700 °C

# 3.3. Glass powder preparation

The glass powder utilized for coating was created through a melt-quench technique, designed according to a specific batch composition aimed at achieving optimal characteristics for high-temperature uses. The preparation involved several essential stages: formulation of the batch, mixing, melting, quenching, and processing into powder, which are outlined below.

#### 1. Batch Composition

As precursors higher purity oxides, other chemical regions were applied including silicon dioxide, calcium carbonate, magnesium carbonate, sodium carbonate, ammonium hydrogen phosphate, calcium fluoride and others. (Table 3.1).

These chemical reagents were selected to facilitate the formation of the glass network, improve bioactivity, and customize thermal and chemical stability. Modifiers like



calcium oxide, magnesium oxide, sodium oxide were added as needed to modify properties such as thermal expansion and viscosity.

**Table 3.1.** Chemical compositions (batches) of the investigated glasses G-1d and G-1e (the composition of glassG-1b is presented for comparison purposes)

Glass	SiO <sub>2</sub>	$B_2O_3$	CaO	MgO	$P_2O_5$	Na <sub>2</sub> O	CaF <sub>2</sub>
G-1b							
wt%	40,08	5,16	29,10	8,96	6,32	4,59	5,79
mol%	39,82	4,43	30,97	13,27	2,65	4,43	4,43
mol ratio	9	1	7	3	1	1	1
G-1d							
wt%	46,60	-	28,66	8,83	6,22	4,53	5,70
mol%	45,45	-	30,30	12,99	2,60	4,33	4,33
mol ratio	11	-	7	3	1	1	1
G-1e							
wt%	43,48	-	30,44	8,75	7,19	4,49	5,65
mol%	43,10	-	32,33	12,93	3,02	4,31	4,31
mol ratio	10,00	-	8	3	1	1	1

## 2. Mixing

The chemical reagents were precisely weighed according to the desired composition and thoroughly combined to achieve uniformity. This mixing occurred in a clean, inert vessel using either manual stirring or mechanical mixing based on the batch size. Consistent mixing is crucial to avoid compositional variations and ensure reliable melting behavior.

#### 3. Melting

The homogeneous mixture of powders was placed into a crucible resistant to high temperatures (usually made from platinum or alumina). This crucible was then positioned inside a preheated muffle or resistance furnace where the temperature gradually raised to between 1250°C and 1400°C. Once this target temperature was attained, the melt was maintained at that level for 1–2 hours to guarantee complete fusion and chemical homogeneity among the glass components. Intermittent stirring of the melt may be conducted when feasible to improve uniformity and eliminate any trapped bubbles.



#### 4. Quenching

After reaching a fully molten and homogeneous state, cooling of the glass occurred swiftly utilizing one of two quenching methods:

- Metal Plate Quenching: The molten glass was poured onto a preheated steel or graphite plate, allowing it to spread rapidly and solidify into a brittle glassy mass.
- Water Quenching: Alternatively, the melt could be poured into deionized water, resulting in thermal shock that fractured it into small granules.

Both techniques were employed with the aim of preventing crystallization by quickly lowering the temperature, thereby maintaining the amorphous nature of the glass.

#### 5. Grinding and Sieving

For samples obtained through water quenching, initial drying ensured removal of any residual moisture from the resulting granules. Subsequently, this solidified glass, whether frit or granules, was ground into fine powder using either a ball mill or mortar and pestle. To achieve a consistent particle size distribution suitable for, sieving was performed typically selecting particles within the range of 10–20 microns. The typical appearance of glass powder after grinding is shown in Figure 3.7.



**Figure 3.7.** Glass powder (G1-d) after grinding



## 3.4. Characterization of glass

The dilatation curves of the experimental glass compositions are plotted in Fig. 3.8. A thorough examination of these curves reveals critical insights regarding the transition temperature (Tg) and softening points (Ts), as well as the coefficients of thermal expansion (CTE).

These findings are comprehensively summarized in Table 3.2. The results indicate that the transition temperatures (Tg) for the analyzed glasses range between 580°C and 600°C, while the softening points (Ts) vary from 644°C to 672°C. Such temperatures are pivotal in understanding the thermal behavior and stability of these glass materials, especially in applications where thermal stress could impact their performance.

Furthermore, the CTE values, which were generally observed to be at a high level, play a significant role in assessing how these glasses will respond to temperature fluctuations in real-world scenarios. Notably, the coefficient of thermal expansion for glass G-1e is slightly lower than that of G-1d, suggesting a nuanced variation in thermal stability and expansion characteristics that could impact their suitability for various technological applications.

In further exploration of the impact of heat treatment on these glass compositions, it was observed that when the glass powder compacts were subjected to heat treatment at 700°C—which is notably above the transition temperature (Tg)—the samples retained their amorphous nature while achieving complete density. This finding indicates that sintering, a process where particles adhere and densify without melting, precedes crystallization in these glass systems. The implications of this behavior are profound, particularly as the future of glass technology increasingly leans towards enhancing performance through controlled thermal processes.



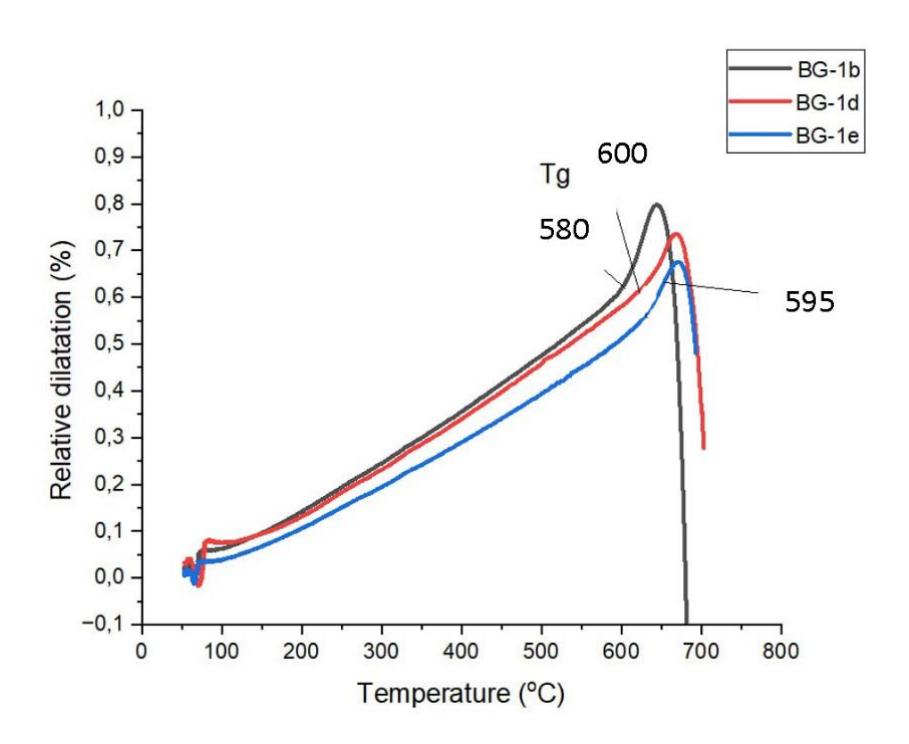


Figure 3.8. Dilatation curves of the glasses

**Table 3.2.** Characteristic temperatures (Tg and Ts) of the glasses G-1b, G-1d and G-1e and their thermal expansion coefficients (CTE) for the temperature ranges of 200–400°Cand 200–500°C determined from the dilatometry curves of Fig. 3.8.

Property	G-1b	G-1d	G-1e
Tg (°C)	580	600	595
Ts (°C)	644	669	672
CTE (×10 <sup>-6</sup> K <sup>-1</sup> )			
200-400°C	10,67	10,44	9,18
200-500°C	11,11	10,87	9,56



# 3.5. Coating deposition and functionalization

As the coating material deposition of Ti substrate, glass powder is composition G1-d was used. The coating procedure utilized a slurry-based method that combined G1-d with glycerol at room temperature. This approach enabled an even distribution of the glass material over titanium substrates, followed by a carefully controlled heating process to promote bonding and densification.

#### 1. Slurry preparation and deposition

To assess how composition influences coating efficacy, two distinct mass ratios of glass powder to liquid glycerol were prepared:

- **70:30** (Glass G1-d: glycerol)
- **50:50** (Glass G1-d: glycerol)

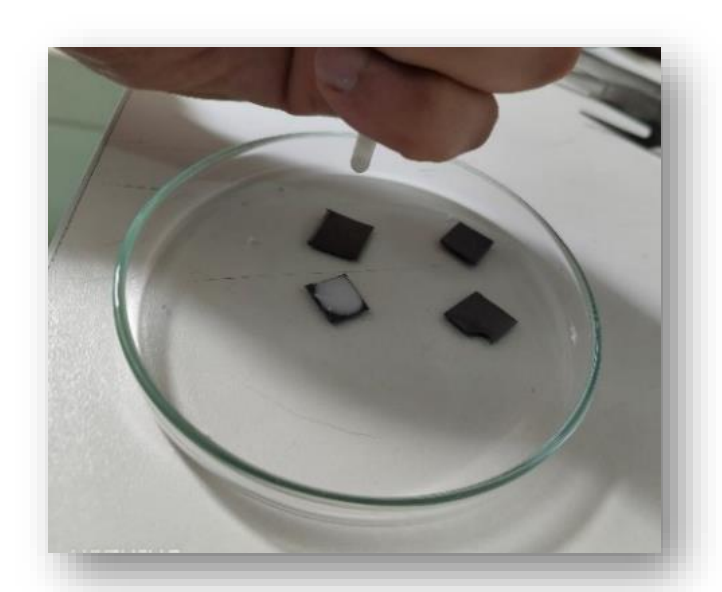


**Figure 3.9.** Glass powder-glitserol slurry is deposited on surface of Ti substrate

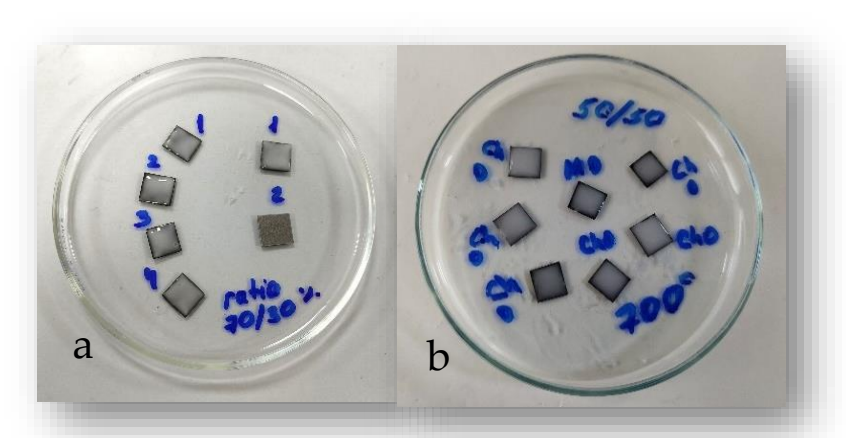


**Figure 3.10.** Preparation of coating using glass powder-glycerol in proportion a) 70/30 b) 50/50 mass % ratio

Each mixture was thoroughly stirred to achieve a uniform slurry. A micropipette was then employed to precisely fix a small droplet of the slurry onto each substrate's surface. This drop-casting method ensured consistent thickness and coverage of the substrate (Fig. 3.9 and 3.10).

# 2. Drying Process

After deposition, the coated samples were placed in a Memmert UN55 plus drying oven, where they underwent drying at 80 °C for four hours. This phase was crucial for the gradual evaporation of glycerol and the initial solidification of the glass layer before thermal treatment (Fig. 3.11).



**Figure 3.11.** Drying was performed in a Memmert UN55plus drying cabinet



# 3.6. Heat treatment process optimization

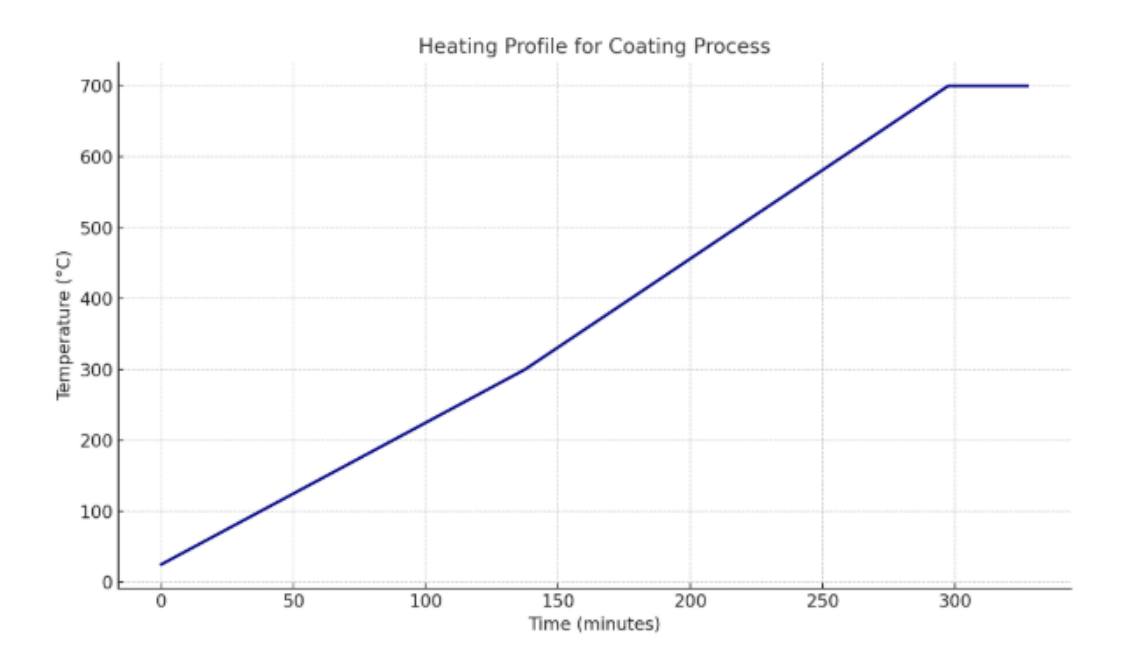
# **Heat Treatment (Sintering)**

Following drying, the samples were moved to a Carbolite<sup>™</sup> CWF chamber furnace for sintering under controlled temperature conditions (Fig. 3.5).

Two different sintering profiles were implemented to examine how peak temperature affects the final morphology and adhesion of the coating:

- 1. In the first profile, temperatures similarly increased to 300 °C at a rate of 2 °C/min before reaching 700 °C at 2.5 °C/min, with a subsequent dwell time of 30 minutes at this lower temperature level. This protocol aimed to investigate potential variations in coating densification and interaction with the substrate (Fig. 3.12 a).
- 2. In the second profile, the furnace temperature was gradually raised from ambient levels to 300 °C at a rate of 2 °C/min, followed by an increase to 750 °C at 2.5 °C/min. A dwell time of 30 minutes at this peak temperature facilitated viscous flow and enhanced bonding between the glass and titanium substrate (Fig. 3.12 b).
- 3. In the third profile, the furnace temperature gradually rose from ambient levels to 300 °C at a rate of 2 °C/min, followed by an increase to 800 °C at 2.5 °C/min. A dwell time of 30 minutes at this peak temperature facilitated viscous flow and enhanced bonding between the glass and titanium substrate.





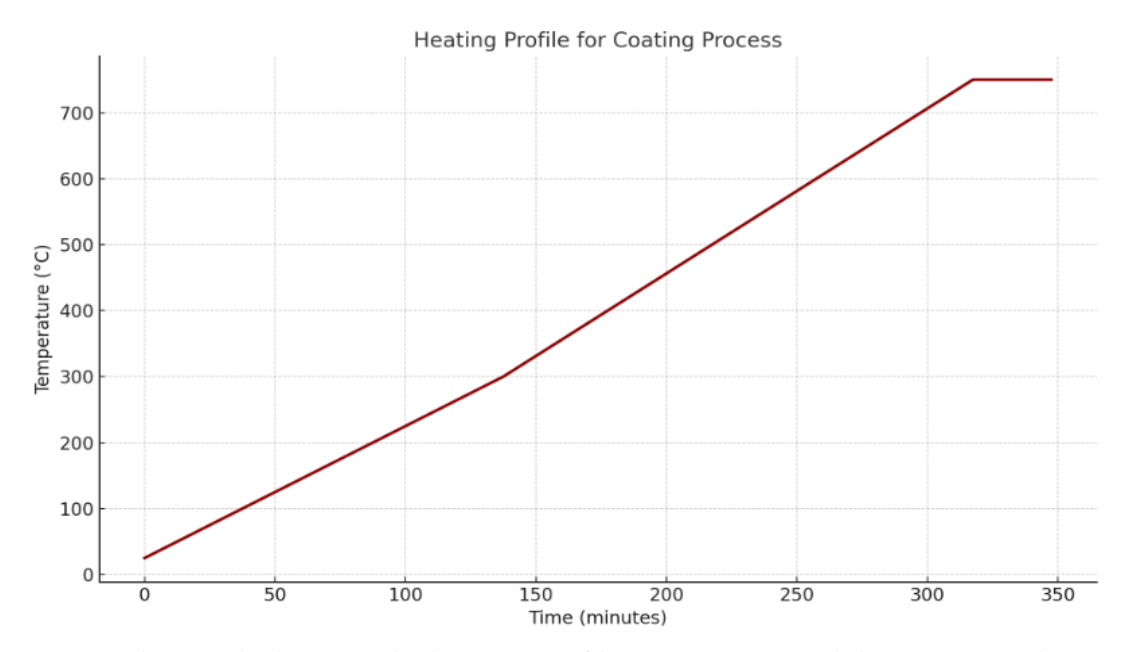


**Figure 3.12.** The graph showing the heating profile at (a) 700 °C and (b) 750 °C. Cooling profile of samples followed the cooling profile of furnace after switching off.



The appearance of samples after treatment at 700, 750 and 800  $^{\circ}$ C are shown in Fig. 3.13-3.15.

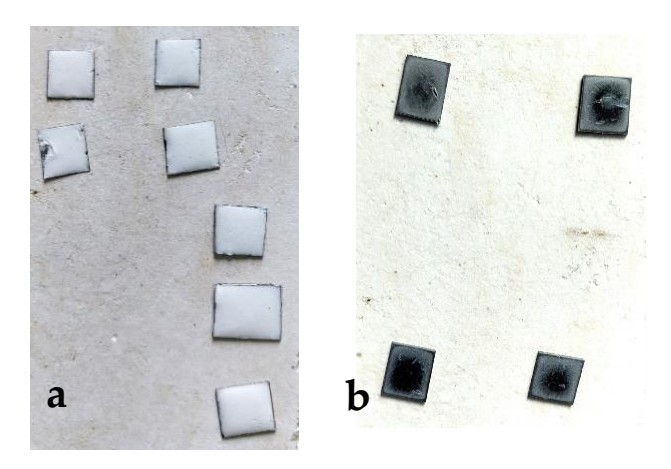


**Figure 3.13.** Coated sample. The finished product from the furnace temperature at 700 °C (a) and 750 °C (b).

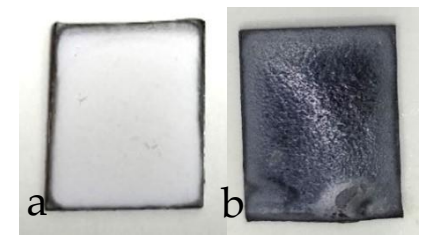


**Figure 3.14.** Individual images of coated samples heat treated at at 700 °C(a) and 750 °C(b).

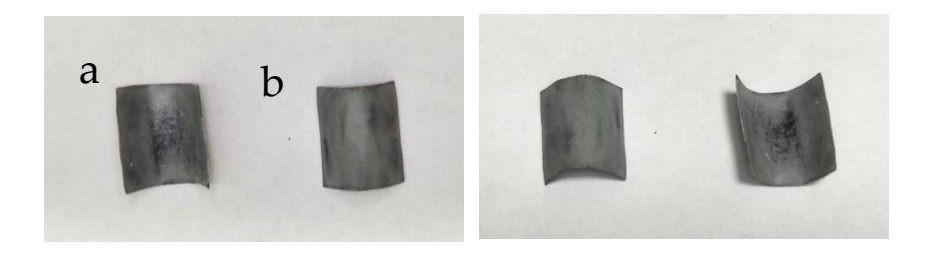


**Figure 3.15.** Glass coating at round shape surfaces at heat treated at 750 °C concave(a) and convex(b).



# Preparation of sample cross section for microstructural analysis

After mounting, systematic grinding and polishing of cross section coating-substrate was carried out using the LS1 machine (Fig. 3.5).



**Figure 3.16**. Surface grinding and polishing, the type of carborundum surface (grit size)

The grinding process employed water-assisted techniques to mitigate overheating, commencing with coarse abrasive papers (240 grit) and advancing through progressively finer grits up to 1000 or 1200 (Fig. 3.16).

This approach effectively eliminated surface irregularities and distortions caused during sectioning. Following grinding, polishing commenced using diamond suspension or an alumina slurry applied on a polishing cloth to achieve a smooth, reflective surface. The final polishing stage was crucial for removing any remaining scratches and revealing the material's true microstructure.

Upon completion of polishing, thorough cleaning of the sample was performed using ethanol or isopropyl alcohol to eliminate surface contaminants. To ensure all particulates were fully removed, the sample also underwent treatment in an ultrasonic bath for final cleansing.



In certain instances, etching was employed as an additional step to enhance contrast in microstructural features; appropriate chemical reagents like ammonium persulfate selectively attacked grain boundaries. The prepared—and where applicable, etched—sample was then examined under scanning electron microscopy (SEM) for detailed analysis of its microstructure.

# 3.7. SEM analysis

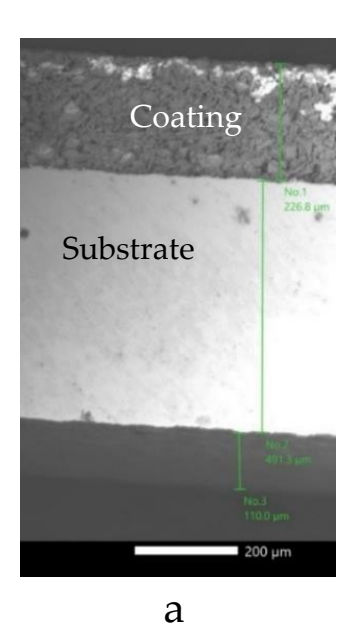
Cross sections of glass coating – Ti substrate were analyzed using analytical SEM-EDS: JEOL JSM-IT200LA apparatus (Fig. 3.17).

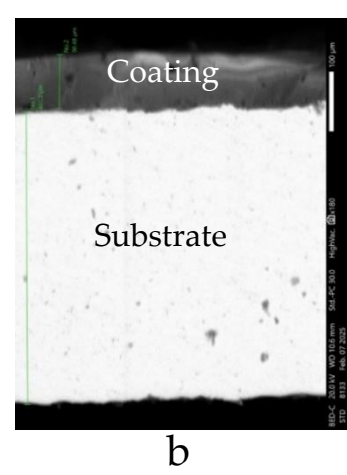


Figure 3.17. Analytical SEM-EDS: JEOL JSM-IT200LA apparatus

Figure 3.18. Shows microstructure of polished cross section of glass coating – Ti substrate after heat treatment at 700 °C and at 750 °C. In both cases uniform glass coating on Ti substrate was achieved, no cracks and gaps were observed.







**Figure 3.18.** Microstructure of polished cross section of glass coating – Ti substrate after heat treatment at (a) 700 °C and (b) 750 °C

The microstructure of glass coating and the microstructure of Ti substrate heat treated at 700 °C for 30 minutes are shown in Fig. 3.19 and 3.20 respectively.

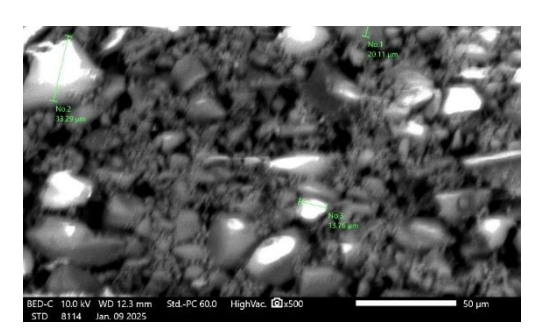


**Figure 3.19.** The microstructure of glass coating at 700°C

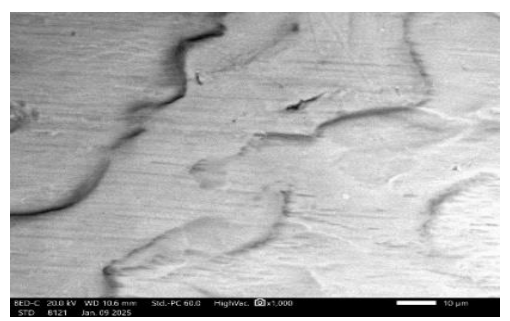


**Figure 3.20.** The microstructure surface of Ti substrate



# 3.8. EDS analysis

# 3.8.1. EDS analysis of Ti substrate

Energy-Dispersive X-ray Spectroscopy (EDS) analysis of Ti substrate as presented in Table 3.3.

The spatial distribution of Ti was analyzed using elemental experiments, as shown in Fig. 3.21. From this experimental data the Ti substrate was found to be pure titanium.

EDS elemental mapping experiment of Ti substrate is shown in Fig. 3.22.

**Table 3.3.** The mass and atomic ratio of Titanium sample

Element Line		Mass%	Atom%	
Ti	K	100.00±0.28	100.00±0.28	
Total		100.00	100.00	

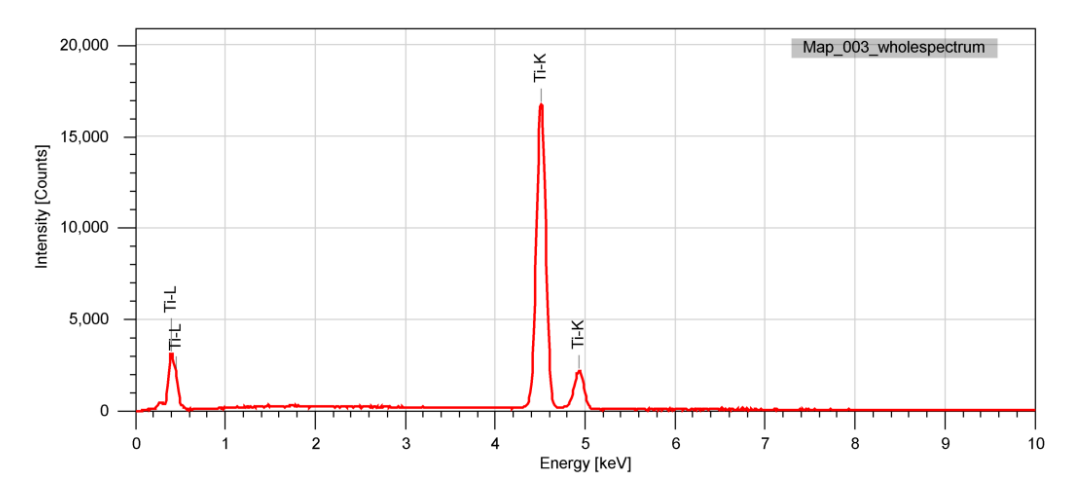


Figure 3.21. EDS of Ti substrate



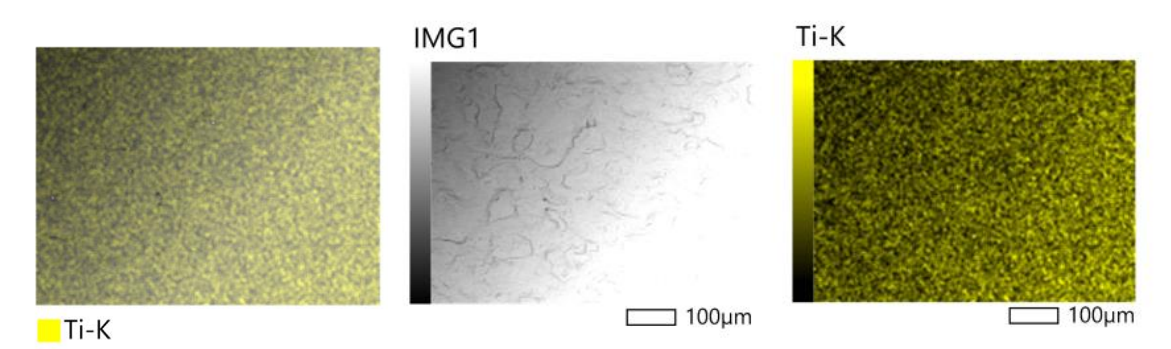


Figure 3.22. EDS elemental mapping experiment of Ti substrate

Data from EDS analysis of Ti substrate confirms that distribution of elements corresponds to its chemical composition.

# 3.8.2. EDS analysis of glass coating

EDS of glass coating after heat treatment at 700°C for 30 minutes is presented in Table 3.4 and shown in Fig. 3.23.

The spatial distribution of elements in glass coating was analyzed using elements mapping as presented in Fig.3.24.

Data from EDS analysis of glass coating confirms that distribution of elements corresponds to chemical composition of the parent glass.

**Table 3.4.** The mass and atomic ratio of the front and back sides of the coated sample

Element	Mass%	Atom%
0	48.95±0.17	65.15±0.23
Na	3.36±0.04	3.11±0.04
Mg	4.45±0.04	3.90±0.03
Si	19.71±0.07	14.94±0.05
P	2.54±0.03	1.74±0.02
Ca	21.00±0.08	11.16±0.04
Total	100.00	100.00

Element	Mass%	Atom%	
Ti	100.00±0.28	100.00±0.28	
Total	100.00	100.00	



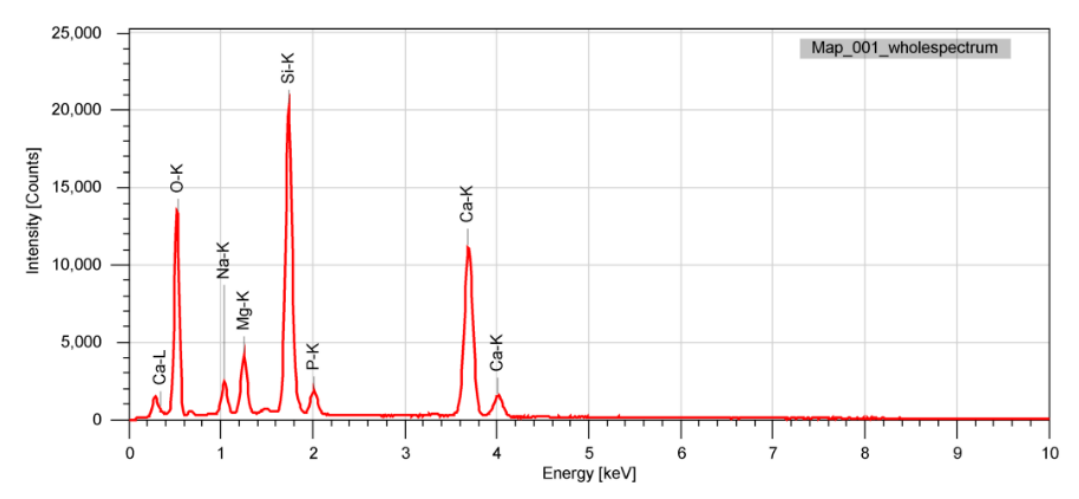
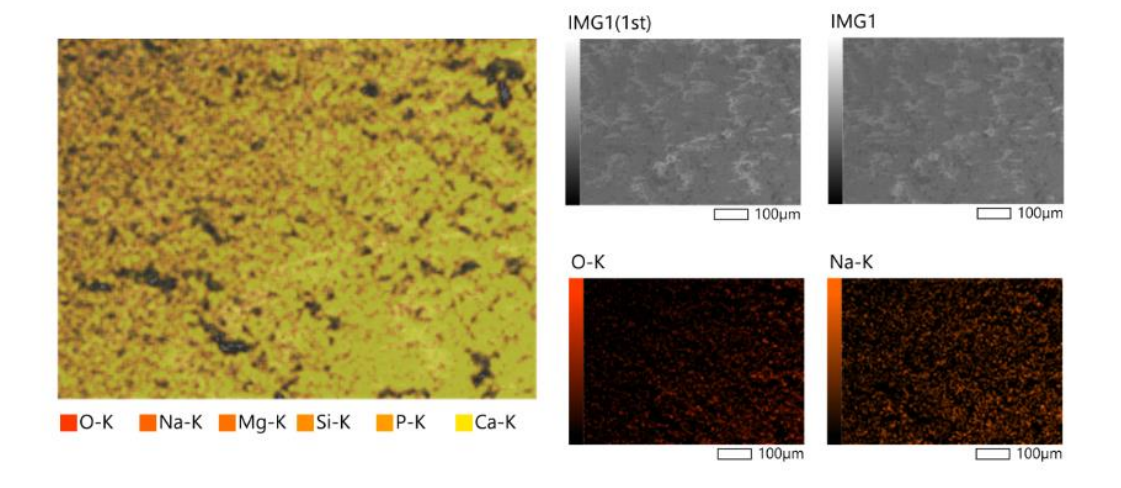


Figure 3.23. EDS of the powders of the investigated coating glass





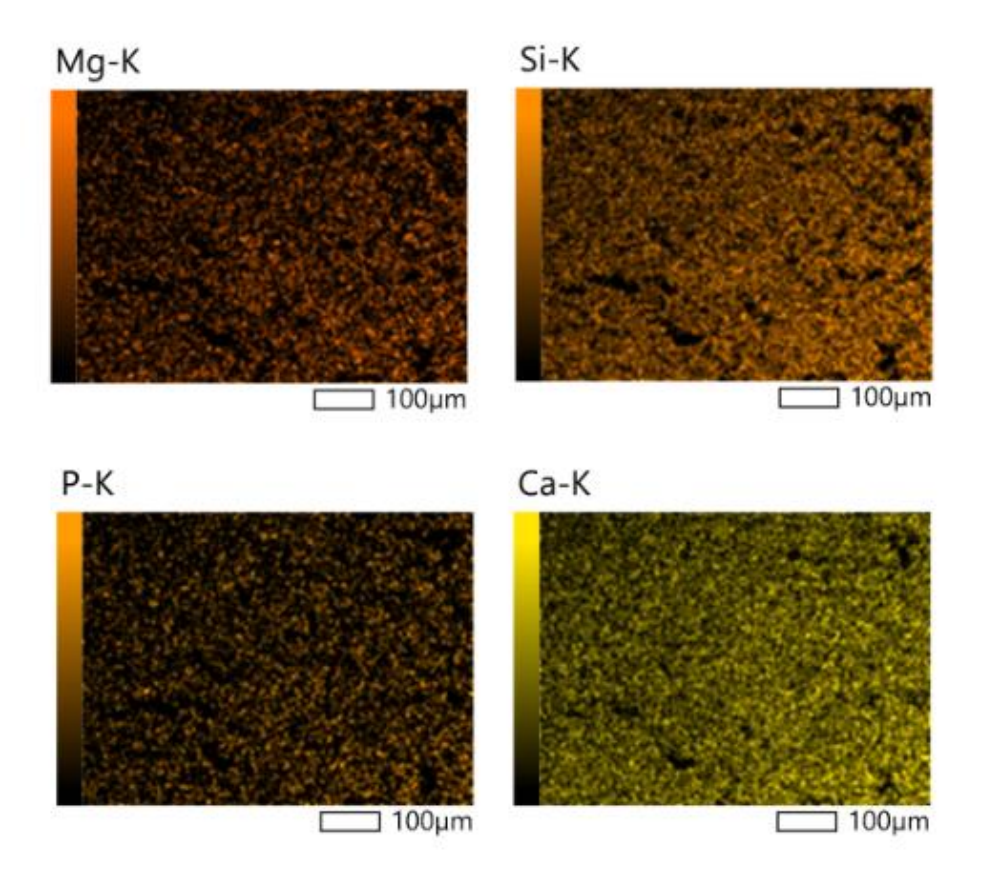
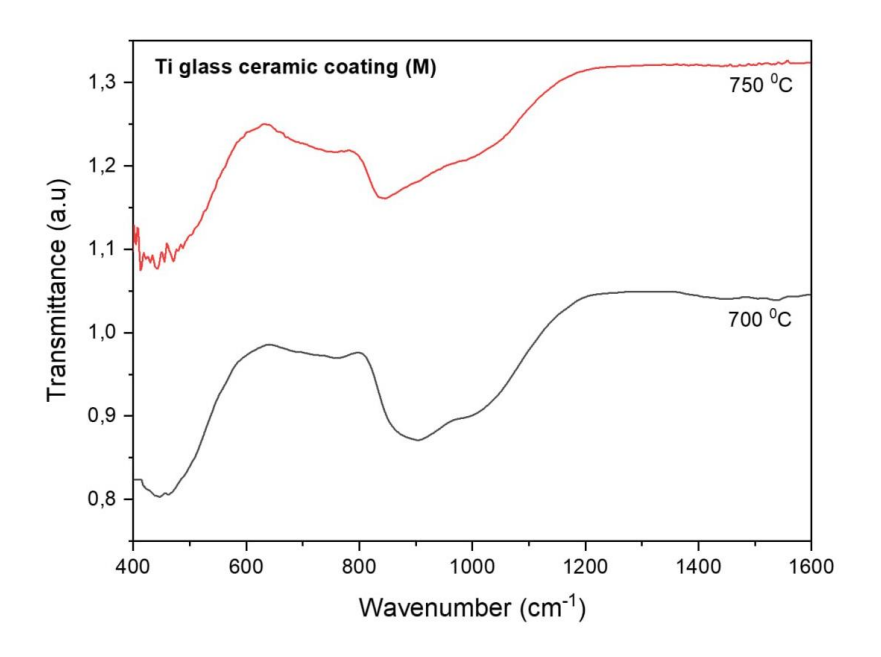


Figure 3.24. Spatial distribution of elements in glass coating



# 3.9. Fourier Transform Infrared spectroscopy analysis (FTIR) analysis of glass coating



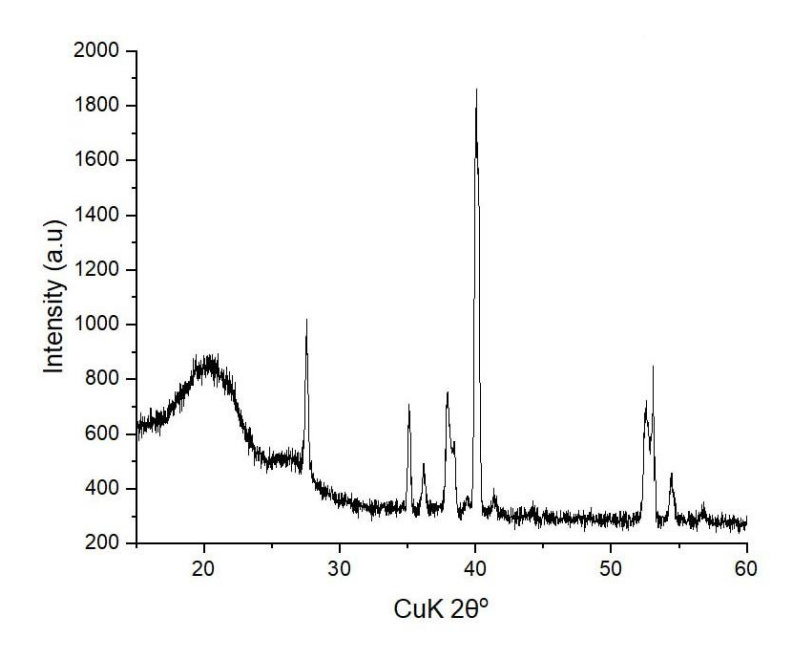
**Figure 3.25.** FTIR for coating at 700°C and 750°C

FTIR spectra of the BG glass (Fig.3.25) exhibit three broad transmittance bands in the region of 300–1300 cm<sup>-1</sup> that is indicative of the general disorder in the silicate and phosphate network mainly due to a wide distribution of Q<sup>n</sup> (polymerization in the glass structure, where n denotes the number of bridging oxygens) units occurring in these glasses. The most intense bands in the 800–1300 cm<sup>-1</sup> region correspond to the stretching vibrations of the SiO<sub>4</sub> tetrahedron with a different number of bridging oxygen atoms. Thus, the band around 1030 cm<sup>-1</sup> indicated the distribution of silicate Q<sup>n</sup> units centered on Q<sup>3</sup> while the transmittance band near 916 cm<sup>-1</sup> may be attributed to the polymerization in silicate network structure with two bridging oxygens as Q<sup>2</sup> units along with some Q<sup>1</sup> units. Supporting information and extended results are provided in Annex A (Figure 5.1-5.5 A)



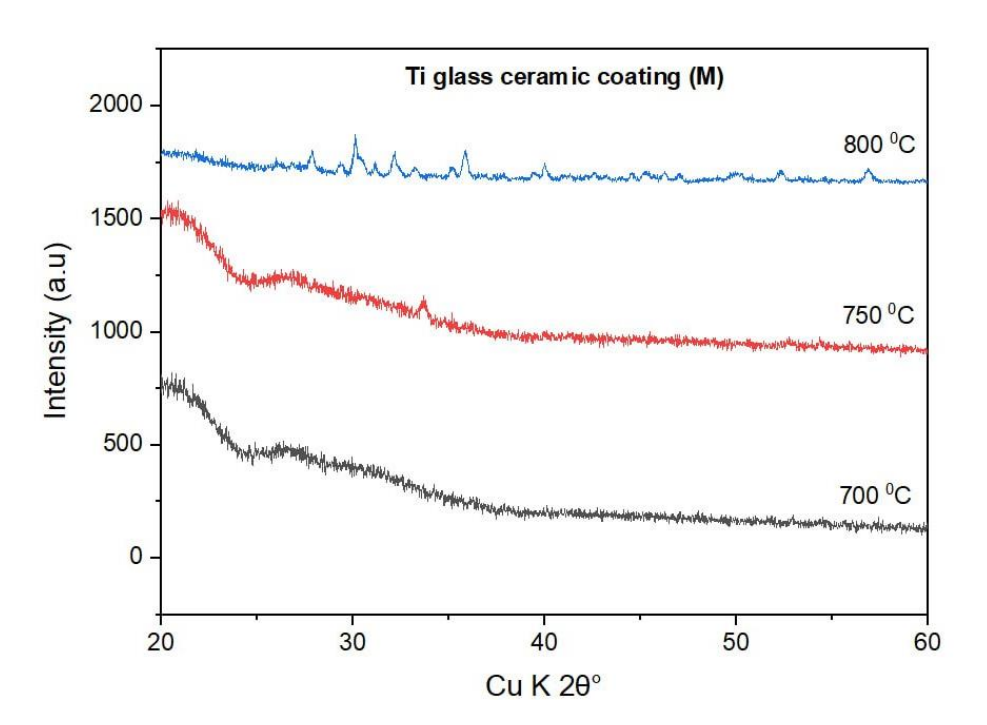
# 3.10. X-ray diffraction analysis (XRD) of Ti substrate and glass coating.

Fig. 3.26 shows XRD pattern of titanium substrate after heat treatment at  $700^{\circ}$ C for 30 minutes.



**Figure 3.26.** XRD pattern of Ti substrate after heating at 700 °C





**Figure 3.27**. XRD patterns of glass coatings heat treated at 700°C, 750 °C and 800 °C

Fig. 3.27. demonstrate XRD patterns of the coatings subjected to heat treatments at 700 °C and 750 °C. No evidence of crystallization was observed at these temperatures; the glass retains amorphous structure. The glass matrix remains disordered, indicating that the thermal energy provided was insufficient to initiate crystallization. This suggests that the glass preserved its amorphous nature and did not undergo any significant structural rearrangement.

In contrast, after heat treatment at 800 °C, clear signs of crystallization were observed. X-ray diffraction analysis revealed the appearance of distinct diffraction lines corresponding to crystalline phases such as diopside, wollastonite, and fluorapatite. These findings confirm that the higher thermal energy at 800 °C was sufficient to overcome the energy activation barrier for nucleation and crystal growth within the glass structure in Fig. 3.27. Additional data related to this analysis can be found in Annex A (Figure 5.6-5.14).



# 3.11. Metallographic analysis of glass coating.

Morphology of glass coating after treatment at 750°C obtained using metallographic microscope are shown in Fig. 3.28. The absence of well-defined grain boundaries or crystalline patterns indicates that the coating remains amorphous after heat treatment at this temperature. It shows the coated surface with a relatively uniform distribution of pores or microbubbles. Fig. 3.29 shows the morphology of Ti substrate. That is typical for heat treated at 700°C shows clusters separated from each other by voids. That apparently will be important to get adhesion between glass and substrate.



**Figure3.28.** Morphology of coating at 750 °C (magnification 12.5×)

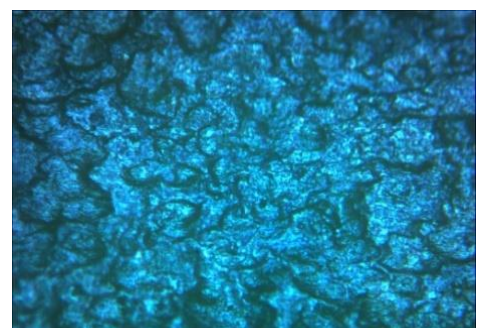


**Figure 3.29.** Morphology of pure Ti substrate (magnification 12.5×)



# 3.12. Thermal shock analysis of glass coating Ti substrate

To assess the thermal shock resistance of coatings on Ti substrate the tests were performed involving rapid temperature cycling (result illustrates in Table 3.5).

**Table 3.5.** Results of Thermal shock resistance tests

	Picture						
	Time interval	(10	Sample 1	Sample 2	Sample 3	Sample 4	Sample 5
№	№ minutes)			1	I	1	1
1	11:10-11:20	Crack defined	x	x	x	x	x
2	11:25-11:35	Crack defined	Х	x	x	x	х
3	11:40-11:50	Crack defined	х	x	x	x	х
4	11:55-12:05	Crack defined	х	x	x	x	х
5	12:10-12:20	Crack defined	х	x	x	x	х
6	12:20-12:30	Crack defined	х	х	x	х	х
7	12:30-12:40	Crack defined	х	х	Yes	Yes	х
8	12:45-12:55	Crack defined	х	х			х
9	13:00-13:10	Crack defined	х	х			х
10	13:20-13:30	Crack defined	х	X.			Yes

The samples were subjected to alternating conditions between room temperature  $(20\,^{\circ}\text{C})$  and  $250\,^{\circ}\text{C}$ . The main aim of this evaluation was to observe the initiation and development of crack formation under these extreme thermal variations.

The experiment lasted for 2 hours and 20 minutes, five samples (Samples 1 through 5) were analyzed under uniform cycling conditions (Table 3.5).

During the initial phase of testing (Intervals 1 to 6, 10 minutes duration each sample), no cracks were observed in any of the samples. This indicates that all five specimens successfully maintained their structural integrity while undergoing repeated cycles of thermal expansion and contraction during the first 70 minutes.

Evidence of degradation first emerged during Interval 7, when both Sample 3 and Sample 4 showed visible cracks (Fig. 3.32).

The simultaneous appearance of these cracks implies a possible threshold temperature or time-dependent mechanism contributing to material failure. In contrast, Samples 1, 2, and 5 remained free of cracks at this stage.

Notably, during Interval 10, a new crack was identified in sample 5, indicating a delayed failure response due to prolonged thermal exposure (Fig. 3.31).



These findings suggest that while all coatings initially resisted damage, their durability under extended thermal cycling varied among different samples. Such insights are essential for assessing the reliability of coated components subject to fluctuating high-temperature conditions, particularly in applications like exhaust systems and thermal barriers.



**Figure 3.30.** Morphology of coating before the thermal shock test (sample 5)



**Figure 3.31.** Fracture occurs after 10th cycles (sample 5)





Figure 3.32. Fracture occurs after 7th cycles in (a) sample 3 and (b) sample 4

The result of thermal shock experiments demonstrated that all tested samples can resist to 6 cycles of temperature change in the interval 250°C - 20 °C while 40% of samples to 10 of similar cycles.



#### **Discussion:**

The thermal shock test can serve as a practical method for testing the thermal compatibility of all ceramic crown systems. It can be used to identify systems where residual stresses are not of sufficient magnitude to cause failure upon completion of the initial firing cycle, but which could cause failure at it can be used to identify systems where **residual stresses** are not of a sufficient magnitude to cause failure upon completion of the initial firing cycle, but which could cause failure at a where the critical temperature difference ( $\Delta T_f$ ) that a coating can withstand without failure is often estimated using the following equation:

$$\Delta T_f = rac{\sigma_f (1-\mu)}{lpha E} \cdot S$$

 $\Delta T_f$  is temperature difference when fracture occurs,  $\sigma_f$  is the fracture stress,  $\mu$  is Poisson's ratio, E is modulus of elasticity,  $\alpha$  is linear Coefficient of Thermal Expansion (CTE), and S is a shape factor. This equation highlights the relationship between mechanical properties and thermal mismatch. A high CTE mismatch between the glass coating and the titanium substrate increases internal stress during cycling, making crack formation more likely.

- After 7 cycles, microcracking begins to appear (Sample 3/4).
- After 10 cycles, distinct, continuous cracks are visible (Sample 5).

These cracks likely propagate due to the thermal expansion mismatch and the brittle nature of the glass, especially under rapid thermal gradients. This aligns with the theoretical prediction that coatings with low fracture toughness and high stiffness are more prone to thermal shock-induced damage.

This relationship applies when the quench is so rapid that the surface temperature reaches its final value before the average temperature changes. By this criterion of failure, a material with high fracture stress, low modulus of elasticity, and low thermal expansion coefficient will likely be resistant to thermal stress failure. Therefore, glass sample characterized by a low thermal expansion coefficient typically exhibit a high resistance to thermal shock, as demonstrated by the findings of this study. Nonetheless, these systems showed sufficient resilience against thermal shock since occurrences of thermal shocks exceeding 200-250°C are unlikely. The stresses generated by thermal shock are temporary; however, they can lead to failure if they induce tensile stress on the surface, which is likely during rapid cooling.



If these surface stresses reach significant levels (where  $\Delta T$  is large in the equation referenced), cracks may form on the surfaces of brittle materials. In the system examined in this study, it is anticipated that such surface cracks would emerge because this material possesses lower strength compared to the core material, and the outer surface of a crown experiences greater thermal shock than the inner surface adjacent to the core material. These surface cracks will extend into the material and interact with existing internal residual stresses. The characteristics of these residual stresses will influence how the thermally shocked induced cracks progress inward. Although a crown represents a complex system, some general observations can be made regarding residual stresses. When the core's coefficient of thermal expansion exceeds that of the glass sample, radial tensile stresses will affect the body porcelain while hoop stresses will manifest as compressive following cooling post-firing. These residual stresses will be most prominent at the core interface. As a crack propagates inward from the surface, it will be redirected towards areas experiencing higher tensile stress—specifically along a path tangential to the core interface. This type of crack often appears deflected and runs parallel to the core due to prevailing tensile forces. Such fractures typically present as curved lines or half-moon shapes extending in a mesial/distal orientation (see Fig. 3.31). In cases of complete failure, opaque fragments would detach from the core material.

Conversely, when the core's coefficient of thermal expansion is less than that of either opaque or glass materials, tensile hoop stresses arise within those materials while radial stress remains compressive. In this scenario, surface cracks induced by thermal shock are propelled radially inward due to residual tensile hoop stresses. These fractures typically manifest as vertical lines aligned in an occlusal/gingival direction (see Fig. 3.32).

By rotating crowns under light illumination, one can observe both crack orientation and whether they penetrate through or run tangentially along with the core. This observation aids in determining whether cracks result from radial tensile (vertical) or radial compressive (horizontal) stresses and helps identify potential mismatches in thermal expansion of glass components.

Factors such as thermal conductivity and interfacial bond strength between glass coating layers also play roles in influencing thermal shock resistance: increased conductivity tends to reduce resistance to shocks. Furthermore, differences in elastic moduli among glass samples alongside variations in restoration dimensions contribute significantly as well—varying thicknesses across different layers alters stiffness and consequently modifies residual stress profiles.



# 3.13. Simulation of exhaust system at high temperatures

In this research, the thermal characteristics of an exhaust system designed for high-performance automotive applications were modeled using specific boundary conditions to assess the efficacy of protective coatings on titanium substrates (Fig 3.33).

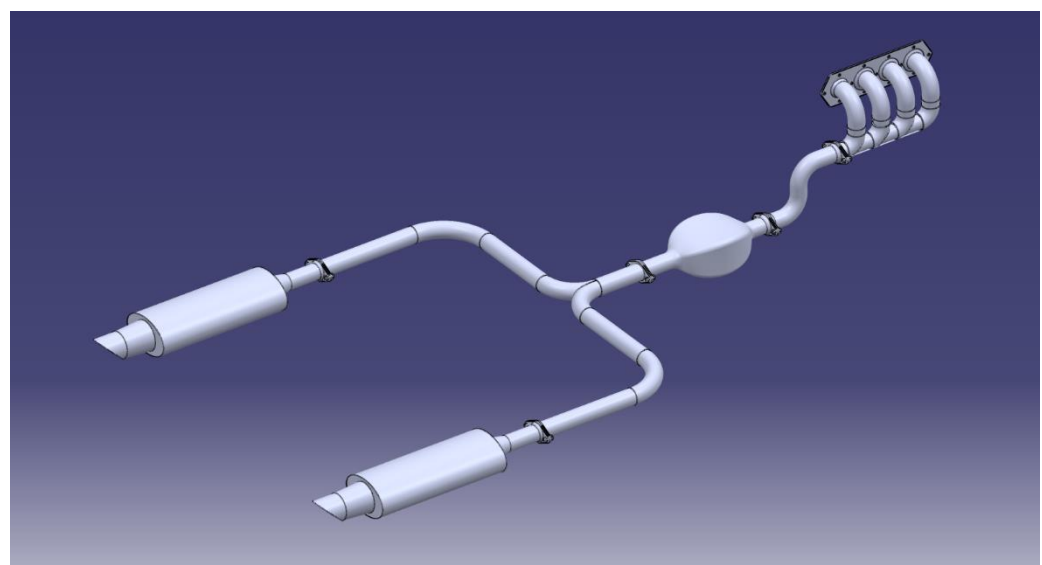
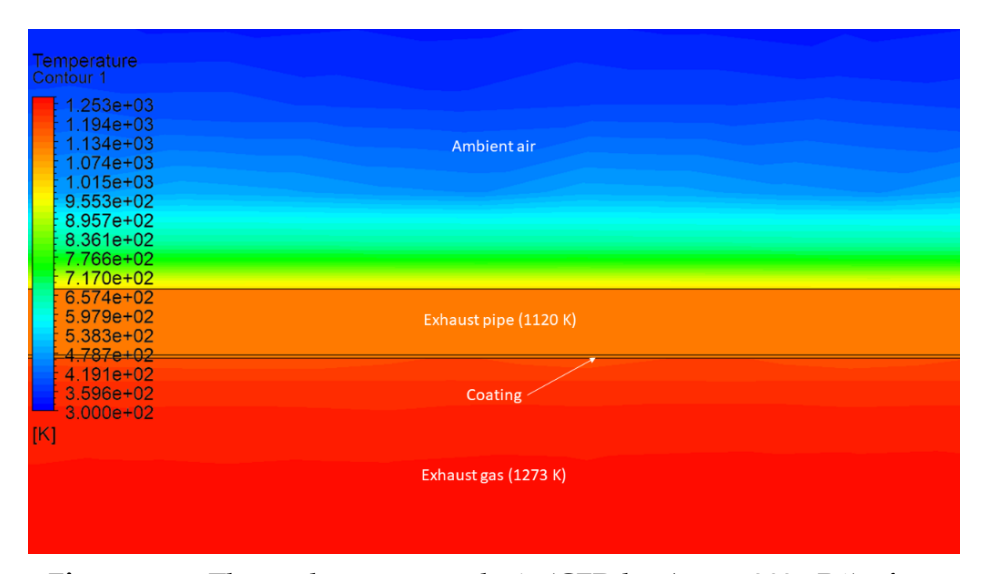


Figure 3.33. Dual-exit performance exhaust system for Inline-4 engine

To evaluate how well a glass-ceramic coating insulates the exhaust pipe and prevents heat transfer from the hot exhaust gas to the cooler ambient air. Figure 3.34 represents a thermal contour plot from a simulation (CFD) analyzing the temperature distribution across a coated titanium exhaust pipe exposed to high-temperature exhaust gas and ambient air. The exhaust gas entering the system was assigned an inlet temperature of 1273 K and a velocity of 50 m/s, reflecting the operational conditions typical of sports car engines under high-load regimes. The ambient air surrounding the exhaust pipe was represented at a temperature of 300 K with a convective flow velocity of 5 m/s, mimicking the external airflow produced during vehicle operation. The exhaust pipe was presumed to be constructed from commercially pure titanium due to its advantageous high-temperature mechanical properties and resistance to oxidation. This pipe featured an outer diameter of 60 mm and a wall thickness of 2 mm.





**Figure 3.34.** Thermal contour analysis (CFD by Ansys 2025 R1) of an exhaust system temperature value in Kelvin (K)

To improve oxidation resistance and thermal protection for the titanium against prolonged exposure to elevated-temperature gases, it was externally coated with a 0.1 mm-thick layer of fused silica (SiO<sub>2</sub>) glass, which was applied through an appropriate chemical vapor deposition (CVD) technique. The selection of glass-silica coating stemmed from its low thermal conductivity, chemical inertness, and superior thermal stability, positioning it as an effective barrier against high-temperature oxidation. The purpose of the analysis is to evaluate how well a glass-ceramic coating insulates the exhaust pipe and prevents heat transfer from the hot exhaust gas to the cooler ambient air (Fig.3.34).

The provided thermal contour plot depicts the temperature distribution across an exhaust system component, simulated under high-temperature operating conditions. Key temperature zones include:

- Exhaust gas core: 1273 K (typical of turbocharged or high-load engine conditions).
- Exhaust pipe surface: 1120 K, indicating significant thermal retention by the pipe material.
- Coating layer: Sharp gradient from ~700 K to 300 K, suggesting active thermal insulation (Fig.3.36).
- Ambient boundary: Stabilizes near 300 K, confirming effective ambient cooling.



The contour labels (e.g., 1.253e+03 K to 3.000e+02 K) demonstrate a non-linear temperature decay from the pipe interior to the coating-air interface, characteristic of systems with high heat flux and insulating layers.

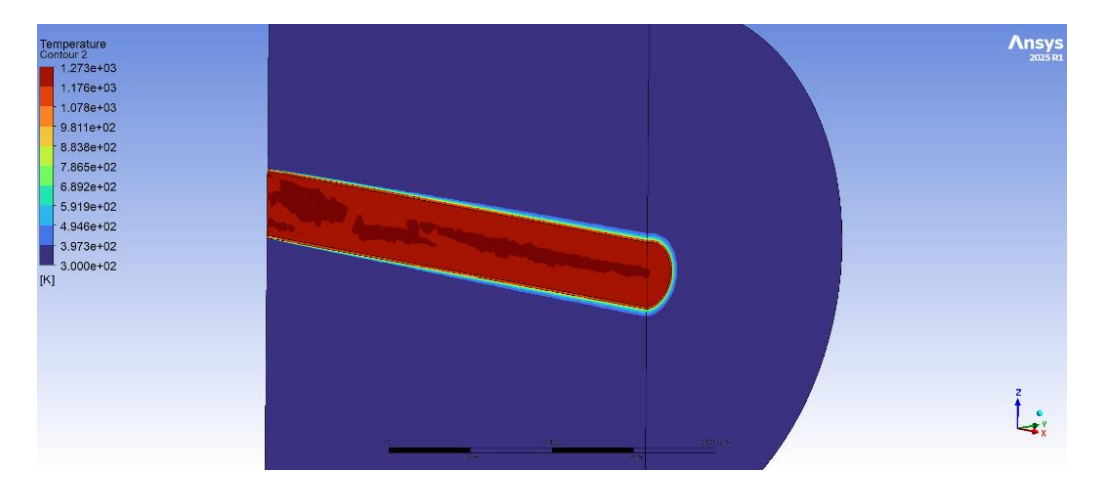


**Figure 3.35.** Thermal distribution in a coated exhaust system simulated under steady-state operating conditions

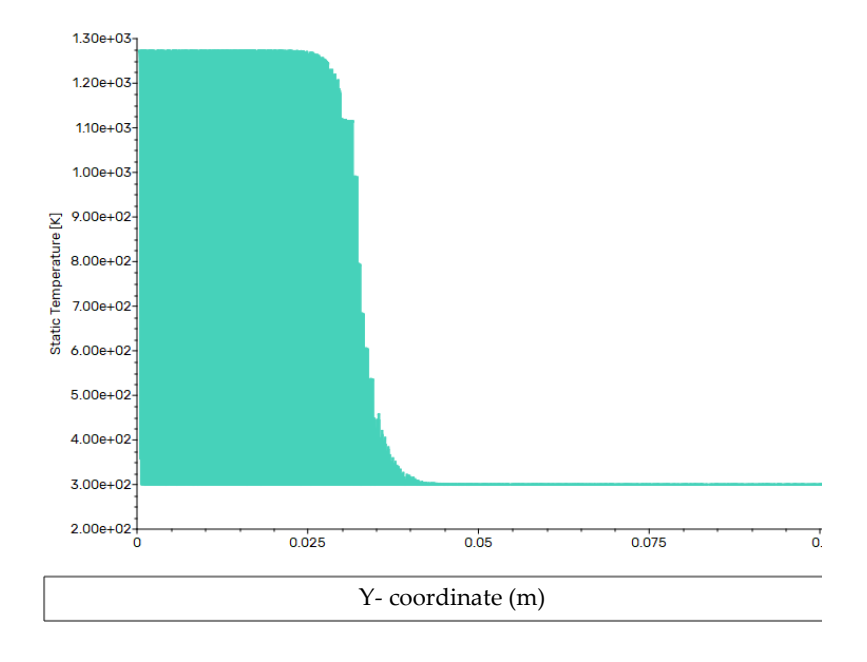


**Figure 3.36.** Temperature change along the Y-axis from the center of the pipe circumference radially outwards



# 4. Conclusion

- 1. The topics highlight the critical role of advanced coatings in enhancing the high-temperature oxidation resistance of titanium and its alloys, particularly for applications in automotive exhaust systems. Silicon-based coatings, such as silicides, effectively create a protective SiO<sub>2</sub> layer that inhibits oxygen penetration, demonstrating excellent thermal stability and oxidation resistance up to 1000°C. Glass and glass-ceramic coatings provide an alternative by forming dense barriers against oxygen infiltration and exhibiting self-repair capabilities, although challenges related to thermal expansion mismatches remain.
- 2. Adhesion in coating/substrate systems is a complex phenomenon influenced by various factors, including surface chemistry, mechanical interlocking, and thermodynamic principles. Intrinsic adhesion arises from molecular attractions at the interface, while measured adhesion quantifies bond strength through specific testing methods. Surface energy and wettability are critical for effective adhesion; substrates with higher surface energy promote better wetting and bonding. Various adhesion testing methods, including pull-off tests, scratch tests, and impact tests, help evaluate the performance of coatings.
- 3. The cleaning and thermal treatment processes employed for the Ti substrate are critical in ensuring the integrity and performance of the samples for subsequent applications. The multi-stage cleaning regimen, which includes washing with pH-balanced water, acetone washing, and ultrasonic immersion in isopropyl alcohol, effectively removes surface impurities and contaminants that could compromise the quality of the titanium. The use of ultrasonic cleaning enhances the removal of residual particles and oils, ensuring a pristine surface condition.
- 4. The cleaning and thermal treatment processes employed for the Ti substrate are critical in ensuring the integrity and performance of the samples for subsequent applications. The multi-stage cleaning regimen, which includes washing with pH-balanced water, acetone washing, and ultrasonic immersion in isopropyl alcohol, effectively removes surface impurities and contaminants that could compromise the quality of the titanium. The use of ultrasonic



- cleaning enhances the removal of residual particles and oils, ensuring a pristine surface condition.
- 5. Experimental results demonstrated that following the cleaning process, the tempering heat treatment at 700°C serves to enhance the structural stability and surface integrity of the titanium substrate. This thermal treatment not only alleviates residual stress from prior mechanical processing but also promotes a uniform microstructure that is essential for the performance of the material in high-temperature applications. The careful management of the heating and cooling processes minimizes the risk of thermal shocks and microcracks, thereby preserving the mechanical strength and chemical performance of the titanium.
- 6. Overall, these meticulous procedures ensure that the titanium substrate are optimally prepared for further modifications, such as coating applications or oxidation testing, thereby enhancing their reliability and effectiveness in practical applications.
- 7. The glass powder was produced using a melt-quench technique with a carefully formulated batch composition. The process involved several key stages: designing of glass compositions, glass batch preparation mixing, melting, quenching, grinding and sieving process. This meticulous process ensures the production of glass powder with optimal properties for high-temperature applications.
- 8. The important finding from this experiment is matching the CTE values of experimental glasses (9.5-10.5) x10-6 K -1 and Ti substrate (9.5-10.0) x10-6 K -1. Various factors can impact all-ceramic systems resistance to thermal shock; notably, any substantial difference in thermal expansion between glass coating layers can generate residual stress.
- 9. The study implemented three distinct sintering profiles to investigate the impact of peak temperature on the morphology and adhesion of glass coatings on titanium substrates. The first profile reached a peak temperature of 700 °C, promoting enhanced bonding through viscous flow, while the second profile, with a peak of 750 °C and 800 °C allowed for examination of coating densification at a higher temperature. Both approaches utilized a slurry-based application of glass powder with glycerol, facilitating uniform coating and effective heat treatment for improved adhesion and densification.
- 10. Data from EDS analysis of Ti substrate confirms that distribution of elements corresponding to chemical composition. Data from EDS analysis of glass



coating confirms that distribution of elements corresponds to the chemical composition of parent glass.

The microstructure of polished cross section of glass coating – Ti substrate after heat treatment at 700 °C and 750°C uniform glass coating of Ti substrate was achieved no cracks and gaps were observed.

- 11. XRD pattern of substrate confirms presents of Ti diffraction lines only. that confirms the result of EDS analysis.
- 12. The study of microstructure of polished cross sections of samples after heat treatment at 700 and 750°C evidenced that uniform glass coating on Ti substrate was achieved with no cracks and gaps.
- 13. XRD patterns of coatings after heat treatment at 700 and 750°C showed that no crystallization of coating occurred and glass remains in its amorphous nature. It means that glass keeps its disordered structure. However, after heat treatment at 800°C crystallization is evident:
  - Diffraction lines corresponding to crystalline phases such as diopside, wollastonite, and fluorapatite were recorded.
- 14. The result of thermal shock experiments demonstrated that all tested samples could resist 6 cycles of temperature change in the interval 250°C 20°C while 40% of samples to 10th of similar cycles 12.
  - Rotating crowns under light reveals crack orientation and penetration, indicating whether cracks arise from radial tensile or compressive stresses, and helps identify thermal expansion mismatches in glass components. Factors like thermal conductivity and interfacial bond strength impact thermal shock resistance, with higher conductivity reducing resistance. Variations in elastic moduli and restoration dimensions also affect stiffness and residual stress profiles. To ensure consistency, an incisor crown shape was uniformly applied across samples.
- 15. The results of this study can be used as the first approach for the development of reliable coatings on titanium for protection against high-temperature oxidation in the automotive industry. The contour analysis highlights critical thermal management challenges in exhaust systems, emphasizing the balance between insulation efficiency and material survivability under extreme conditions.



# 5. Appendix A

# FTIR analysis of glass coating

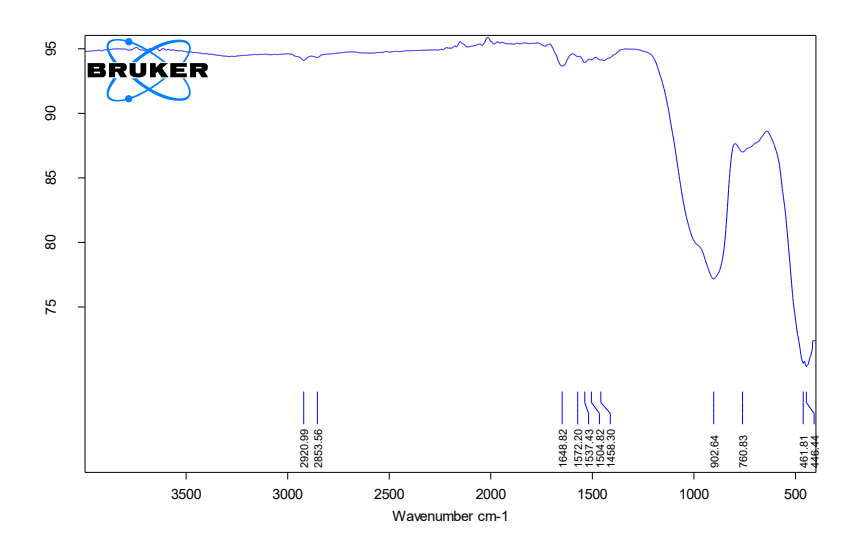


**Figure 5.1 A.** Fourier Transform Infrared Spectroscopy coating at 700°C

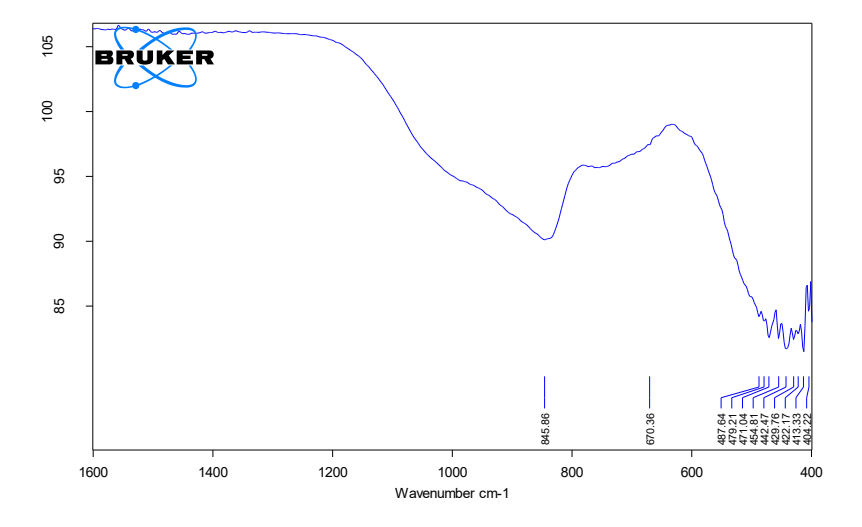


**Figure 5.2 A.** Fourier Transform Infrared Spectroscopy coating at 750°C



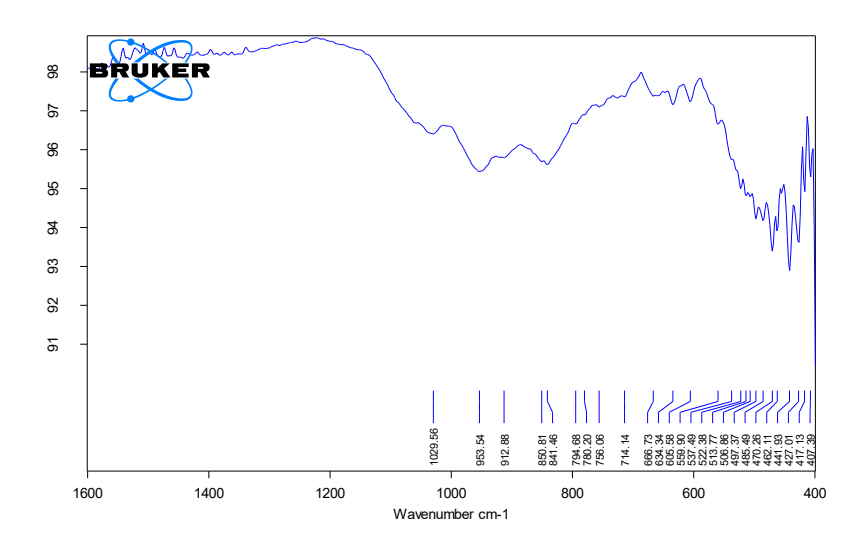


**Figure 5.3 A.** Fourier Transform Infrared Spectroscopy coating at 800°C

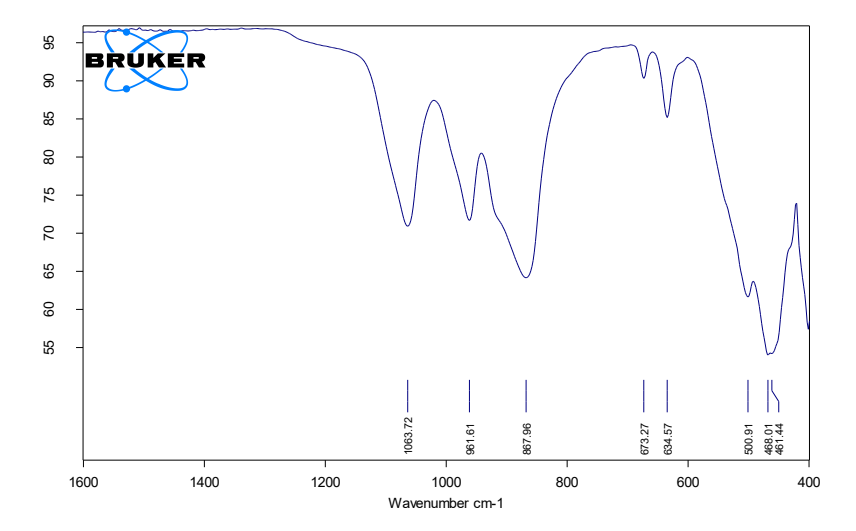


**Figure 5.4 A.** Fourier Transform Infrared Spectroscopy of Ti substrate tempered at 700°C



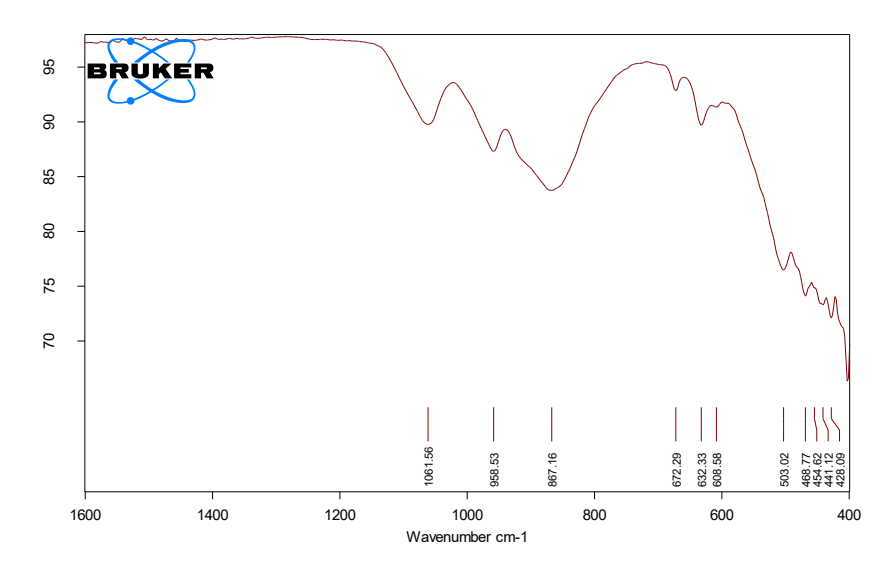


**Figure 5.5 A.** Fourier Transform Infrared Spectroscopy of Ti substrate heated at 700°C

# XRD for Ti substrates and glass powders

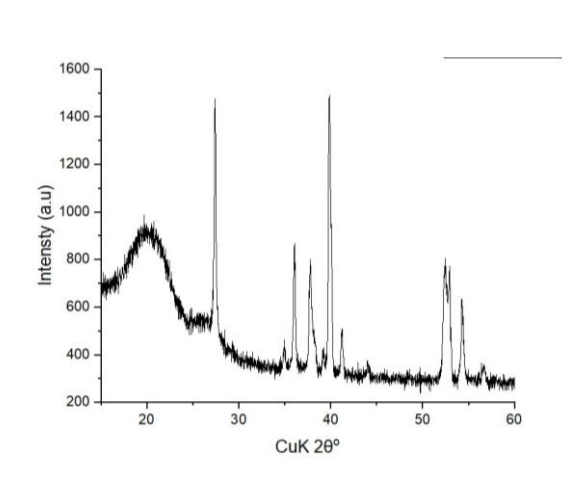


**Figure 5.6 A.** X-ray diffractograms of the Ti substrate after heating at 700 °C

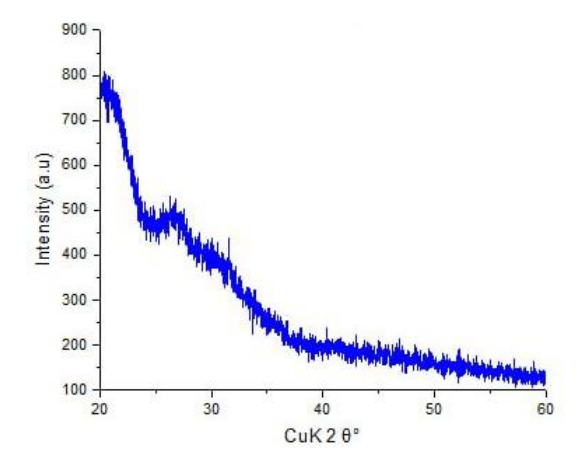


**Figure 5.7 A.** X-ray diffractograms of the glass-powder compacts heat treated at 700°C



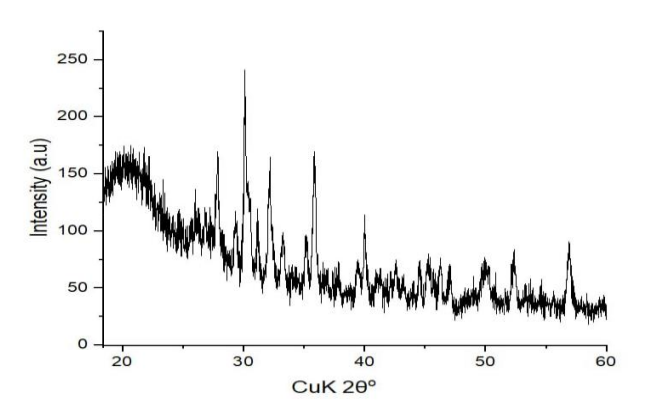


**Figure 5.8 A.** X-ray diffractograms of the glass-powder compacts heat treated at 800°C

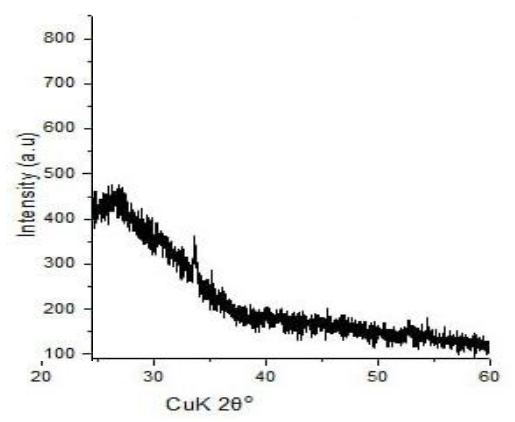


**Figure 5.9 A.** X-ray diffractograms of the glass-powder compacts heat treated at 750 °C

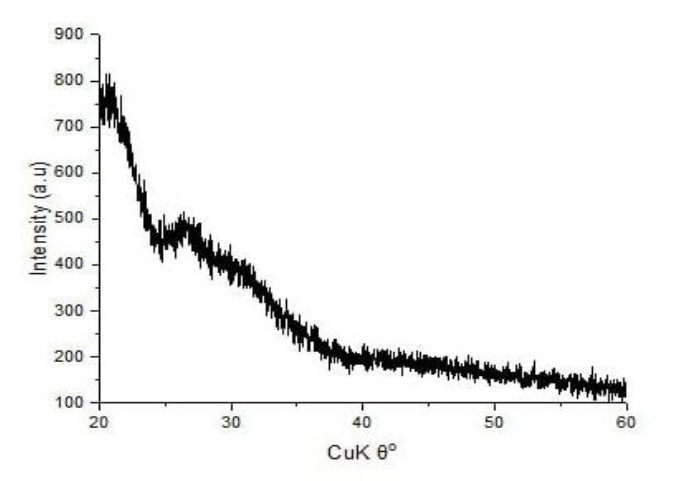


**Figure 5.10 A.** X-ray diffractograms of the glass-powder compacts heat treated at700°C.



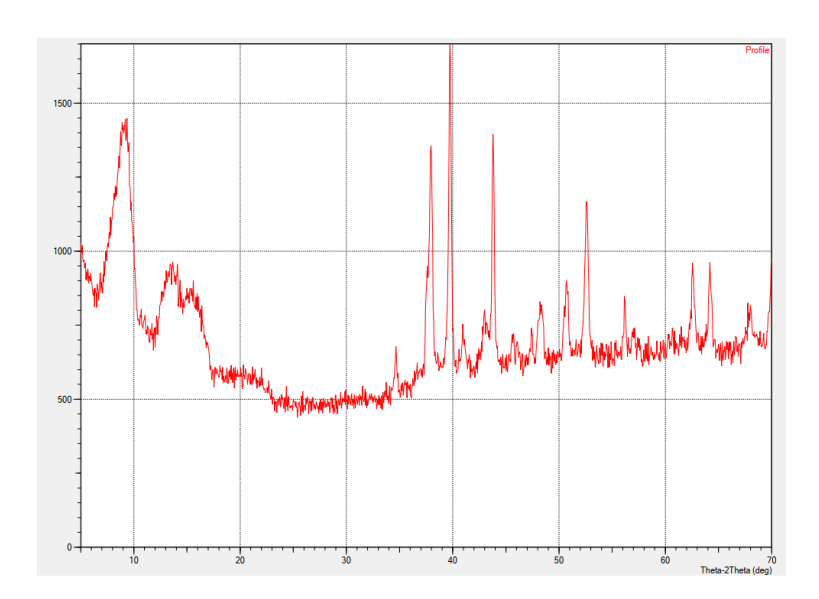


**Figure 5.11 A.** X-ray diffractograms of the Ti substrate sample 1 Grade 2 (ASTM B348)

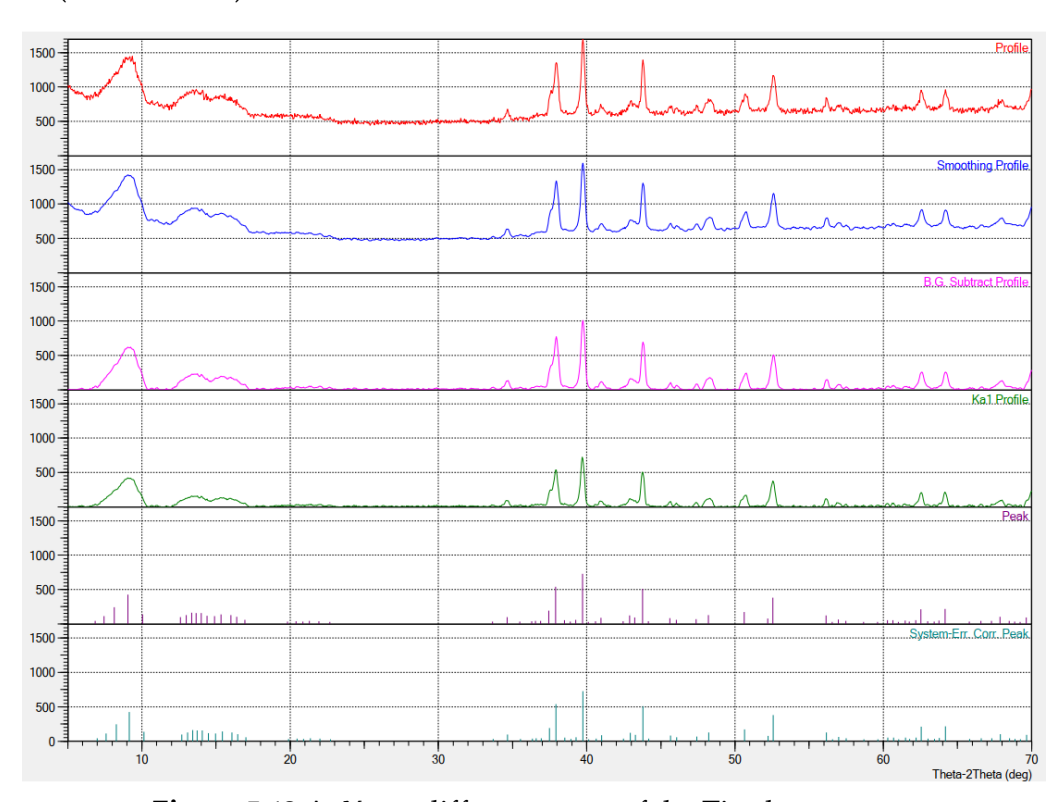


**Figure 5.12 A.** X-ray diffractograms of the Ti substrate



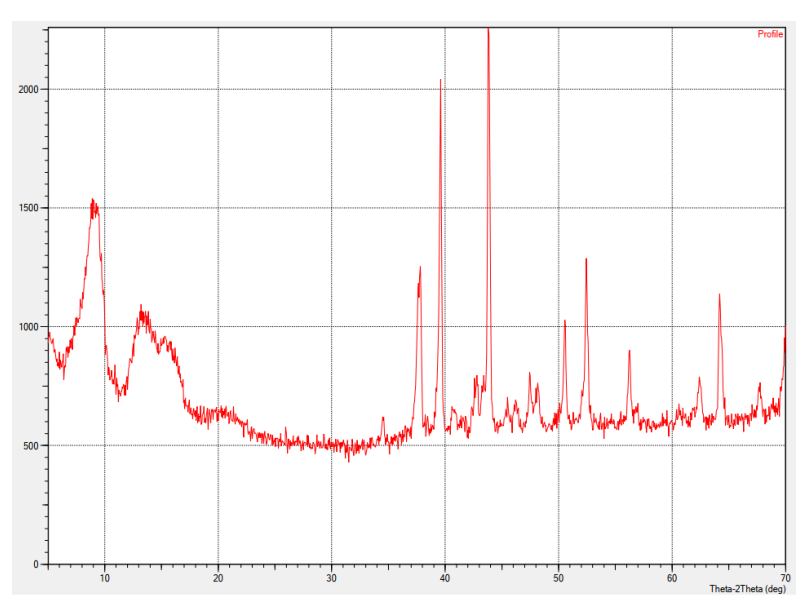


**Figure 5.13 A.** X-ray diffractograms of the Ti substrate sample 2 Grade 2 (ASTM B348)

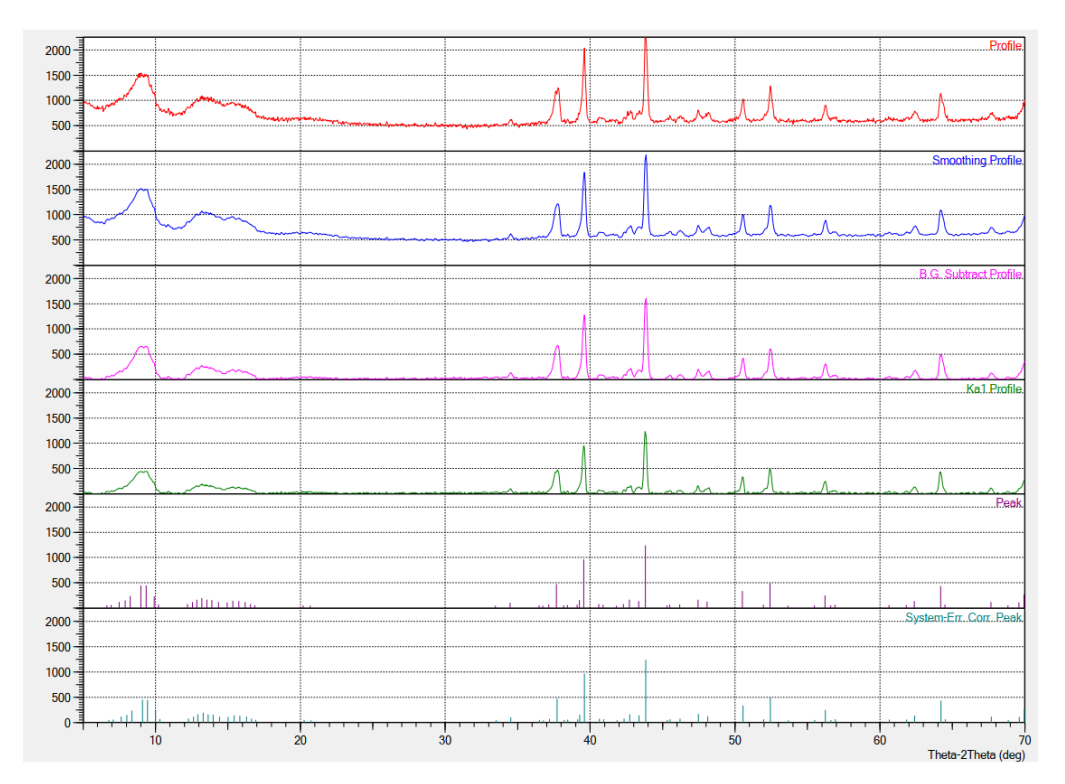


Figure 5.14 A. X-ray diffractograms of the Ti substrate



# **Bibliography**

- [1] J. Smith, A. R. Brown, and T. K. Lee, "High-temperature oxidation mechanisms in titanium alloys under nitrous oxide combustion," Acta Materialia, vol. 210, pp. 116–128, 2021, doi: 10.1016/j.actamat.2021.05.001.
- [2] M. Garcia et al., "Ceramic thermal barrier coatings for exhaust systems: Adhesion failure modes under thermal cycling," Surface & Coatings Technology, vol. 432, p. 128066, 2023, doi: 10.1016/j.surfcoat.2023.128066.
- [2] McAndrew, Anthony. (2015). Modelling of Ti-6Al-4V Linear Friction Welds.
- [4] R. Davis et al., "Engine efficiency losses due to exhaust backpressure at extreme temperatures," in Proc. SAE Int. Conf. Adv. Combust. Engines, Detroit, MI, USA, 2020, pp. 1–9, doi: 10.4271/2020-01-1234.
- [5] National Highway Traffic Safety Administration (NHTSA), "Fire incidence in high-performance vehicles: 2015–2022," NHTSA Tech. Rep. DOT HS 813 521, 2023. [Online]. Available: https://www.nhtsa.gov/fire-risks-sports-cars
- [6] UzAuto Motors, "Annual automotive market report: Uzbekistan," Tashkent, Rep. UAM-2023-09, 2023.
- [7] S. Patel, "Porsche tests 3D-printed titanium exhausts with active cooling," Automotive News Europe, Jan. 15, 2024. [Online]. Available: https://europe.autonews.com/porsche-3d-exhaust
- [8] Fédération Internationale de l'Automobile (FIA), "2025 regulations for sustainable motorsport materials," FIA Standard Doc. 12.4, 2023. [Online]. Available: https://www.fia.com/sustainability-regs
- [9] A. Polishetty, V. Manoharan, G. Littlefair, and C. Sonavane, "Machinability assessment of Ti-6Al-4V for aerospace applications," ASME Early Career Technical Journal, 2013.
- [10] Gerd Lutjering and James C. Williams. Titanium. 2nd ed., Springer, 2007, pp. 45-67. DOI: 10.1007/978-3-540-73036-1
- [11] Froes, F. H. (2015). Titanium: Physical Metallurgy, Processing, and Applications. ASM International.
- [12] Banerjee, D., & Davidson, J. E. (1996). Titanium Alloys: Science and Technology. CRC Press.
- [13] Christoph Leyens and Manfred Peters. Titanium and Titanium Alloys: Fundamentals and Applications. Wiley-VCH, 2003. DOI: 10.1002/3527602119.



- [14] Richard R. Boyer, George Welsch, and E. W. Collings. Materials Properties Handbook: Titanium Alloys. ASM International, 1994. DOI: 10.31399/asm.hb. v02. a0001012.
- [15] F. H. Froes. Titanium: Physical Metallurgy, Processing, and Applications. ASM International, 2018.
- [16] M. Peters, C. Leyens, J. Kumpfert, and J. C. Williams. "Titanium and Titanium Alloys: Fundamentals and Applications." Wiley-VCH, 2003.
- [17] D. Banerjee and J. C. Williams. Perspectives on Titanium Science and Technology. Acta Materialia, vol. 61, no. 3, pp. 844-879, 2013.
- [18] S. Liu and Y. C. Shin. "Additive Manufacturing of Titanium Alloy and Titanium Matrix Composites: A Review." International Journal of Machine Tools and Manufacture, vol. 132, pp. 17-48, 2019.
- [19] Gerd Lütjering and James C. Williams. Titanium. Springer Science & Business Media, 2007. DOI: 10.1007/978-3-540-73036-1.
- [20] Matthew J. Donachie. Titanium: A Technical Guide. ASM International, 2000. DOI: 10.1361/techguide2000.
- [21] Richard Rosenberg, Francis H. Froes, Samuel Semiatin, and Shankar Ankem. "Titanium processing and properties." Journal of Metals, vol. 64, no. 2, 2012, pp. 214-222. DOI: 10.1007/s11837-012-0281-0.
- [22] Boyer, R. R. (1996). "An Overview on the Use of Titanium in the Aerospace Industry." Materials Science and Engineering: A, vol. 213, pp. 103-114. DOI: 10.1016/0921-5093(96)10233-1.
- [23] Firstov, G. S., Rogojina, E. V., Firstov, J. V., & Vladykina, E. Y. (2007). "Titanium and Its Alloys as Biomaterials." Journal of Materials Science, vol. 42, no. 4, pp. 1404-1414. DOI: 10.1007/s10853-006-1461-x.
- [24] Abdul Wahed, Mohd & Gupta, Amit & Sharma, Vaibhav & Mahesh, Katakam & Singh, Swadesh & Kotkunde, Nitin. (2019). Material characterization, constitutive modelling, and processing map for superplastic deformation region in Ti-6Al-4V alloy. The International Journal of Advanced Manufacturing Technology. 104. 10.1007/s00170-019-03956-z.
- [25] Cedeno, A. J. (2005). Titanium Machining and Manufacturing Processes. Journal of Manufacturing Science and Engineering.
- [26] Jamieson, J.C. Crystal Structures of Titanium, Zirconium, and Hafnium at High Pressures. Science 1963, 140, 72–73. [b
- [27] Jamieson, J.C. Crystal Structures of Titanium, Zirconium, and Hafnium at High Pressures. Science 1963, 140, 72–73. [CrossRef] [PubMed]



- [28] Weiss, I.; Semiatin, S.L. Thermomechanical Processing of Alpha Titanium Alloys—An Overview. Mater. Sci. Eng. A Struct. Mater.
- 1999, 263, 243–256. [CrossRef]
- [29] Bania, P.J. Beta Titanium Alloys and Their Role in the Titanium Industry. JOM 1994, 46, 16–19. [CrossRef]
- [30] Koul, M.K.; Breedis, J.F. Phase Transformations in Beta Isomorphous Titanium Alloys. Acta Metall. 1970, 18, 579–588. [CrossRef]
- [31] E. Marin and A. Lanzutti, "Biomedical Applications of Titanium Alloys: A Comprehensive Review," Jan. 01, 2024, Multidisciplinary Digital Publishing Institute (MDPI). doi: 10.3390/ma17010114.
- [32] Mwinteribo, T.V.; Li, C.; Saifu, W.; Li, J.; Xu, X. Mechanical Properties of near Alpha Titanium Alloys for High-Temperature Applications—A Review. Aircr. Eng. Aerosp. Technol. 2020, 92, 521–540.
- [33] Semiatin, S.L.; Seetharaman, V.; Weiss, I. The Thermomechanical Processing of Alpha/Beta Titanium Alloys. JOM 1997, 49, 33–39. [CrossRef]
- [34] Liu, Y.; Lim, S.C.V.; Ding, C.; Huang, A.; Weyland, M. Unravelling the Competitive Effect of Microstructural Features on the Fracture Toughness and Tensile Properties of near Beta Titanium Alloys. J. Mater. Sci. Technol. 2022, 97, 101–112. [CrossRef]
- [35] Sidhu, S.S.; Singh, H.; Gepreel, M.A.-H. A Review on Alloy Design, Biological Response, and Strengthening of  $\beta$ -Titanium Alloys as Biomaterials. Mater. Sci. Eng. C Mater. Biol. Appl. 2021, 121, 111661. [CrossRef]
- [36] Alipour, S.; Taromian, F.; Ghomi, E.R.; Zare, M.; Singh, S.; Ramakrishna, S. Nitinol: From Historical Milestones to Functional Properties and Biomedical Applications. Proc. Inst. Mech. Eng. H 2022, 236, 1595–1612. [CrossRef]
- [37] G. Lutjering and J. C. Williams, Titanium. New York, NY, USA: Springer, 2007.
- [38] M. Niinomi, "Recent research and development in titanium alloys for biomedical applications and healthcare goods," Science and Technology of Advanced Materials, vol. 4, no. 5, pp. 445-454, 2003.
- [39] G. Lütjering and J. C. Williams, Titanium, 2nd ed., Springer, 2007, pp. 45-67. DOI: 10.1007/978-3-540-73036-1.
- [40] D. Banerjee and J. C. Williams, "Perspectives on titanium science and technology," Acta Materialia, vol. 61, no. 3, 2013, pp. 844–879. DOI: 10.1016/j.actamat.2012.10.043.
- [41] M. Niinomi, "Mechanical properties of biomedical titanium alloys," Materials Science and Engineering: A, vol. 243, no. 1-2, 1998, pp. 231–236. DOI: 10.1016/S0921-5093(97)00806-X.



- [42] R. R. Boyer, "An overview on the use of titanium in the aerospace industry," Materials Science and Engineering: A, vol. 213, no. 1-2, 1996, pp. 103-114. DOI: 10.1016/0921-5093(96)10233-1.
- [43] S. Z. Hu, Y. C. Wang, H. J. Rack, and D. C. Dunand, "Processing, structure, and properties of porous titanium," Materials Science and Engineering: A, vol. 559, 2013, pp. 102-117. DOI: 10.1016/j.msea.2012.08.050.
- [44] Gerd Lutjering and James C. Williams. Titanium. 2nd ed., Springer, 2007, pp. 45-67. DOI: 10.1007/978-3-540-73036-1.
- [45] Sohn, H.-S. Production Technology of Titanium by Kroll Process. J. Korean Inst. Resour. Recycl. 2020, 29, 3–14. [CrossRef]
- [46] Agripa, H.; Botef, I. Modern Production Methods for Titanium Alloys: A Review. In Titanium Alloys—Novel Aspects of Their Manufacturing and Processing; IntechOpen: London, UK, 2019.
- [47] Woodside, C.R.; King, P.E.; Nordlund, C. Arc Distribution during the Vacuum Arc Remelting of Ti-6Al-4V. Metall. Mater. Trans. B 2013, 44, 154–165. [CrossRef]
- [48] Blackburn, M.J.; Malley, D.R. Plasma Arc Melting of Titanium Alloys. Mater. Eng. 1993, 14, 19–27. [CrossRef]
- [49] Fashu, S.; Lototskyy, M.; Davids, M.W.; Pickering, L.; Linkov, V.; Tai, S.; Renheng, T.; Fangming, X.; Fursikov, P.V.; Tarasov, B.P. A. Review on Crucibles for Induction Melting of Titanium Alloys. Mater. Des. 2020, 186, 108295. [CrossRef]
- [50] Fang, Z.Z.; Paramore, J.D.; Sun, P.; Chandran, K.S.R.; Zhang, Y.; Xia, Y.; Cao, F.; Koopman, M.; Free, M. Powder Metallurgy of Titanium—Past, Present, and Future. Int. Mater. Rev. 2018, 63, 407–459. [CrossRef]
- [51] Ramamurthy, A.; Sivaramakrishnan, R.; Muthuramalingam, T.; Venugopal, S. Performance Analysis of Wire Electrodes on Machining Ti-6Al-4V Alloy Using Electrical Discharge Machining Process. Mach. Sci. Technol. 2015, 19, 577–592. [CrossRef]
- [52] Hasçalık, A.; Çayda¸s, U. Electrical Discharge Machining of Titanium Alloy (Ti–6Al–4V). Appl. Surf. Sci. 2007, 253, 9007–9016. [CrossRef]
- [53] Ramamurthy, A.; Sivaramakrishnan, R.; Muthuramalingam, T.; Venugopal, S. Performance Analysis of Wire Electrodes on Machining Ti-6Al-4V Alloy Using Electrical Discharge Machining Process. Mach. Sci. Technol. 2015, 19, 577–592. [CrossRef]
- [54] Hasçalık, A.; Çayda, s., U. Electrical Discharge Machining of Titanium Alloy (Ti-6Al-4V). Appl. Surf. Sci. 2007, 253, 9007–9016. [CrossRef]



- [55] Muthuramalingam, T.; Akash, R.; Krishnan, S.; Phan, N.H.; Pi, V.N.; Elsheikh, A.H. Surface Quality Measures Analysis and Optimization on Machining Titanium Alloy Using CO2 Based Laser Beam Drilling Process. J. Manuf. Process. 2021, 62, 1–6. [CrossRef]
- [56] Muthuramalingam, T.; Moiduddin, K.; Akash, R.; Krishnan, S.; Hammad Mian, S.; Ameen, W.; Alkhalefah, H. Influence of Process Parameters on Dimensional Accuracy of Machined Titanium (Ti-6Al-4V) Alloy in Laser Beam Machining Process. Opt. Laser Technol. 2020, 132, 106494. [CrossRef]
- [57] Yang, X.; Richard Liu, C. Machining Titanium and Its Alloys. Mach. Sci. Technol. 1999, 3, 107–139. [CrossRef]
- [58] Singh, R.; Khamba, J.S. Ultrasonic Machining of Titanium and Its Alloys: A Review. J. Mater. Process. Technol. 2006, 173, 125–135. [CrossRef]
- [59] Kumar, J.; Khamba, J.S.; Mohapatra, S.K. An Investigation into the Machining Characteristics of Titanium Using Ultrasonic Machining. Int. J. Mach. Mach. Mater. 2008, 3, 143. [CrossRef]
- [60] Status of Titanium and Titanium Alloys in Automotive Applications
- Ninomi M, Akiyama S, Ikeda M, Hagiwara M, Maruyama the K (2007).
- [61] MSC Direct. (2023). "Challenges in Machining Titanium." Better MRO, Available at: mscdirect.com.
- [62] Lasting Titanium. (2023). "Benefits and Challenges of Forging Titanium Alloys." Titanium Industry Report, Available at: lastingtitanium.com.
- [63] Climate MIT. (2023). "Titanium Availability and Supply Risks for EVs." MIT Climate Portal, Available at: climate.mit.edu.
- [64] U.S. Department of Energy. (2023). "Low-Cost Titanium Alloy Production." Energy.gov, Available at: energy.gov.
- [65] Eplus3D. (2023). "How to Reduce Titanium Manufacturing Costs." Metal 3D Printing Report, Available at: eplus3d.com.
- [66] Titanium Info Group. (2023). "Methods to Improve Economy of Titanium Materials." Titanium Research Journal, Available at: titaniuminfogroup.com.
- [67] Journal of Materials Science. (2023). "Advancements in Additive Manufacturing for Titanium Alloys." Materials Science & Engineering, vol. 543, pp. 112-125. DOI: 10.1002/adem.202301122.
- [68] International Journal of Manufacturing. (2023). "Innovations in Titanium Processing Techniques." Manufacturing & Industrial Research, vol. 32, pp. 67-80. DOI: 10.1007/s00170-021-08218-5.



- [69] Journal of Advanced Materials. (2023). "Development of Next-Generation Titanium Alloys." Advanced Materials & Engineering, vol. 75, pp. 134-150.
- [70] Automotive Materials Report. (2023). "Future Prospects of Titanium in the Automotive Industry." Global Automotive Research, vol. 29, pp. 45-60.
- [71] J. A. Nesbitt and R. M. Nagabhushana, "Protective Coatings for High-Temperature Titanium Alloys: A Review," Surface and Coatings Technology, vol. 76-77, pp. 95-105, 1995. DOI: 10.1016/0257-8972(95)02550-6.
- [72] C. G. Levi, "Emerging Materials and Processes for Thermal Barrier Systems," Current Opinion in Solid State & Materials Science, vol. 8, no. 1, pp. 77-91, 2004. DOI: 10.1016/j.cossms.2004.10.008.
- [73] Ali, H. M. (Ed.). (2022). Titanium dioxide: Advances and applications. IntechOpen. ISBN: 978-1-83969-475-2.
- [74] S. C. Deevi and V. K. Sikka, "Nickel and Iron Aluminides: An Overview on Properties, Processing, and Applications," Intermetallics, vol. 4, no. 5, pp. 357-375, 1996. DOI: 10.1016/0966-9795(96)00002-6.
- [75] F. H. Froes, "The Use of Titanium in Industrial Applications," Journal of Materials Engineering and Performance, vol. 14, pp. 681-685, 2005. DOI: 10.1361/105994905X77611.
- [76] Wikipedia contributors. (n.d.). Coating. Wikipedia. Retrieved June 11, 2025, from https://en.wikipedia.org/wiki/Coating
- [77] Mattox D M. Handbook of Physical Vapor Deposition (PVD) Processing. Oxford UK Else- vier, 2010;
- [78] Wikipedia contributors. (n.d.). Chemical vapor deposition. Wikipedia. Retrieved June 11, 2025, from https://en.wikipedia.org/wiki/Chemical\_vapor\_deposition
- [79] Wikiwand. (n.d.). Chemical vapor deposition. Retrieved June 11, 2025, from http://www.wikiwand.com/en/Chemical\_vapor\_deposition
- [80] Amin S, Panchal H. A Review on Thermal Spray Coating Processes. International Journal of Current Trends in Engineering & Research (IJCTER) e-ISSN 2455 1392 Volume 2 Issue 4, April 2016 pp. 556 563;
- [81] Won-Seock K, Il-Han J, Jung-Ju L, Hee-Tae J. Evaluation of mechanical interlock e ect on adhesion strength of polymer metal interfaces using micro-patterned surface topography. International Journal of Adhesion and Adhesives 30(6):408-417, September 2010;
- [82] https://www.materialstoday.com/metal-nishing/features/fundamentals-of-paint-adhesion;
- [83] Baldan A Adhesion phenomena in bonded joints International. Journal of Adhesion & Ad- hesives 38 (2012) 95 116;



- [84] Neubauer R, Moritz Husmann S, Weinländer C, Kienzl N, Leitner E, Hochenauer C. Acid base interaction and its in uence on the adsorption kinetics and selectivity order of aromatic sulfur heterocycles adsorbing on Ag-Al2O3. Institute of Thermal Engineering (3070);
- [85] Simpson V. Foundamental studies of adhesion. Master Thesis, University of Wollongong, 1997;
- [86] Ebnesajjad C F. Surface Treatment of Materials for Adhesion Bonding. Elvisier, Second edition, 2014;
- [87] Tracton A. Coating technology handbook. Taylor & Francis Group, LLC 2006;
- [88] ASTM International. (2022, July 29). Standard Test Method for Pull-Off Strength of Coatings Using Portable Adhesion Testers (ASTM D4541-22). Retrieved June 11, 2025, from
- [89] Chalker P R, Bull S J, Rickerby D S. A review of the methods for the evaluation of coating- substrate adhesion. Materials Science and Engineering, A 140 (1991) 583-592;
- [90] Cai Y, Zhang S, Zeng X, Qian M, Sun D, Weng W. Interfacial study of magnesium-containing fluoridated hydroxyapatite coatings. Thin Solid Films, 519 (2011) 4629 4633;
- [91] Fletcher J F, Barnes D J. Pull-o adhesion testing of coating- improve your technique. Elcometer Limited;
- [92] Choudhary R K, Mishra P. Use of Acoustic Emission During Scratch Testing for Under- standing Adhesion Behavior of Aluminum Nitride Coatings. Journal of Materials Engineering and Performance, June 2016, Volume 25, Issue 6, pp 2454 2461;
- [93] Campos-Silva I, Martínez-Trinidad J, Doñu-Ruíz M A, Rodríguez-Castro G. Hernández- Sánchez E, Bravo-Bárcenas O. Interfacial indentation test of FeB/Fe2B coatings. Surface and Coatings Technology, Vol. 206, Issue 7, 25 December 2011, pp 1809-1815;
- [94] Bouzakis K D, Gerardis S Skordaris G, Bouzakis E. Nano-impact test on a TiAlN PVD coating and correlation between experimental and FEM results. Surface and Coatings Tech-nology, Vol. 206, Issue 7, 25 December 2011, pp 1936-1940;
- [95] Mittal K L. Adhesion Measurement of thin lms. Electrocomponent Science and Technology 1976, Vol. 3, pp. 21-42;
- [96] Martin P M. Handbook of Deposition Technologies for Films and Coatings Science. Appli- cations and Technology Book, 3rd Edition, 2010;
- [97] Moira e Silva CW, Alves E, Ramos AR, Sandu CS, Cavaleiro A. Adhesion failures on hard coatings induced by interface anomalies. Vacuum 83 (2009) 1213-1217;
- [98] Poorna Chander K, Vashista M, Sabiruddin K, Paul S, Bandyopadhyay P P. E ects of grit blasting on surface properties of steel substrates. Materials and design 30 (2009) 2895-2902;



- [99] Varacalle D J, Guillen D, Deason D M, Rhodaberg W. E ect of Grit-Blasting on Substrate Roughness and Coating Adhesion. Journal of Thermal Spray Technology, 15(3):348-355, September 2006;
- [100] Danlos Y, Costil S, Liao H, Coddet C. In uence of Ti-6Al-4Vand Al 2107substrate morphol- ogy on Ni-Al coating adhesion-impacts of laser treatment. Surface and coating technology,205 (2011) 2702-2708;
- [101] Kromer R, Costil S, Cormier J, Courapied D, Berthe L, Peyre P, Boustie M. Laser surface patterning to enhance adhesion of plasma sprayed coatings. Surface and coatings technology, 278 (2015) 171-182;
- [102] Rahamati B, Zalnezhad E, Sarhan A A D, Kamiab Z, Nasiri Tabrizi B, Abas W A B W. Enhancing the adhesion strength of tantalum oxide ceramic thin lm coating on biomedical Ti-6Al-4V alloy by thermal surface treatment. Ceramics international, 41 (2015) 13055- 13063;
- [103] T. I. H. P. K. T. G. J. S. C. R. P. M. L. C. M. Y. F. R. F. A. I. S. B. H., "The Strength-to-Weight Ratio of Titanium Alloys," Journal of Materials Science, vol. 45, no. 6, pp. 1501-1512, 2010.
- [104] A. K. S. D. R. T. H. K. N. S. P. A., "Corrosion Resistance of Titanium Alloys," Corrosion Science, vol. 52, no. 2, pp. 303-315, 2011.
- [105] J. D. F. R. J. T. M. H. P., "Thermal Stability of Titanium," Materials Science and Engineering A, vol. 527, no. 1, pp. 83-89, 2010.
- [106] R. L. R. P. N., "Durability of Glass Ceramic Coatings in Automotive Applications," Journal of Thermal Spray Technology, vol. 22, no. 2, pp. 145-153, 2013.
- [107] Y. C. H. K. E. T., "Impact of Glass Ceramic Coatings on Engine Performance," Energy, vol. 36, no. 12, pp. 4943-4950, 2011.
- [108] H. P. C. J. M. E., "Aesthetic Aspects of Glass Ceramic Coatings," Journal of Coating Science and Technology, vol. 12, no. 3, pp. 245-254, 2014.
- [109] J. G. T. R. P. P. F., "Future Directions in Automotive Coatings," Automotive Engineering, vol. 25, no. 2, pp. 105-112, 2013.
- [110] L. N. A. M. E. T., "Sustainability in Coating Technologies," Environmental Science & Technology, vol. 45, no. 4, pp. 365-372, 2011.
- [111] Renugadevi, R & Vasu, Rajkumar & Arasappan, Rajesh. (2016). MODELLING AND ANALYSIS OF DAMPING EFFECT IN EXHAUST SYSTEM USING ANSYS. 3. 38-43.
- [112] R. Brown, "Chemical Vapor Deposition: Advantages and Applications," Surface Engineering, vol. 36, no. 7, pp. 455-462, Jul. 2021.
- [113] P. Black and S. Gray, "Economic Impact of Coating Technologies in Automotive Applications," Automotive Engineering Journal, vol. 52, no. 6, pp. 34-40, Jun. 2021.



[114] ASTM B348, "Standard Specification for Titanium and Titanium Alloy Bars and Rods for Aerospace Applications," ASTM International, West Conshohocken, PA, USA, 2021.

[115] L. Davis, "Thermal Stability of Glass-Ceramic Coatings," Materials Science and Engineering, vol. 55, no. 2, pp. 78-85, Feb. 2019.

# **Images**

# Figure 1.1.

[F1] QuesTek Innovations. "Running Your Engines Hotter Enhances Performance and Reduces Carbon Emissions." https://questek.com/...

[F2] Nickel Institute. "High-Temperature Characteristics of Stainless Steels." https://nickelinstitute.org/...

[F3] Dey, A. et al. "High-temperature oxidation behavior of titanium alloys." \*Journal of Alloys and Compounds\*, 753, 61–74, 2018.

[F4] HowStuffWorks. "Top 10 Causes of a Car Fire." https://auto.howstuffworks.com/...

[F5] ScienceDirect. "Fracture Analysis of Thermal Barrier Coating Delamination under Thermal Shock." https://www.sciencedirect.com/...

# Figure 1.2.

[F6] S. Patel, "Porsche tests 3D-printed titanium exhausts with active cooling," Automotive News Europe, Jan. 15, 2024. [Online]. Available: https://europe.autonews.com/porsche-3d-exhaust

#### Figure 1.3.

[F7] Bruce, Sam & Delaval, Beni & Moisi, Anthea & Ford, Jerad & West, James & Loh, Joanne & Hayward, Jennifer. (2021). Critical Energy Minerals Roadmap. The global energy transition: Opportunities for Australia's mining and manufacturing sectors. 10.13140/RG.2.2.16659.60968.

# Figure 1.4.

[F8] "Titanium Processing: What You Need to Know," Hyson Etch, Oct. 22, 2022. [Online]. Available: https://www.hysonetch.com/titanium-processing/. [Accessed: Mar. 8, 2025].

#### Figure 1.5.

[F9] Ali, H. M. (Ed.). (2022). Titanium dioxide: Advances and applications. IntechOpen. ISBN: 978-1-83969-475-2



# Figure 1.6.

[F10] Abdul Wahed, Mohd & Gupta, Amit & Sharma, Vaibhav & Mahesh, Katakam & Singh, Swadesh & Kotkunde, Nitin. (2019). Material characterization, constitutive modelling, and processing map for superplastic deformation region in Ti-6Al-4V alloy. The International Journal of Advanced Manufacturing Technology. 104. 10.1007/s00170-019-03956-z.

# Figure 1.7.

[F11] E. Marin and A. Lanzutti, "Biomedical Applications of Titanium Alloys: A Comprehensive Review," Jan. 01, 2024, Multidisciplinary Digital Publishing Institute (MDPI). doi: 10.3390/ma17010114.

# Figure 1.8.

[F12] M. Niinomi, "Mechanical properties of biomedical titanium alloys," Materials Science and Engineering: A, vol. 243, no. 1-2, 1998, pp. 231–236. DOI: 10.1016/S0921-5093(97)00806-X.

# Figure 1.9.

[F13] Application of Titanium in the Automotive Industry. Stanford Advanced materials. https://www.samaterials.com/content/application-of-titanium-in-the-automotive-industry.html

# Figure 1.10, Figure 1.11, Figure 1.12, Figure 1.13, Figure 1.14, Figure 1.15.

[F14] Status of Titanium and Titanium Alloys in Automotive Applications Ninomi M, Akiyama S, Ikeda M, Hagiwara M, Maruyama The K (2007).

# Figure 1.16.

[F15] D. S. Brauer, "Bioaktive Gläser: Struktur und Eigenschaften," Angewandte Chemie, vol. 127, no. 14, pp. 4232–4254, Mar. 2015, doi: 10.1002/ange.201405310.

# Figure 2.1.

[F16] Sigma-Aldrich. (n.d.). \*Materials science and engineering\*. https://www.sigmaaldrich.com/UZ/en/applications/materials-science-and-engineering?utm\_source=redirect&utm\_medium=promotional&utm\_campaign=materials-science

#### Figure 2.2.

[F17] Pajkic Z, Wolf H, Gerdes T, Willert-Porada M. Microwave plasma uidized bed arc-PVD coating of particulate materials, Surface and Coatings Technology, May 2008, 202(16):3927-3932;



# Figure 2.3.

[F18] Mattox D.M. Handbook of Physical Vapor Deposition (PVD) Processing, Oxford UK Elsevier, 2010;

# Figure 2.4.

[F19] Mathur S, Shen H, Altmayer J. Nanostructured funcional ceramic coatings by molecule- based chemical vapor deposition., Reviews on Advanced Materials Science, 15(2007) 163-23;

# Figure 2.5.

[F20] SlideShare. (n.d.). \*Share & discover presentations\*. https://www.slideshare.net

# Figure 2.6.

[F21] https://www.researchgate.net/ gure/Thermal-spray-process-principle-Source-An-Introduction-to-Thermal-Spray-Issue-4-C\_ g1\_307944165;

# Figure 2.7.

[F22] Amin S, Panchal H. A Review on Thermal Spray Coating Processes. International Journal of Current Trends in Engineering & Research (IJCTER) e-ISSN 2455 1392 Volume 2 Issue 4, April 2016 pp. 556 563;

#### Figure 2.8.

[F23] Advanced Coating. (n.d.). \*Advanced Coating SA\*. Advanced-Coating.com. https://www.advanced-coating.com/

#### Figure 2.9.

[F24] Li J,Li C, Yang G, Li C. E ect of vapor deposition in shrouded plasma spraying on morphology and wettability of the metallic Ni20Cr coating surface. Elsevier Journal of Alloys and Compounds, Vol. 735, 25 February 2018, pp 430-440;

#### Figure 2.10.

[F25] IndiaMART. (n.d.). Phosphate coating. Retrieved June 11, 2025, from https://www.indiamart.com/proddetail/phosphate-coating-16503155030.html

#### Figure 2.11.

[F26] Aluminum Electroplating Using Bromide Salts, FEBRUARY 1, 2018, MANUFACTUR- ING & PROTOTYPING, MATERIALS;

# Figure 2.12.

[F27] F Jones Jewelers. (n.d.). \*Rochester's home for fine jewelry, diamonds & engagement rings\*. Retrieved October 27, 2023, from https://www.jfjonesjewelers.com;



# Figure 2.13, Figure 2.14

[F28] Amin S, Panchal H. A Review on Thermal Spray Coating Processes. International Journal of Current Trends in Engineering & Research (IJCTER) e-ISSN 2455 1392 Volume 2 Issue 4, April 2016 pp. 556 563;

# Figure 2.15. Figure 2.17, Figure 2.18, Figure 2.19, Figure 2.22.

[F29] Baldan A Adhesion phenomenon in bonded joints International. Journal of Adhesion & Adhesives 38 (2012) 95 116;

# **Figure 2.20, Figure 2.23.**

[F30] Tracton A. Coating technology handbook. Taylor & Francis Group, LLC 2006;

# Figure 2.21.

[F31] Ray A. Intermolecular forces give rise to cohesion in water molecules. Jul 16, 2017;

# **Figure 2.16.**

[F32] Neubauer R, Moritz Husmann S, Weinländer C, Kienzl N, Leitner E, Hochenauer C. Acid base interaction and its in uence on the adsorption kinetics and selectivity order of aromatic sulfur heterocycles adsorbing on Ag-Al2O3. Institute of Thermal Engineering (3070);

#### Figure 2.24.

[F33] Chalker P R, Bull S J, Rickerby D S. . A review of the methods for the evaluation of coating-substrate adhesion. Materials Science and Engineering, A 140 (1991) 583-592;

# Figure 2.25.

[F34] DFD Instruments. (n.d.). ASTM D4541 – ISO 4624. Retrieved June 11, 2025, from https://dfdinstruments.com/astm-d4541-iso-4624/

#### Figure 2.26.

[F35] Cai Y, Zhang S, Zeng X, Qian M, Sun D, Weng W. Interfacial study of magnesium- containing uoridated hydroxyapatite coatings. Thin Solid Films, 519 (2011) 4629 4633;

#### Figure 2.27.

[F36] Tracton A. Coating technology handbook. Taylor & Francis Group, LLC 2006;

# Figure 2.28.

[F37] Sergici Onur A, Randall N. Scratch Testing of Coatings. Advanced Materials and Pro- cases, April 2006;



# **Figure 2.29, Figure 2.30.**

[F38] Choudhary R K, Mishra P. Use of Acoustic Emission During Scratch Testing for Understanding Adhesion Behavior of Aluminum Nitride Coatings. Journal of Materials Engineering and Performance, June 2016, Volume 25, Issue 6, pp 2454 2461;

# **Figure 2.31, Figure 2.32.**

[F43] Tracton A. Coating technology handbook. Taylor & Francis Group, LLC 2006;

# Figure 2.33.

[F44] Campos-Silva I, Martínez-Trinidad J, Doñu-Ruíz M A, Rodríguez-Castro G. Hernández-Sánchez E, Bravo-Bárcenas O. Interfacial indentation test of FeB/Fe2B coatings. Surface and Coatings Technology, Vol. 206, Issue 7, 25 December 2011, pp 1809-1815;

# **Figure 2.34, Figure 2.35.**

[F45] Tracton A. Coating technology handbook. Taylor & Francis Group, LLC 2006;

# **Figure 2.36, Figure 2.37.**

[F46] Moira e Silva CW, Alves E, Ramos AR, Sandu CS, Cavaleiro A. Adhesion failures on hard coatings induced by interface anomalies. Vacuum 83 (2009) 1213-1217;

# Figure 2.38, Figure 2.39, Figure 2.40.

[F47] Varacalle D J, Guillen D, Deason D M, Rhodaberg W. E ect of Grit-Blasting on Substrate Roughness and Coating Adhesion. Journal of Thermal Spray Technology, 15(3):348-355, September 2006;

# Figure 2.41, Figure 2.42, Figure 2.45.

[F48] Kromer R, Costil S, Cormier J, Courapied D, Berthe L, Peyre P, Boustie M. Laser surface patterning to enhance adhesion of plasma sprayed coatings. Surface and coatings technology, 278 (2015) 171-182;

# **Figure 2.44, Figure 2.45.**

[F49] Rahamati B, Zalnezhad E, Sarhan A A D, Kamiab Z, Nasiri Tabrizi B, Abas W A B W. Enhancing the adhesion strength of tantalum oxide ceramic thin lm coating on biomedical Ti-6Al-4V alloy by thermal surface treatment. Ceramics international, 41 (2015) 13055-13063;

# Figure 2.46.

[F50] Tracton A. Coating technology handbook. Taylor & Francis Group, LLC 2006;

#### Figure 2.47.

[F51] Renugadevi, R & Vasu, Rajkumar & Arasappan, Rajesh. (2016). MODELLING AND ANALYSIS OF DAMPING EFFECT IN EXHAUST SYSTEM USING ANSYS. 3. 38-43.



# Figure 2.48.

[F52] R. Brown, "Chemical Vapor Deposition: Advantages and Applications," Surface Engineering, vol. 36, no. 7, pp. 455-462, Jul. 2021.

# **Tables**

#### Table 1.1.

[T1] Abdul Wahed, Mohd & Gupta, Amit & Sharma, Vaibhav & Mahesh, Katakam & Singh, Swadesh & Kotkunde, Nitin. (2019). Material characterization, constitutive modelling, and processing map for superplastic deformation region in Ti-6Al-4V alloy. The International Journal of Advanced Manufacturing Technology. 104. 10.1007/s00170-019-03956-z

#### Table 1.2.

[T2] E. Marin and A. Lanzutti, "Biomedical Applications of Titanium Alloys: A Comprehensive Review," Jan. 01, 2024, Multidisciplinary Digital Publishing Institute (MDPI). doi: 10.3390/ma17010114.

#### Table 1.2.

[T3] A. Nesbitt and R. M. Nagabhushana, "Protective Coatings for High-Temperature Titanium Alloys: A Review," Surface and Coatings Technology, vol. 76-77, pp. 95-105, 1995. DOI: 10.1016/0257-8972(95)02550-6.